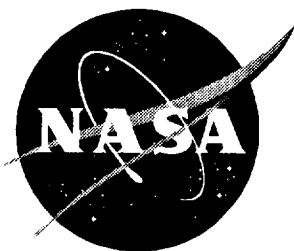NASA/CR-97-206243

Surface Modeling and Grid Generation of Orbital Sciences X34 Vehicle (Phase I)

Stephen J. Alter
Lockheed Martin Engineering & Sciences Company, Hampton, Virginia

National Aeronautics and
Space Administration

Langley Research Center
Hampton, Virginia 23681-2199

November 1997

Abstract

The surface modeling and grid generation requirements, motivations, and methods used to develop Computational Fluid Dynamic volume grids for the X34-Phase I are presented. The requirements set forth by the Aerothermodynamics Branch at the NASA Langley Research Center serve as the basis for the final techniques used in the construction of all volume grids, including grids for parametric studies of the X34. The Integrated Computer Engineering and Manufacturing code for Computational Fluid Dynamics (ICEM/CFD), the Grid Generation code (GRIDGEN), the Three-Dimensional Multi-block Advanced Grid Generation System (3DMAGGS) code, and the Volume Grid Manipulator (VGM) code are used to enable the necessary surface modeling, surface grid generation, volume grid generation, and grid alterations, respectively. All volume grids generated for the X34, as outlined in this paper, were used for CFD simulations within the Aerothermodynamics Branch.

1

Contents

4

List of Tables

List of Figures

Nomenclature

interp Interpolated angle boundary condition for PDEs

ortho Orthogonality boundary condition for PDEs

CADCAM Computer Aided Design tool

CFD Computational Fluid Dynamics

GEOLAB GEOmetry LABoratory at NASA-Langley Research Center

GPSG Grid-Point-Spacing-Gradient or point-to-point spacing in any direction

PDE Partial Differential Equation

TFI Trans-Finite Interpolation

ALGNSHK Grid alignment procedure of LAURA for adapting the third computational direction to outer domain limits and near wall cell sizing for proper boundary layer modeling.

HVI Hermite Vector Interpolation

LAURA The Langley Aerothermodynamic Upwind Relaxation Algorithm code

3DMAGGS The Three-Dimensional Multi-block Advanced Grid Generation System code

GRIDGEN Code used to develop three-dimensional surface grids

ICEM/CFD The Intergrated Computer Engineering and Manufacturing CAD tool for CFD

VGM The Volume Grid Manipulation code

$\|\vec{r}\|_{\eta\eta}$ Magnitude of second derivative in the J-direction.

$\|\vec{r}\|_{\eta}$ Magnitude of first derivative in the J-direction.

$\|\vec{r}\|_{\xi\xi}$ Magnitude of second derivative in the I-direction.

$\|\vec{r}\|_{\xi}$ Magnitude of first derivative in the I-direction.

A_i Area of a cell face for $1 \leq i \leq 6$

n Multigrid and sequencing number for determining grid dimensionality

r Radius of shock limit in the vehicle pitching plane

R_n Nose radius

X, x Physical coordinate from body center line to tail tip

12

Y, y Physical coordinate of body symmetry

Z, z Physical coordinate from forebody to aftbody

c A computational coordinate

α Angle of attack

β Shock angle

χ_η Skewness of inserting grid lines in an J-plane

χ_ξ Skewness of inserting grid lines in an I-plane

χ_ζ Skewness of inserting grid lines in an K-plane

ΔS_c^+ Distance to the $c + 1$ point

ΔS_c^- Distance to the $c - 1$ point

η, J Computational coordinate in cross-section direction

Γ_η Point-to-point spacing in the J-direction

Γ_ξ Point-to-point spacing in the I-direction

Γ_ζ Point-to-point spacing in the K-direction

μ Mach cone angle

Ω Cell volume

ρ_2/ρ_1 Density change across a normal shock

σ Safety factor for grid domain sizing

θ Effective geometry cone angles for domain sizing

ξ, I Computational coordinate in streamwise direction

ζ, K Computational coordinate in body to outer domain direction

Chapter 1

Methods and Requirements

1.1 Surface and Volume Grid Requirements

The primary Computational Fluid Dynamics (CFD) code used by the Aerothermody-namics Branch is the Langley Aerothermodynamic Upwind Relaxation Algorithm[1] (LAURA) code. This code, like other CFD programs, requires a grid to be of a certain fidelity to accu-rately compute aerodynamic and thermodynamic properties of a high-speed flowfield about a given configuration. The desired computational grid for the LAURA code should satisfy the following requirements:

(1) Cross-directional grid lines need to be sectionally planar everywhere except for the leading edges of the wing and tail, where they are to be orthogonal.

(2) Grid-point-spacing gradients (cell-to-cell sizing) need to be less than 1.5.

(3) Section and subface dimensions must be of $(8 * n + 1)$ where a subface exists between changes in geometry features.

(4) Cell spacings must be monotonic, either increasing or decreasing over short spans (30-50 percent of length).

(5) Grid line intersections must be as orthogonal as possible but fit within the topology framework.

(6) Corners of the vehicle, where flow expands or compresses must have tight spacings to capture flow gradients.

(7) The surface grid must adhere to a database provided by GEOLAB, if the wall definition is defined by GEOLAB.

(8) A single block topological volume grid is to be used, unless otherwise specified.

(9) Grid points on the nose and forebody must be equally spaced, circumferentially.

(10) The volume grid must encompass the entire flow domain influenced by the vehicle.

(11) All breaks and discontinuities on the surface must be preserved.

(12) Grid lines emanating from the wall must be orthogonal.

(13) Grid-point-spacing gradients must be less than 1.2 in the third compuational direction.

(14) All lines traversing from the body to the outer domain should be as straight as possible to enable ALiGN-SHocK adaption.

(15) Lines traversing from the body to the outer boundary should be divergent at the outer boundary, to allow grid domain expansion if necessary.

(16) Lines traversing from the body to the outer boundary should be in the third computational direction to enable turbulence modeling.

(17) No negative volumes can be in the volume grid, according to a right-handed coordinate system.

(18) Skewness in the volume grid must be kept to a minimum (i.e., orthogonal intersections of grid lines must be maximized).

(19) All cells within the volume grid should not exceed an aspect ratio of 100.0 to enable efficient capture of the initial flowfield.

(20) All grids have to be generated in as little time as possible.

(21) Where appropriate, a bow shock adapted volume grid is to be used as the starting point.

1.2 Methods to Meet Requirements

To adhere to this formidable list of requirements, the algebraic grid generation algorithm, Trans-Finite Interpolation (TFI) combined with the smoothing capability provided by the solution of an elliptic system partial differential equations (PDE), is used. The combination of these techniques provides the greatest control over grid quality as the algebraic method requires accurate placement of boundaries,[2] and the elliptic PDE solvers in GRIDGEN[3] and the Three-Dimensional Multi-block Advanced Grid Generation System (3DMAGGS)[4] categorically smooth by averaging grid points in the solution to Poisson's heat conduction equation. Incidentally, the placement of grid points is based on the intersection of isothermals on the interior domain.[5]

Improvement of all volume grids is performed with the Volume Grid Manipulation (VGM)[6] code. The VGM code embodies a language rich with commands and associated arguments to ensure that all requirements can be met, providing that the database received from NASA-Langley's GEOLAB adheres to the grid requirements (1) through (6).

1.3 Grid Generation Process

...ess of generating volume grids, starting from a surface grid provided by GEO-...

The following steps:

...the domain that encompasses the entire flowfield (see requirement 10).

...the domain defined in step 1.

...etizing the faces of each...

...erating the volume grid.

...of these steps are described in more detail in the following sections.

1 Defining the Flow Domain

Step 1 is accomplished by using flowfield quantities to establish the limits of the expected flow domain. The quantities used include Mach number, Reynold's number, effective nose radius, and angle of attack. For supersonic and hypersonic flowfields, these quantities are used first in computing the shock standoff distance at the nose with equation 1.1:

$$\Delta S = distance = \frac{0.78 * R_n \sigma}{\rho_2 / \rho_1}$$

(1.1)

where σ is a safety factor, typically set to 2.0. The safety factor is used to enable the elliptic solvers to generate a grid in the nose region. Otherwise the outer boundary is so close to the nose, the cell sizes at the wall may cause the elliptic solver to go instable due to increased stiffness in the PDEs.[7] The density ratio is determined from the normal shock relationships for the Mach number to be modeled.

The outer limits of the volume grid are determined by using effective cone angles from the nose to the tail combined with angle-of-attack variations. The effective cone angle the windside of the vehicle is computed by connecting the most forward point on the to the aft bottom point of the configuration as shown in figure 1.1.

The effective cone angle for the leeside is computed similarly. The actual limit the outer shock is expected to exist on the windside is computed by using the solutic Taylor-Maccoll[8] equation for conical flow. This equation computes the angle, β the bow shock and the body axis, as shown in figure 1.2. The tangent of this an used to compute the distance away from the body, using the distance to the end c with equation 1.2.

$$x = -z \tan(\beta)$$

Figure 1.1: Effective cone angles for computing the flow domain limits.

Figure 1.2: Approximate bow shock location resulting from vehicle movement

1.3 Grid Generation Process

The process of generating volume grids, starting from a surface grid provided by GEO-LAB, entails the following steps:

(1) Defining the domain that encompasses the entire flowfield (see requirement 10).

(2) Discretizing the faces of each domain defined in step 1.

(3) Generating the volume grid.

Each of these steps are described in more detail in the following sections.

1.3.1 Defining the Flow Domain

Step 1 is accomplished by using flowfield quantities to establish the limits of the expected flow domain. The quantities used include Mach number, Reynold's number, effective nose radius, and angle of attack. For supersonic and hypersonic flowfields, these quantities are used first in computing the shock standoff distance at the nose with equation 1.1:

$$\Delta S = distance = \frac{0.78 * R_n \sigma}{\rho_2 / \rho_1} \tag{1.1}$$

where σ is a safety factor, typically set to 2.0. The safety factor is used to enable the elliptic solvers to generate a grid in the nose region. Otherwise the outer boundary is so close to the nose, the cell sizes at the wall may cause the elliptic solver to go instable due to increased stiffness in the PDEs.[7] The density ratio is determined from the normal shock relationships for the Mach number to be modeled.

The outer limits of the volume grid are determined by using effective cone angles from the nose to the tail combined with angle-of-attack variations. The effective cone angle for the windside of the vehicle is computed by connecting the most forward point on the nose to the aft bottom point of the configuration as shown in figure 1.1.

The effective cone angle for the leeside is computed similarly. The actual limits where the outer shock is expected to exist on the windside is computed by using the solution to the *Taylor-Maccoll*[8] equation for conical flow. This equation computes the angle, β, between the bow shock and the body axis, as shown in figure 1.2. The tangent of this angle is then used to compute the distance away from the body, using the distance to the end of the body, with equation 1.2.

$$x = -z \tan(\beta) \tag{1.2}$$
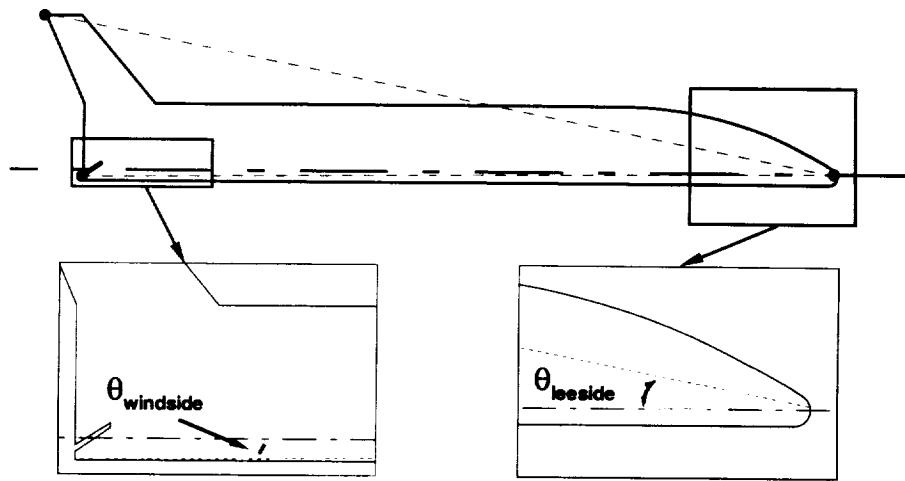
Figure 1.1: Effective cone angles for computing the flow domain limits.
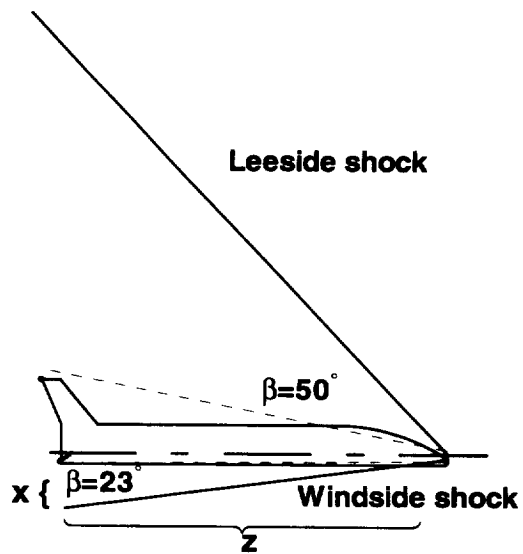
Figure 1.2: Approximate bow shock location resulting from vehicle movement.

The leeside limit is computed by using the limit of the Mach cone for the flowfield. The Mach cone angle, μ, as determined by equation 1.3a, is used to compute the effective flow domain for the geometry of a <u>slender</u> body. The leeside flow domain, as shown in figure 1.2, is computed by using the tangent of the Mach cone angle to compute the ratio between the X- and Z- coordinates for the LAURA code reference frame (see section 2.1). The computed ratio is then used to compute the leeside outer domain limit by taking the Mach cone for the flow and rotating it by the angle of attack, α, according to equations 1.3e and 1.3f:

$$\mu = \sin^{-1}\left(\frac{1}{M_\infty}\right) \tag{1.3a}$$

$$\frac{x}{z} = \tan(\mu) \tag{1.3b}$$

$$x = z\tan(\mu) \tag{1.3c}$$

$$r = \sqrt{z^2 + z^2\tan^2(\mu)} = z\sqrt{1 + \tan^2(\mu)} = z\sec(\mu) \tag{1.3d}$$

$$x_{leeside} = r\cos(\alpha) \tag{1.3e}$$

$$z_{leeside} = -r\,sin(\alpha) \tag{1.3f}$$

The equations 1.3d through 1.3f are solved iteratively on z until the streamwise distance along the body from the last equation matches the end of the configuration, assuming the nose to be at (X, Y, Z) of $(0, 0, 0)$. Note that the seed value for z is not the configuration length but a value larger than the length. The final result of $x_{leeside}$ is then increased by 20 percent to guarantee the flowfield capture of requirement (10).

The computed limits are then connected to the shock standoff point at the nose with ellipses such that the grid line produces an orthogonal intersection with the exit domain on the windside and an extrapolated flow on the leeside. To complete the domain, the leeside point and windside point are connected with a circular arc to generate the final ellipsoidal shape for the outer boundary. This technique is used throughout the grid generation process and serves as the basis for domain definition of the entire flow domain comprised of six computational faces as shown in figure 1.3.

1.3.2 Discretizing the Defined Flow Domain

The grid generation process continues by generating three-dimensional (3D) surface grids[1] on all block boundaries. The surface grid is generated by first defining the grid point distributions along each edge, generating the grid with TFI, and smoothing with an elliptic solver. Grid refinements to develop a grid to adhere to the requirements of section 1.1 are accomplished by dividing the face into subdomains (i.e., subfaces). Algebraic and elliptic solvers are then used on the subfaces to improve grid quality.[7,9]

---

[1] surface grids are computationally two-dimensional (2D)
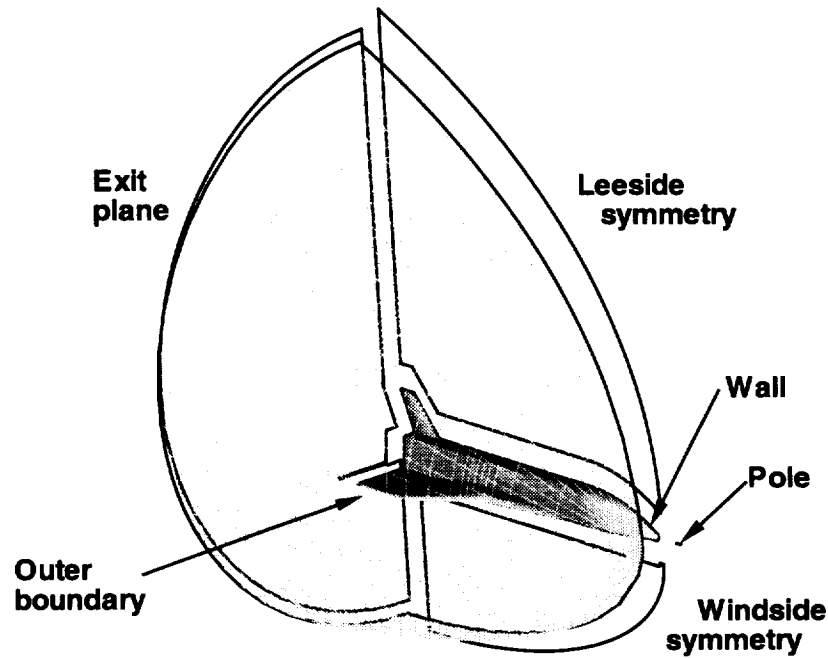
Figure 1.3: Six faces of a single block on a configuration.

The typical elliptic solver controls used on each face and boundary to obtain a usable surface grid are based on the following **GRIDGEN** nomenclature:

Face number	Boundary type	First edge	Second edge	Third edge	Fourth edge
1	Pole	$K_{min}=none$	$J_{max}=none$	$K_{max}=none$	$J_{min}=none$
2	Exit	$K_{min}=$ortho	$J_{max}=$ortho	$K_{max}=$interp	$J_{min}=$ortho
3	Leeside symmetry	$I_{min}=$ortho	$K_{max}=$interp	$I_{max}=$interp	$K_{min}=$ortho
4	Windside symmetry	$I_{min}=$ortho	$K_{max}=$interp	$I_{max}=$interp	$K_{min}=$ortho
5	Wall	$J_{min}=$ortho	$I_{max}=$ortho	$J_{max}=$ortho	$I_{min}=none$
6	Wall	$J_{min}=$ortho	$I_{max}=$interp	$J_{max}=$ortho	$I_{min}=none$

Table 1.1: Typical **GRIDGEN** boundary conditions for each block, face, and edge.

where, **ortho** identifies orthogonality and **interp** indicates that the angles are interpolated from the edge limits.

1.3.3 Generating the Volume

All volume grids are originally generated with Trans-Finite Interpolation in three dimensions (3DTFI) and subsequently smoothed with the elliptic solver 3DMAGGS The 3DMAGGS code offers control on cell height and decay rate of the orthogonality source terms at a boundary, which enables the generation of high-fidelity grids. Orthogonality is usually specified on all boundaries except singularities. Default decay rates are used on all source terms unless specified in the boundary condition tables for each volume grid.

20

The grid generation process is augmented in all stages by the use of the VGM code. This code embodies the necessary language to alter existing grid data and to generate grid data that is difficult to construct without the use of a Computer Aided Design (CAD) tool.

Chapter 2

Topology and Configuration

2.1 Computational Orientation

The computational orientation of coordinates used in this work is shown in figure 2.1. The coordinate reference frame dictated by the use of the LAURA code, shown in figure 2.1, has I (or ξ) increasing in the downstream direction, J (or η) increasing from top to bottom of the vehicle, and K (or ζ) increasing from the wall to the outer boundary. In addition, the grid line parametrically orthogonal to the outer domain will be called the K-line.
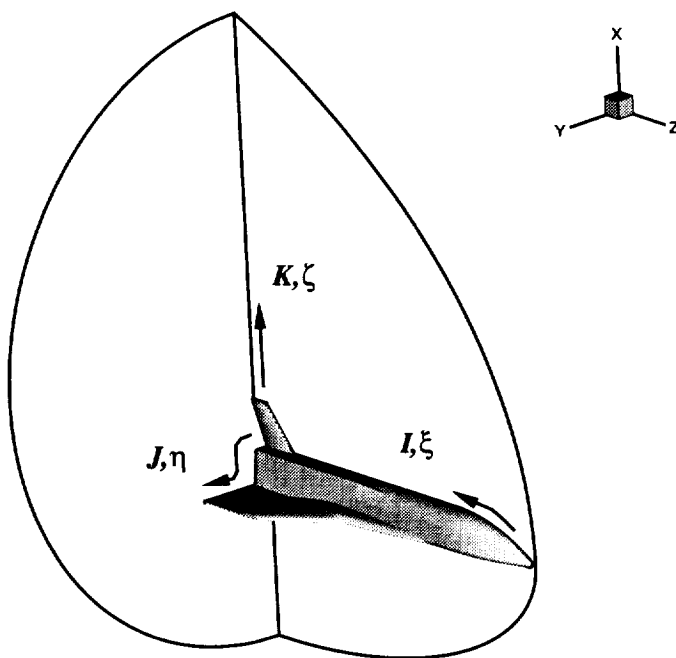
Figure 2.1: Grid point coordinate and computational coordinate orientation for the X34.

2.2 Computational Topology for All Geometry

The topology chosen for this vehicle was an O-H grid with the most complex cross-section at a constant Z dictating the number of points necessary for the J-direction (i.e., cross-flow) and the number of changes in curvature along the I-direction dictating the number of points to be used in the streamwise direction. The most complex cross-section is comprised of the wing and vertical tail. To meet requirements (7), (8) and (11), the point distribution used is shown in figure 2.2. Similarly for the streamwise direction, the distribution required is shown in figure 2.3. In the cross-sectional plane, the break points are easily identifiable by the discontinuities or large changes in curvature. The break points in the streamwise direction are based on these type of discontinuities as well as geometrical features of the vehicle such as the leading edge root of the strake and the leading edge tip region of the wing. Each of these point distributions are shown with every other point missing for clarity and identification of point clusterings.
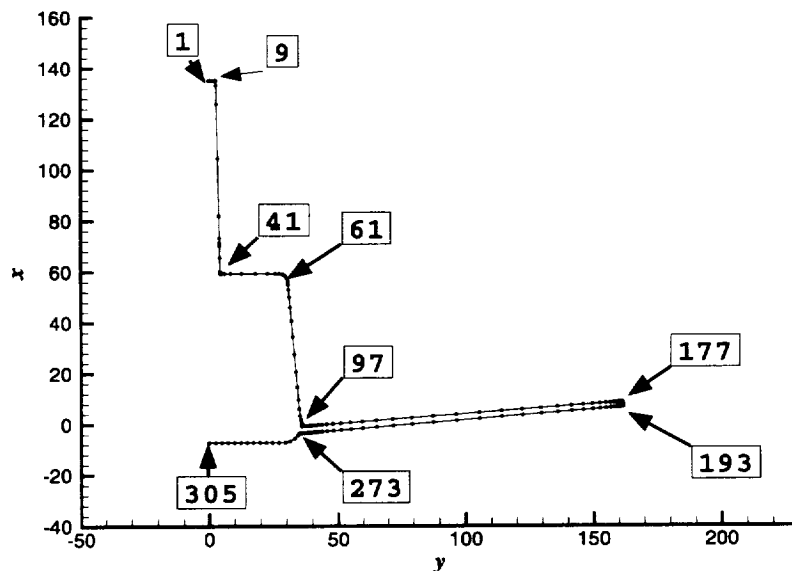
Figure 2.2: Distribution of control grid points in the cross-sectional direction.

The actual topology required the generation of two blocks. The main flowfield block encompasses the configuration, with a ficticious extension of the wing rearward to the end of the fuselage, with an O-grid. The section of the flowfield behind the wing that was omitted from the O-grid uses an H-grid to ensure capture of gradients behind the wing, as well as modeling the side of the fuselage. This topology, shown in figure 2.4, was chosen as it allows the wing, the fuselage, and the vertical tail to be in a single block to guarantee adherence of requirements (8), (9), (14), and (16).

The H-grid was originally constructed with the I-index in the streamwise direction, the J-index along the wing starting at the wingtip and increasing towards the fuselage, and the K-index extending from the bottom of the wing to the top of the wing. This topology was

24
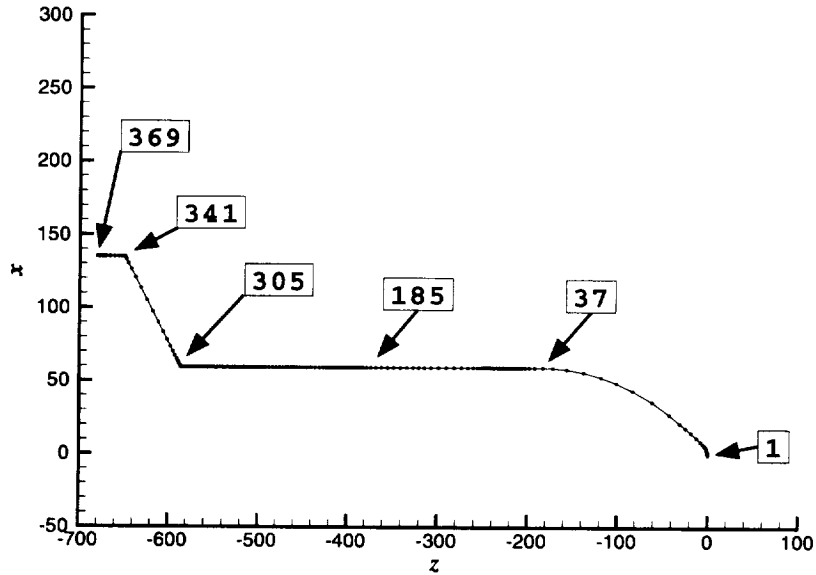
Figure 2.3: Distribution of control grid points in the streamwise direction.
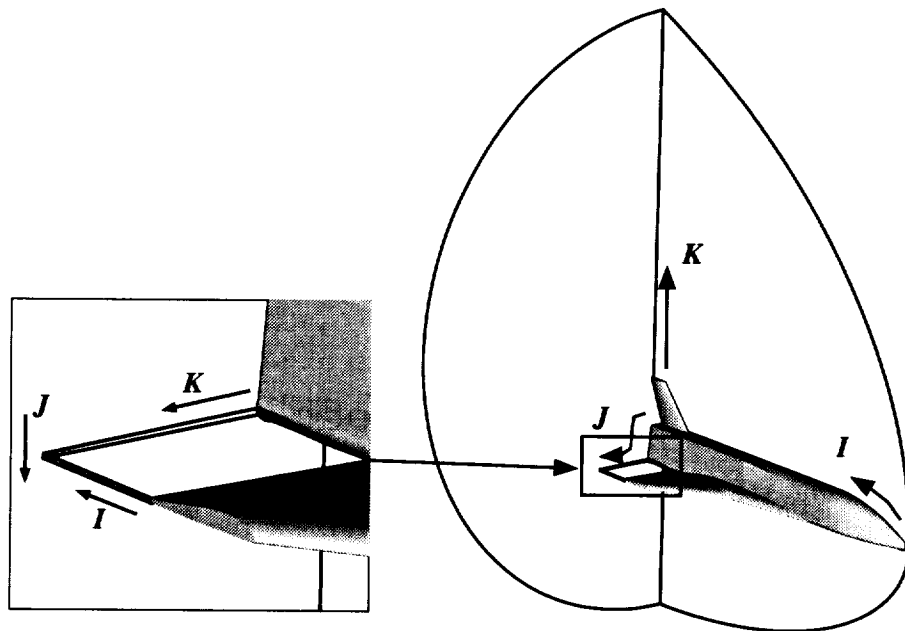
Figure 2.4: Topology of volume grids for the X34.

changed so that the K-index was in the opposite direction of the J-index and the J-index was in the opposite direction of the K-index. This ensured requirement (16) was met. The topology change was solely due to changes in customer requirements for flowfield modeling.

The remaining topological portions of this configuration, including the trailing body

flaps, were continued as O-H grids into the wake regions with another H-grid added in the notched region of the bodyflap behind the base of the configuration as shown in figure 2.5. The topology of the added H-grid was identical to the modified H-grid in the wing trailing edge region to meet requirement (16). This extra zone is isolated and shown in figure 2.6.
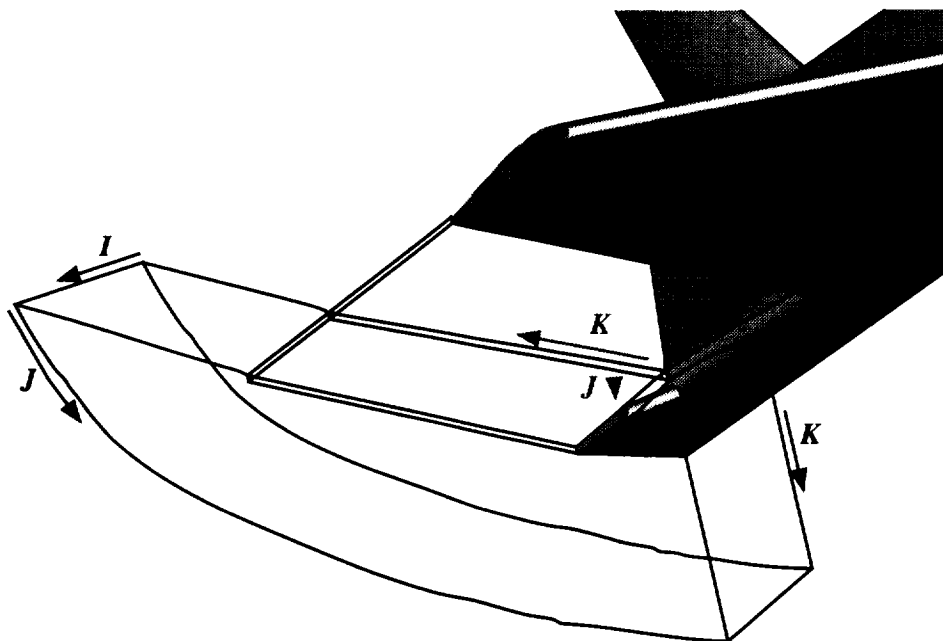
Figure 2.5: Wake topology about bodyflap volume grids for the X34.

These grids represent the overall topography used. The topology changed many times to satisfy the requirements of boundary condition application using the LAURA code and to ease the complexity of the computations. The various changes will be discussed later in chapter 8.

2.3 Configurations to be Modeled

The baseline vehicle geometry to be modeled is shown in figure 2.7. This represents the forebody of the configuration for both inviscid and viscous computations. The inviscid portion ends at the trailing edge of the wing because the front portion is to be used for the determination of aerodynamic heating as computed by the Langley Approximate Three-dimensional Convective Heating (LATCH[10]) code. The LATCH code requires the use of a single block topology for all computations.

The design parametrics to be evaluated for this configuration, shown in figure 2.8, are grouped on the basis of the CFD run matrices in tables 2.1 and 2.2.
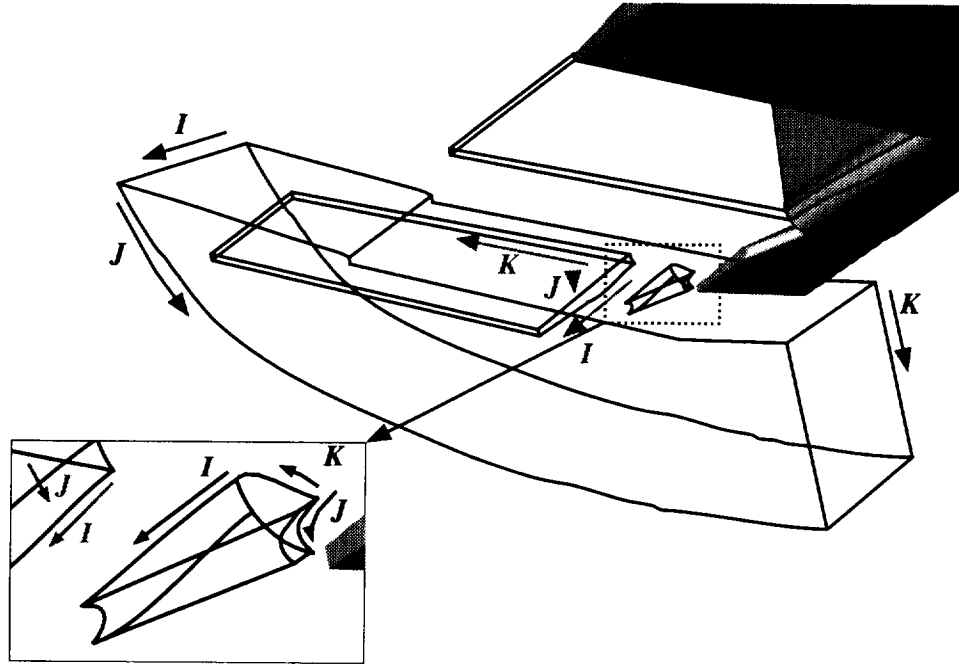
Figure 2.6: Expanded view of wake topology with isolated notched volume.
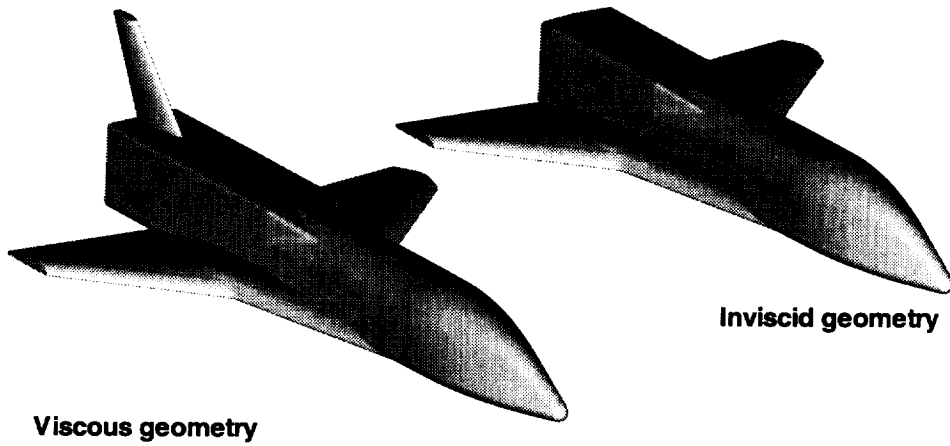
Figure 2.7: Baseline geometries for inviscid and viscous flow computations.
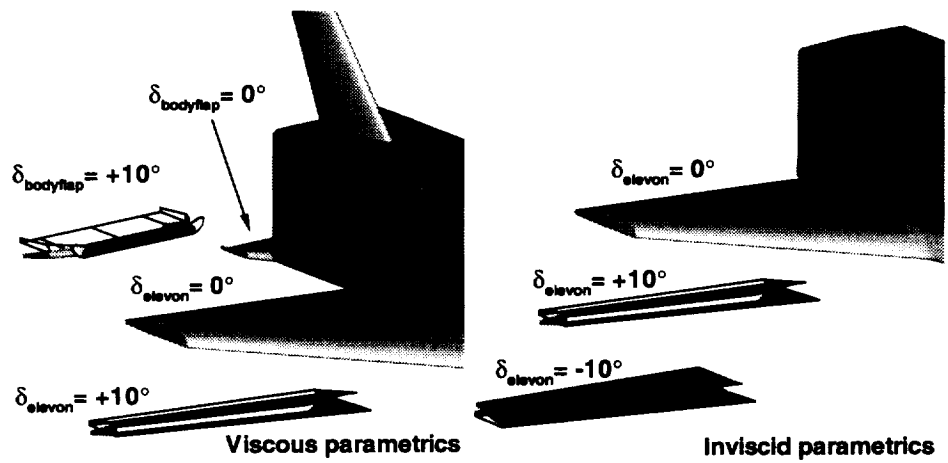
Figure 2.8: Vehicle design parametrics to be evaluated.

Case number	Mach number	α, (deg.)	Elevon angle, (deg.)	Bodyflap angle, (deg.)	Trajectory description
1	6.32	23.0	0	0	Maximum heating/nominal deflection
2	6.32	23.0	10	10	Maximum heating/+10 deflection
3	5.8	8.0	-10	-10	Minimum α /maximum heating
4	6.83	11.0	0	0	Maximum heating on ascent
5	6.0	15.22	0	0	Nominal deflection for wind tunnel
6	3.6	6.48	-10	-10	Reentry maximum q/maximum heating
7	6.0	9.0	0	0	Mach 6 ascent

Table 2.1: CFD run matrix for inviscid computations.

Case number	Mach number	α, (deg.)	Elevon angle, (deg.)	Bodyflap angle, (deg.)	Trajectory description
1	6.32	23.0	0	0	Maximum heating/nominal deflection
2	6.32	23.0	10	10	Maximum heating/+10 deflection
3	6.0	15.22	0	0	Nominal deflection for wind tunnel

Table 2.2: CFD run matrix for viscous computations.

Although the inviscid CFD run matricies identify bodyflap deflections for the inviscid cases, these were not generated because requirement 8 could not be ensured for the LATCH code. The geometry portion to be analyzed ended at the trailing edge of the elevons.

Chapter 3

Geometry and Grid Quality

3.1 Definition of Geometry Quality

For all grids generated and geometries analyzed with CFD, an evaluation of the quality of the surface definition to be used is a necessity. The quality of the geometry upon which subsequent volume grids are based, is evaluated to determine any problems associated with CFD simulations to be performed. Numerous surface quality measures can be found in the literature but, for the scope of the current grid generation, are limited to the following quantities of table 3.1:

Description	Symbol
X-direction component of a surface normal vector.	n_x
Y-direction component of a surface normal vector.	n_y
Z-direction component of a surface normal vector.	n_z
Gaussian curvature[11] on a surface.	Gauss

Table 3.1: Surface quality measures of geometry for grid generation.

For the configurations at hand, the quality measures for the three normal vector components and the Gaussian curvature are illustrated in figures 3.1 through 3.4. Of most importance is the curvature changes identified near the nose and along the leading edges of the strake and wing. These curvature changes may contribute to inaccuracies in heating computations as the boundary layer is thin in these regions.
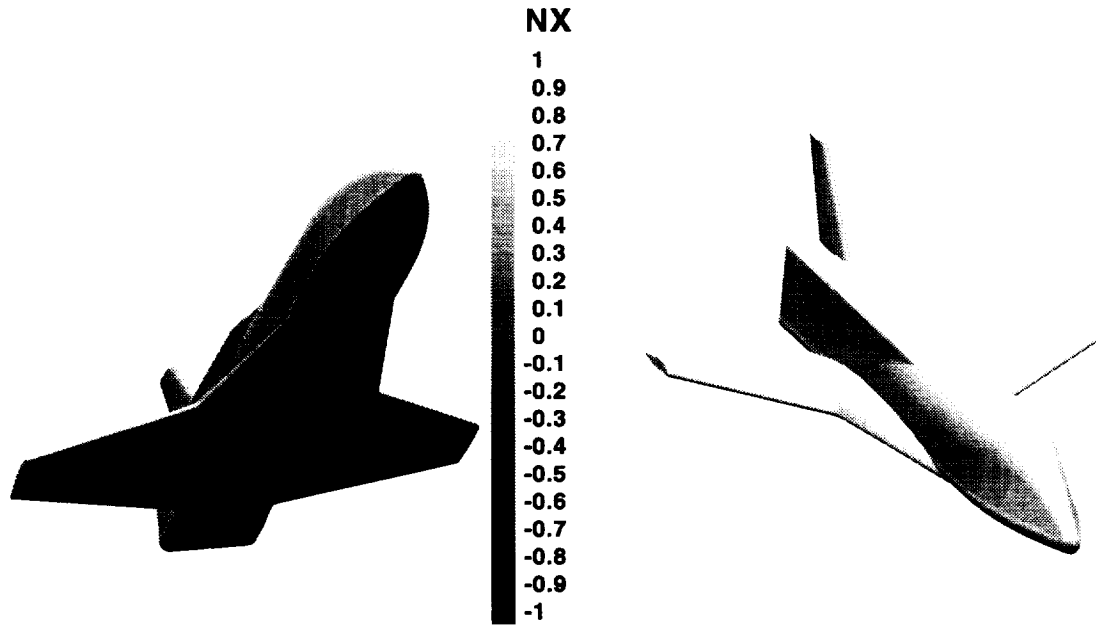
Figure 3.1: X-direction component to a surface-normal vector on the baseline geometry.
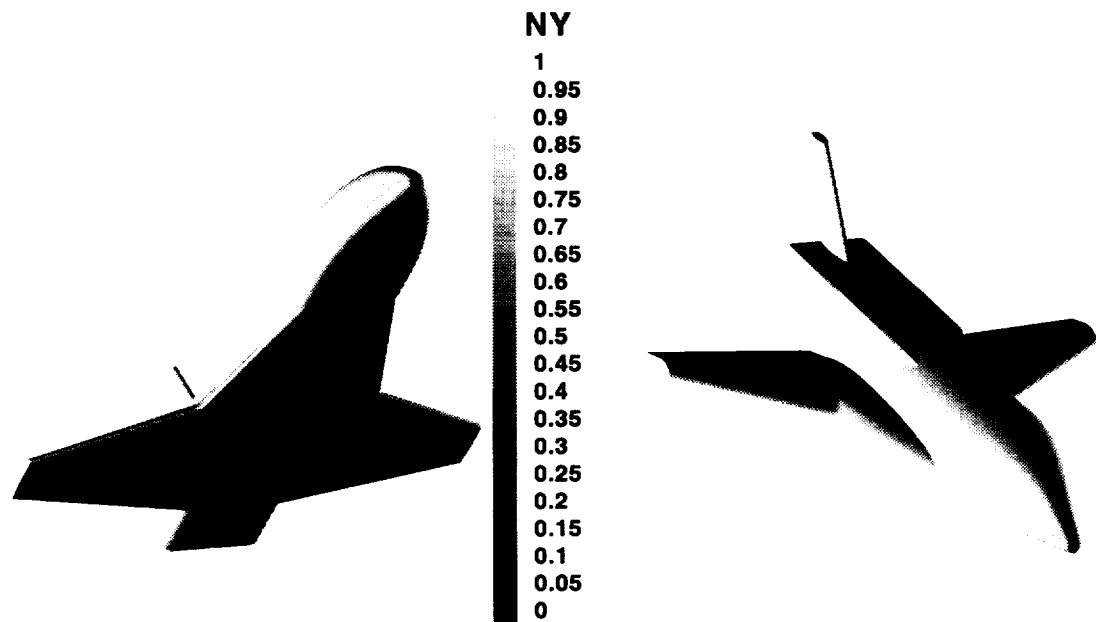
Figure 3.2: Y-direction component to a surface normal-vector on the baseline geometry.
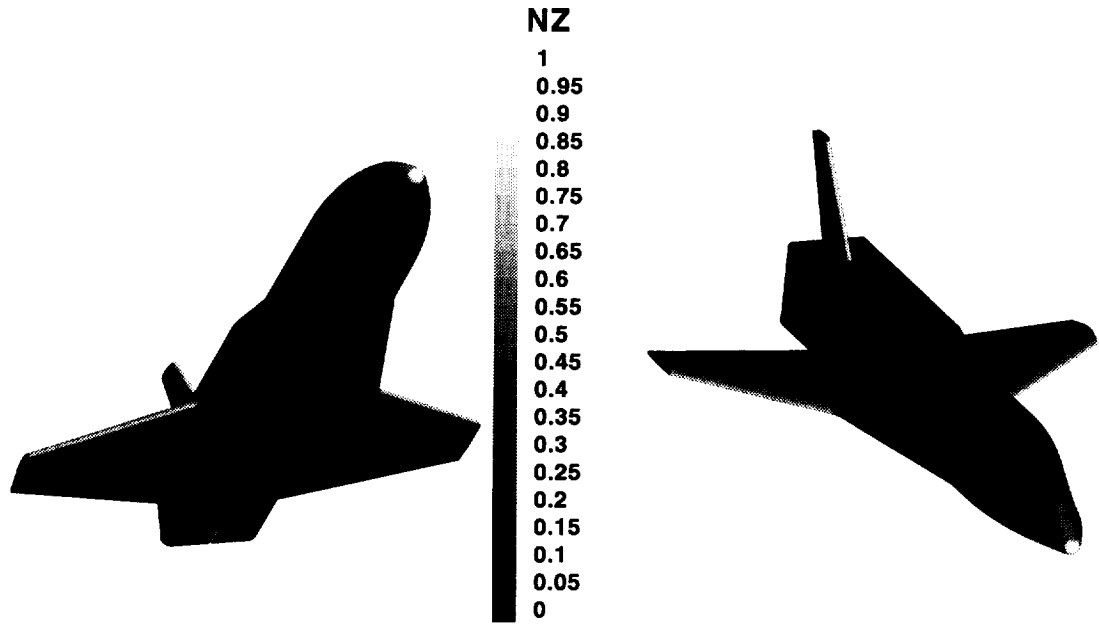
Figure 3.3: *Z*-direction component to a surface normal-vector on the baseline geometry.
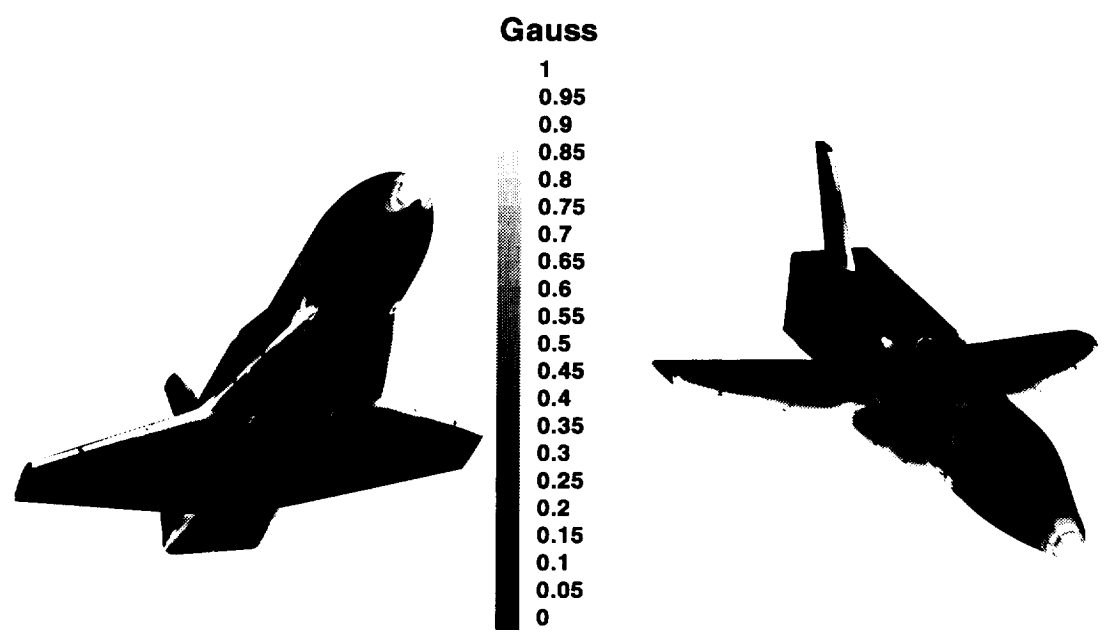
Figure 3.4: Gaussian curvature on the baseline geometry.

3.2 Grid Quality

To guarantee that the requirements governing grid quality are met, the analysis of surface and volume grid quality is performed using the quantities identified in Table 3.2:

Parameter	Symbol
Aspect Ratio of a cell.	AR
Cell volume.	Ω
Grid-point-spacing gradient in the I-direction.	Γ_ξ
Grid-point-spacing gradient in the J-direction.	Γ_η
Grid-point-spacing gradient in the K-direction.	Γ_ζ
Constant I surface grid skewness.	χ_ξ
Constant J surface grid skewness.	χ_η
Constant K surface grid skewness.	χ_ζ
Magnitude of the first derivative in the I-direction.	$\|r\|_\xi$
Magnitude of the second derivative in the I-direction.	$\|r\|_{\xi\xi}$
Magnitude of the first derivative in the J-direction.	$\|r\|_\eta$
Magnitude of the second derivative in the J-direction.	$\|r\|_{\eta\eta}$

Table 3.2: Quality measures of surface and volume grids.

The aspect ratio of a two dimensional cell is measured by calculating the ratio of the average lengths and widths of the cell. In three dimensions, the aspect ratio is determined with equation 3.1:

$$AR = \frac{\sum_{i=1}^{6} A_i}{6\Omega^{\frac{2}{3}}} \tag{3.1}$$

The aspect ratio ranges from 1.0 which represents a square or cube to the maximum in requirement (19). The volume of a cell is always positive and is computed using a tetrahedral discretization to account for curvature of the cell.[12] This is the same method used by the LAURA code and is used to guarantee the grid loaded into LAURA for computations will be free of negative volumes based on the LAURA definition for the volume.

The Grid-Point-Spacing Gradient (GPSG) is the scale factor of distance from point to point along a grid line. As specified by requirements (2) and (13), this value should be less than 1.5, as anything larger will cause the truncation errors of the finite-difference discretizations in the flow solver to become significant. The GPSG is computed in each computational direction for a grid, be it 2D or 3D. The equation is simple, as illustrated in equation 3.2:

$$\Gamma_c = \frac{\max(\Delta S_c^+, \Delta S_c^-)}{\min(\Delta S_c^+, \Delta S_c^-)} \tag{3.2}$$

where,

34

c is the computational coordinate

ΔS_c^+ is the distance to the $c + 1$ point

ΔS_c^- is the distance to the $c - 1$ point

The orthogonality[1] is a final measure of grid quality and is based on measuring planar computations. Orthogonality should be maximized at the wall of a configuration and reduced until grid line curvature is eliminated as the K-line approaches the outer boundary. This type of grid line would produce a grid that satisfies requirements (5), (12), (14), (15), and (18). To get a measure of the orthogonality throughout the grid, equations 3.3a, 3.3b, and 3.3c are used for the ξ, η, and ζ constant planes, respectively.

$$\chi_\xi = cos^{-1} \left[\frac{\vec{r}_\eta \cdot \vec{r}_\zeta}{\sqrt{(\vec{r}_\eta \cdot \vec{r}_\eta)(\vec{r}_\zeta \cdot \vec{r}_\zeta)}} \right] \tag{3.3a}$$

$$\chi_\eta = cos^{-1} \left[\frac{\vec{r}_\xi \cdot \vec{r}_\zeta}{\sqrt{(\vec{r}_\xi \cdot \vec{r}_\xi)(\vec{r}_\zeta \cdot \vec{r}_\zeta)}} \right] \tag{3.3b}$$

$$\chi_\zeta = cos^{-1} \left[\frac{\vec{r}_\xi \cdot \vec{r}_\eta}{\sqrt{(\vec{r}_\xi \cdot \vec{r}_\xi)(\vec{r}_\eta \cdot \vec{r}_\eta)}} \right] \tag{3.3c}$$

As stated above, orthogonality is expected to be greatest near the wall but not at the outer boundary. Hence, the overall orthogonality measurement in each direction should average close to 90 percent or 10° from the orthogonal vector from a surface. Grids that exhibit this type of measurement, or larger, are considered to be high-fidelity grids.

The derivatives listed in table 3.2 are provided to evaluate how well the grid models the underlying surfaces that comprise the wall grid. They are computed in the computational domain as second-order derivatives.[13] Although the second order accurate first derivatives may not assess discontinuities along grid lines, the second derivative will. So the grid line intersection skewness and the magnitudes of the first and second derivatives need to be evaluted to assure odd-even decoupling in the CFD simulations is not attributed to the surface and volume grids. Because these quality measures are grid dependent, each chapter addressing the generation of a surface or volume grid will have a quality assessment section. Each of the terms in table 3.2 will be discussed for individual contributions made to CFD simulations, by assisting in explaining possible anomalies of flowfield characteristics.

---

[1] orthogonality is measured indirectly by computing grid skewness

Chapter 4

Viscous Baseline Grid

This chapter identifies all of the methods and techniques used to develop the viscous volume grids for the X34 baseline geometry as shown in figure 2.7. This chapter consists of several sections covering the assessment of surface grid quality, domain and surface discretizations, and volume generation. The parametrics and topology changes used in the flow computations of the X34 will be in subsequent chapters.

4.1 Surface Grid Quality

The surface grid which was used for the development of the volume grids for the viscous computations was received from GEOLAB. The wall was discretized with 305 points in the I-direction and 369 points in the J-direction. This plethora of points was required to maintain the GPSG of less than 1.5, to provide adequate clustering at the concavities and convexities of the wall grid, and to produce a grid that was multigridable based on requirement (3).

Prior to grid generation, the quality was assessed with the 2D measures identified in section 3.2 and illustrated in appendix A. Most importantly, the wall grid quality, as computed by the GRIDQUAL code, identified several issues that needed attention. The computed measures listed in figure 4.1, indicate GPSG problems in the I-direction, as shown in figure A.1, and highly skewed cells on the surface, as shown in figure A.5.

The skewness is a result of attempting to place a single-block volume grid on this configuration, while maintaining a nearly equally spaced grid on the nose of the configuration; requriements (8) and (11). For this configuration, these requirements produce conflicts with requirements (1) and (5). The compromise of all the pertinent requirements is the wall grid delivered by GEOLAB. Note that the volume generation will only aggravate the GSPG problem as the volume grid is dictated by the wall grid.

The quality measures of the surface grid derivatives shown in figures A.6 through A.9 indicate the effects of the nonmonotonicity of the grid point spacings in each direction. These fluctations in derivatives may be a source of convergence difficulty with the CFD solvers and may provide increased resolution of flowfield gradients where it is not warranted. This data are offered as a check of all CFD simultions.

37

```
Wall Grid Dimensions:  (369 X 305)
```

Measure	Minimum	Maximum	Average	Units
Orthogonality	0.239038E+02	0.151936E+03	0.910516E+02	(degrees)
Cell Area	0.341284E-03	0.176939E+02	0.119581E+01	(square inches)
I-direct GPSG	0.100000E+01	0.184795E+01	0.106493E+01	(none)
J-direct GPSG	0.100000E+01	0.590892E+01	0.106635E+01	(none)

```
Avg. in I of Area Gradients (>1.5)=    1.557990    TOTAL I=      555
Avg. in J of Area Gradients (>1.5)=    0.000000    TOTAL J=        0
Minimum orthogonality =     23.90378      degrees.
```

Figure 4.1: Viscous wall surface grid quality.

4.2 Domain Discretization

To generate the domain that will encompass the entire flow domain, the limits in angle of attack and Mach number are extracted from the CFD run matrix in table 2.2. Based on this matrix and use of equation 1.1 the shock standoff is computed to be:

$$R_{nose} = 0.533 \text{ feet}$$

$$\text{For Mach} = 6.0: \quad \frac{\rho_2}{\rho_1} = 5.268$$

$$\Delta S_{standoff} = \frac{0.78 \times 0.533 \times 2.0}{5.268} \times 12.0 = 1.894 \quad \text{inches}$$

The computation of the limits for the exit flow domain was based on the method described in section 1.3.1, resulting in the following quantities for the leeside:

$$\mu = 9.594°$$
$$z_{seed} = 1716.867$$

$$X_{leeside} = 1200 \text{ inches}$$
$$Z_{leeside} = -714 \text{ inches}$$

and for the windside:

$$\theta = 0.64°$$
$$\beta = 9.5°$$

$$X_{windside} = -130 \text{ inches}$$
$$Z_{windside} = -647 \text{ inches}$$

With these values for the exit limits and these points connected according to the process for domain discretization, the domain for the X34 viscous computation is defined as shown in figure 4.2.
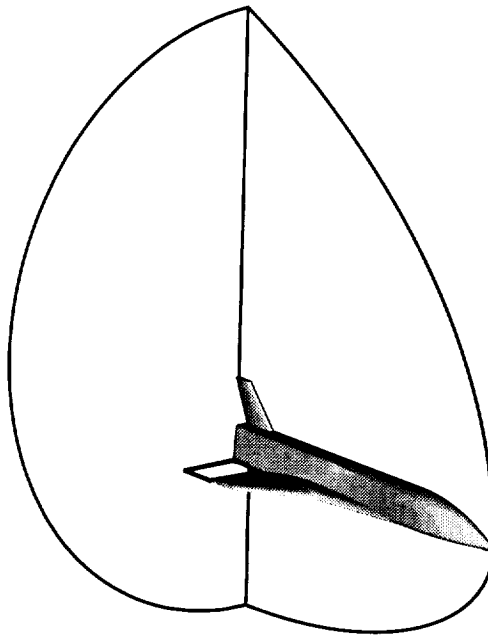
Figure 4.2: Viscous flow domain definition based on flowfield to be simulated.

4.3 Block and Face Construction

Generation of the domain usually begins by sequentially generating the symmetry planes, the exit or exhaust plane, the inflow or pole boundary at the nose, and the outer boundary. This sequence is used because the symmetry planes dictate the distribution needed to get the grid lines from the wall grid to be as straight as possible and easily promote the development of orthogonality at the wall. The same is true for the exit plane, as it is used to determine the distribution in the cross-sectional direction. The exit plane is usually the most complex surface, besides the wall grid. Generation of this plane and the symmetry planes makes the process of generating the pole boundary and outer boundary easier and quicker. The latter boundary is simply a polar TFI of the domain edges. The following sections detail the construction techniques used for each of the domain faces.

4.3.1 Symmetry Plane Generation

The construction of the faces for the computational block of the viscous computations for the X34 was accomplished by first generating the symmetry planes. These surfaces were generated by selecting a point distribution on the outer boundary edge that produces nearly orthogonal grid lines at the wall edge and straight grid lines toward the outer boundary edge as shown in figure 4.3. To ensure monotonicity of grid point spacing, the connecting grid lines from the wall to the outer boundary were distributed with a Vinokur[14] function which usually provides cell-to-cell spacing ratios less than 1.5 to meet requirement (2). The dimension of these grid lines was limited to 33 points as this is adequate for volume generation, while keeping the overall grid dimensions small enough to fit within existing computer architecture for grid generation.
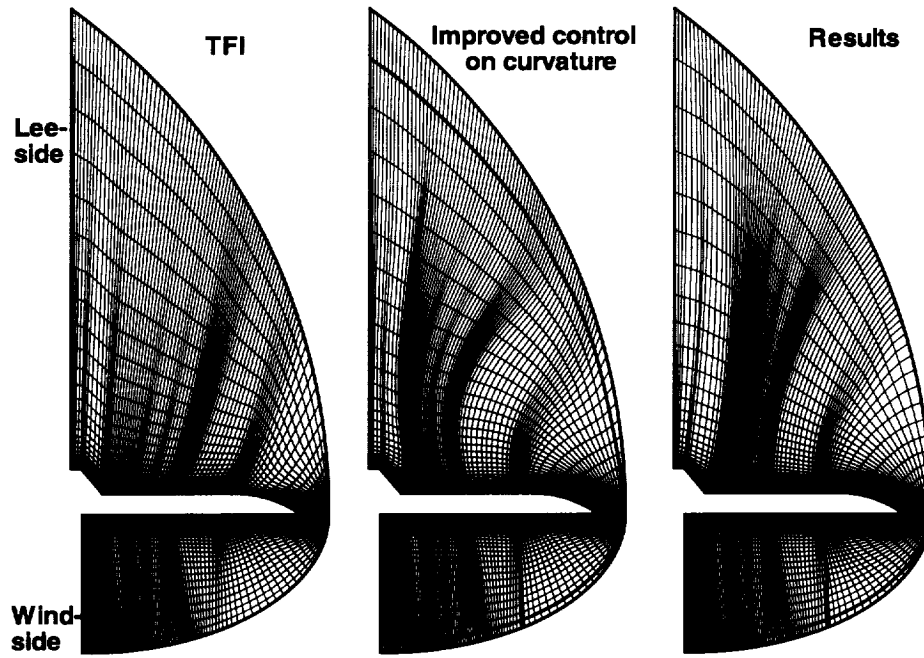
Figure 4.3: Viscous grid - symmetry surface generation process.

The symmetry surface grids were initially generated with TFI. The surfaces were then elliptically smoothed with a Poisson solver for 40 iterations with an orthogonal boundary condition at the pole boundary and wall edges and an interpolated angle boundary condition on the outer boundary and exit edges. This produced grid lines that have minimal orthogonality at the outer boundary edge as shown in figure 4.3. To improve the straightness of the K-lines, a subface of one cell at the outer boundary was created to maintain the current angle constraints. This single-cell layer was modified several times until a grid of reasonable quality was obtained on the interior. The interior domain was smoothed with the Poisson solver to convergence with identical boundary conditions, except for the outer boundary, where a slope continuity boundary condition was imposed. The result is a windside surface grid that meets requirements (2), (4), (8), and (12) through (15).

The leeside symmetry surface grid required more decomposition to improve near-wall orthogonality at the vertical tail root and tip. This was achieved by subdividing the subface into 3 more domains separated by interfaces at the tail leading edge root $I = 305$ and the tail tip leading edge intersection at $I = 345$. Each domain was subsequently generated with TFI and elliptically smoothed with orthogonality at the wall and pole boundary edges, interpolated angles at the outer boundary and exit plane edges, and a slope continuity boundary condition at the subface interfaces. This produced a new leeside grid that adhered to the requirements met by the windside surface grid, shown in figure 4.4.

4.3.2 Exit Plane Generation

The exit plane was most complex surface grid to be generated, and was initially generated by using a distribution that copied the wall grid cross-sectional point distribution to the outer boundary edge. This produced a grid that was not adequate for any requirement and
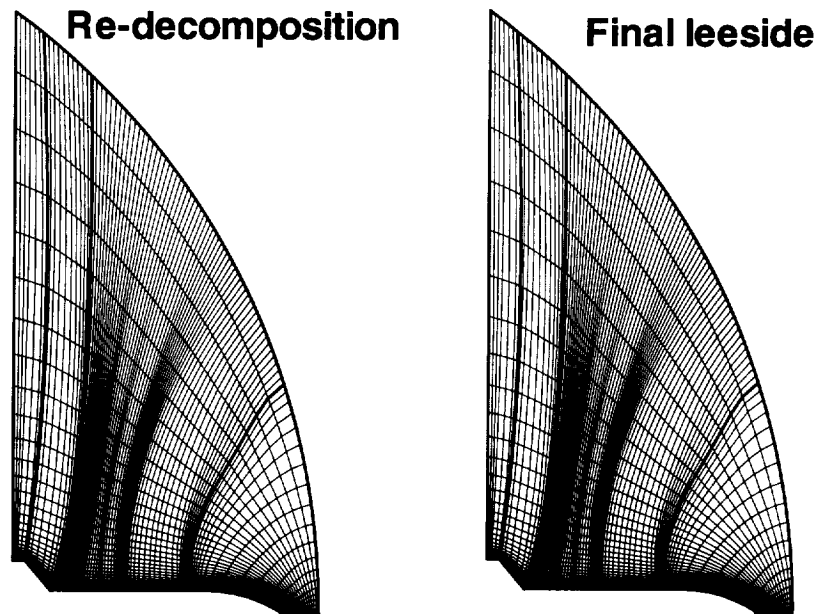
Figure 4.4: Viscous grid - leeside symmetry surface grid improvement process.

resulted in the redistribution of the outer boundary edge to get nearly straight grid lines at key locations on the wall grid, as follows:

- Vertical tail and fuselage intersection.

- Leeside fuselage and wing root intersection.

- Middle of the wing tip.

- Windside fuselage and wing root intersection.

Subfaces were constructed to connect these key geometrical features to the outer domain with grid lines so that orthogonality was ensured at the wall and nearly straight grid lines approached the outer boundary edge. The subfaces were initially generated with TFI again and subsequently smoothed with orthogonality boundary conditions on the symmetry plane and wall edges, interpolated angle boundary conditions on the outer boundary edge, and slope continuity at the subface interfaces. The resulting grid had several problems with the convexities near the top of the vertical tail and the wingtip and concavities at the wing root, as shown in figure 4.5. Elliptic solvers categorically compress grid points onto convexities and pull points out of concavities.[9] For clarity, the grid shown in figure 4.5 is reduced in cross-section dimensionality; so the spacing gradients appear to be worse.

These problems were alleviated through surface grid manipulations with the VGM code. The grid was smoothed using Hermite Vector Interpolation (HVI) with corner packing[9] in the concave regions and redistributing the grid points in the wingtip region to reduce GPSGs at the interfaces to the undisturbed grid. The results of these manipulations produced a grid that was inadequate because the cross-sectional curvature and distributions on the interior produced less than orthogonal grids at the wall. The entire wing region was regenerated

41
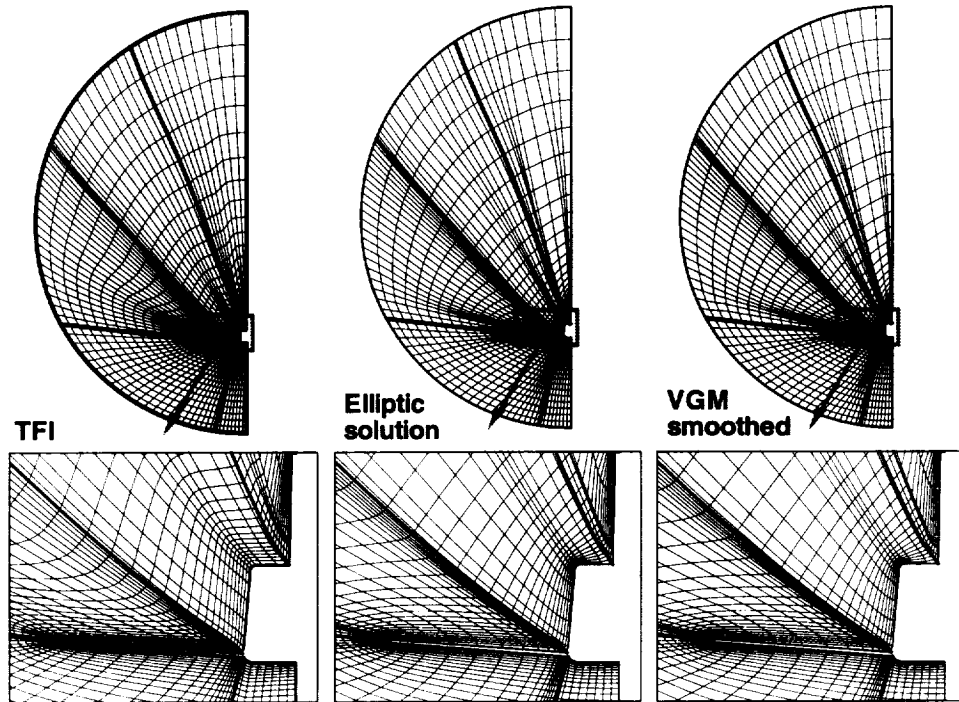
Figure 4.5: Viscous grid - exit domain initial subface decomposition and generation.

by subdividing it into three subfaces that included the leeside and windside portions of the wing and the wingtip in a separate zone, as shown in figure 4.6. The connecting edges of the wing subfaces of the tip were regenerated with piecewise cubic splines and ellipses to get the compromising grid line of 45° at the corners. Each new subface was regenerated with TFI and elliptically smoothed with identical boundary conditions as the first subface decomposition, as shown in figure 4.6.

Again, the elliptic solver produced the usual point spacing mismatch at the interface of the wingtip subface to the leeside and windside subfaces, and the interface of the leeside wing subface to the undisturbed leeside region. These point spacing mismatches were alleviated with VGM. The final result is an exit plane surface grid that is smooth, and adheres to all requirements, illustrated in figure 4.6.

4.3.3 Pole and Outer Boundary Generation

The remaining surfaces to be generated were the outer boundary and the pole boundary on the nose. The outer boundary surface was generated with polar TFI with the axis along Z-coordinate, and the pole grid was generated with standard TFI. All generated surfaces were output in a GRIDGEN face file in preparation for volume grid generation.
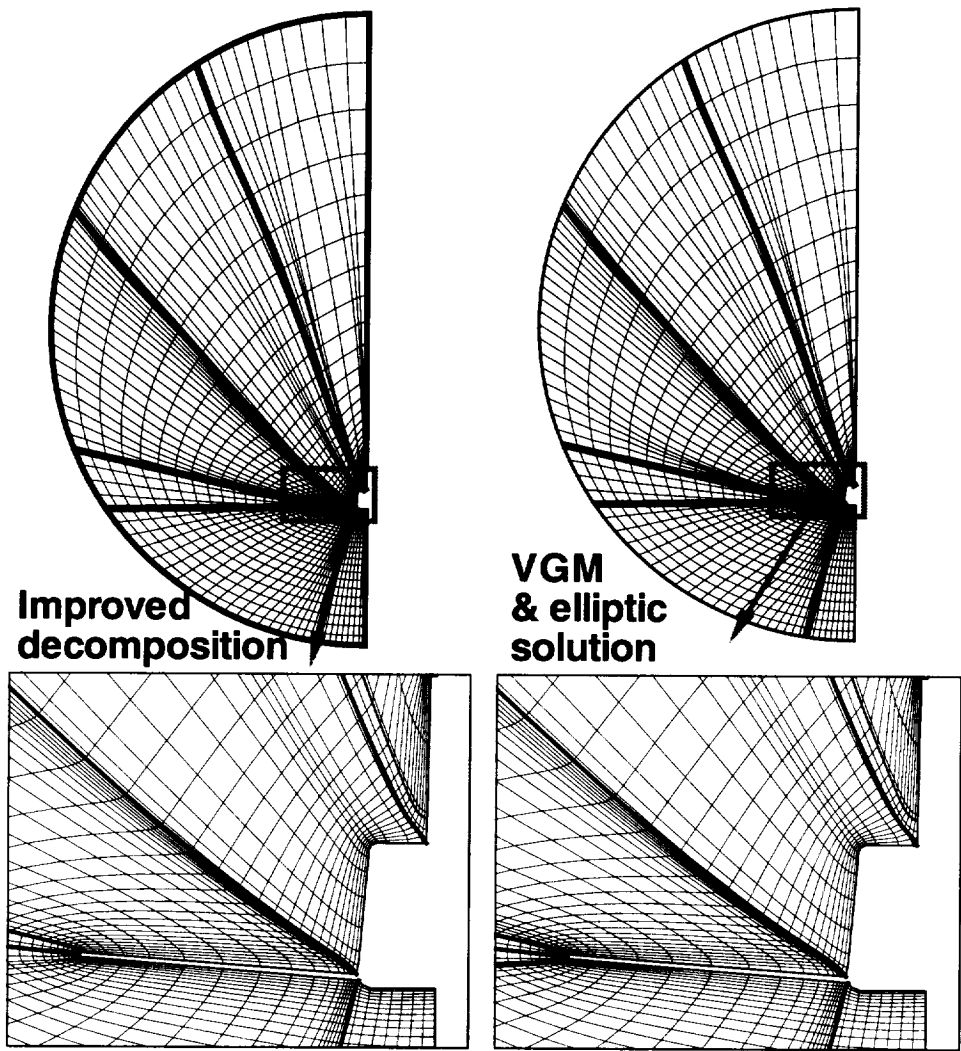
Figure 4.6: Viscous grid - exit domain re-decomposition for improved wingtip regional control.

4.4 Volume Generation

The viscous volume grid is originally generated as an inviscid grid and subsequently converted to the viscous grid through the use of the VGMThe process of generating the volume grid was accelerated by reducing the number of points in the I- and J-directions by an increment of four points. This reduced the size of the grid by a factor of 16, which significantly reduced the time to generate the volume grid.

The boundary conditions used in the development of the volume grid are listed in table 4.1. These controls were chosen to obtain the greatest orthogonality at the symmetry planes and the outer boundary. The latter was most important because the outer boundary is an ellipsoid, and orthogonal grid lines at this boundary would ensure meeting requirement (15).

Face description	Boundary condition	Decay rate
Pole (singularity)	(none)	<Default>
Exit	Orthogonality	0.40
Leeside Symmetry	Orthogonality	0.35
Windside Symmetry	Orthogonality	0.35
Wall	Orthogonality	<Default>
Outer Boundary	Orthogonality	0.40

Table 4.1: Volume grid generation Poisson solver boundary conditions.

The development of the inviscid grid used for the conversion is generated with the 3DMAGGS code. To use the 3DMAGGS code, the GRIDGEN data must first be converted into 3DMAGGS input data. This conversion is accomplished by utilizing the preprocessing code to 3DMAGGS called PREMAGGS. The 3DMAGGS code was executed for 200 iterations using 30 minutes of Central Processing Unit (CPU) time on a Silicon Graphics Incorporated R10000 (SGI-R10k) workstation to get the initial basis grid for creating the inviscid volume grid. The number of iterations did not produce a solution-converged[1] grid, but resulted in an excellent starting place for redensification towards the generation of the viscous volume grid.

Initially, the thinned volume grid was adequate for building a viscous basis grid. The grid was increased in dimensionality to the full I- and J-dimensions using VGM but some of the regions between the elliptically generated grid lines had highly skewed lines. This problem was corrected by using the blend command of VGM to interpolate the wall distributions obtained from the GEOLAB grid to serve as the basis functions for redistributing the regions. The grid qualities of the aft regions were improved by importing the exit plane of the originally generated domain face, and ensuring the symmetry planes to be symmetric by setting the Y-coordinate to zero on the symmetry faces of the volume block. This solution was the eighth method used which resulted in a usable viscous basis volume grid shown in

---

[1]A solution-converged grid is one in which the grid point coordinates are differ by less than 0.001 percent of the smallest cell size in the volume domain for any of the computational directions, between iterations.

figure 4.7. Representative surface grids from the grid interior are shown at $I = 77$, $I = 333$, and $J = 185$, where the black lines indicate the 3DMAGGS generated grid, and the gray lines represent the grid with increased dimensions and quality from VGM work.

I=77   I=333   J=185
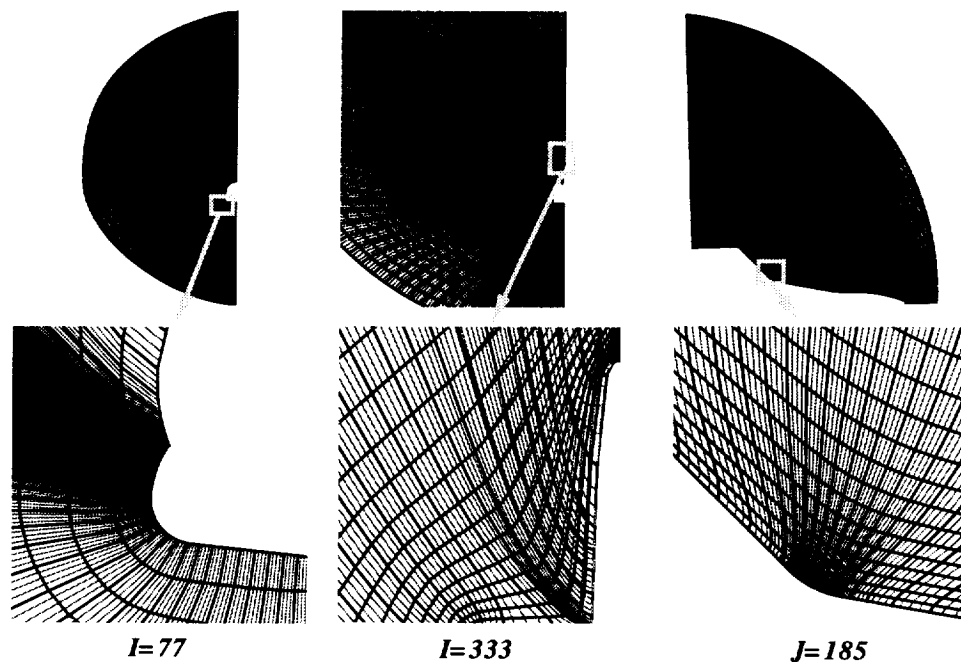
Figure 4.7: Evolution of viscous basis grid from 3DMAGGS to VGM.

The final VGM alterations required to obtain the viscous volume grid were conversion of the viscous basis grid to viscous dimensionality of 65 points on the K-lines, clustering at the wall, re-orientation of the GEOLAB-supplied wing trailing edge wake volume, and translation of the entire volume grid so that the nose starts at $(0,0,0)$. The conversion from inviscid grid spacings to viscous grid spacings is shown in figure 4.8 for identical interior surface grids. The viscous basis grid, colored in black, has been thinned in the I- and J-directions by an increment of 8 to offer clarity in viewing the gray viscous grid lines.

4.5 Volume Grid Quality

The quality of the delivered volume grid, assessed using the measures of table 3.2, was determined with the Three-dimensional VOLume CHecKing code (3DVOLCHK). The output from this code is listed in appendix B. Although the GPSGs in the main volume grid appear to violate the requirements, the values given are the averages of those cell-to-cell scalings greater than the 1.5 maximum, indicated in the dimensions to the right in the table. Considering that the volume has over 7 million cells, the number of cells in question is significantly less than the overall volume grid. As shown by the surface grid quality assessment in section 4.1, the I-direction GPSG is already locally in violation of the requirements. As indicated, these violations propagated into the volume, and accounts for the violations here. Although there

45
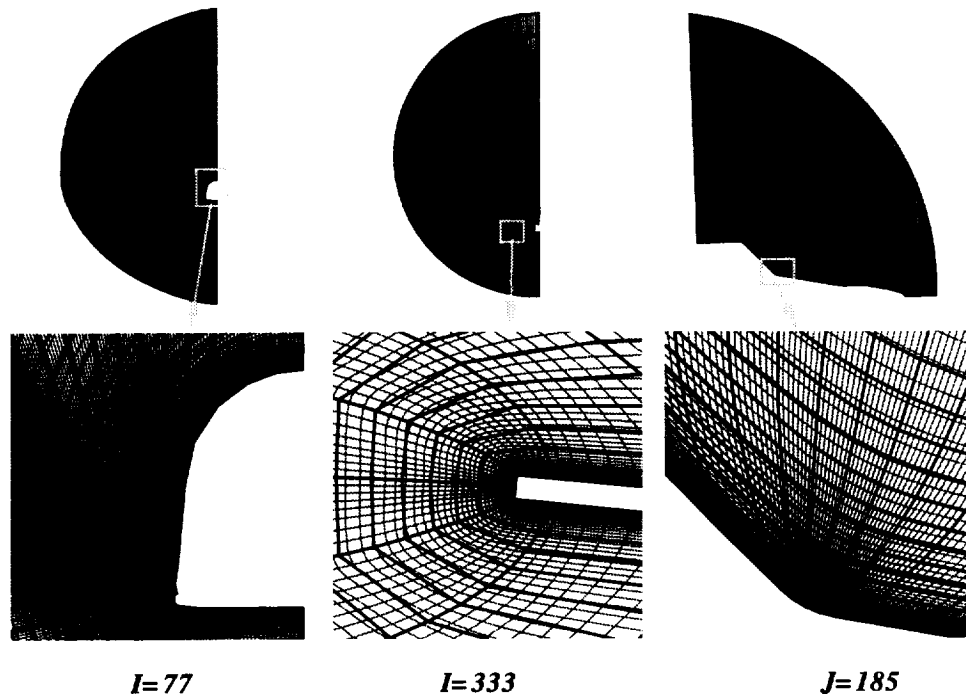
Figure 4.8: Conversion of viscous basis grid to viscous grid.

are local violations of some requirements, all requirements are met globally, and the local violations are insignificant with respect to the entire volume.

Chapter 5

Inviscid Baseline Grid

This chapter addresses the techniques and processes used to generate the inviscid volume grids for the X34 baseline geometry, as shown in figure 2.7. The geometry is the viscous grid geometry truncated at the wing trailing edge. This geometry was chosen because it enables the use of the LATCH code for inviscid heating correlations. The LATCH code requires the entire geometry to reside in a single block; hence the wake regions are not included. This chapter has six sections which cover the following:

(1) Conversion of the viscous wall grid to the inviscid wall grid.

(2) Surface modeling efficiency through quality assessment.

(3) Domain definition for the flowfields to be simulated.

(4) Block and face discretization for the baseline volume grid.

(5) Volume generation.

(6) Quality of deliverable.

The parametrics and topology changes used in the flow computations of the X34 are included in subsequent chapters. This chapter only addresses the methods to obtain the initial inviscid baseline volume grid.

5.1 Wall Grid Generation

Initially, the wall grid to be used was the truncated grid portion from the viscous computations. This grid provided flow resolution through grid point clustering in regions that were not necessary for the computation of the inviscid flowfields. The number of grid points used in the viscous computations was excessive when compared to those required for inviscid computations. The efficient use of a reduced number of avaiable grid points was necessary to limit the size of the problem but offer appropriate modeling of the vehicle features.

The generation of the wall grid was done completely with VGM by converting the wall grid from the viscous computations. The conversion commenced by eliminating the grid point

clustering on the top of the configuration where a transition to the vertical tail had begun. Then, the streamwise direction grid point spacings in the regions of the wing leading-edge root, the crank in the wing which coinsides with the change in fuselage geometry, the leading edge of the wingtip, and the wing trailing edge were redistributed to obtain an approximately equal monotonic spacing of grid points. Finally, the distributions in the cross-sectional direction were modified to improve the modeling of the vehicle features while maintaining a reduced number of grid points and still adhere to requirement 6. The streamwise direction distributions were improved slightly to get closer to the monotonic point spacings of requirement (4).

This conversion process, sequentially shown in figure 5.1, resulted in a wall grid that was redistributed with linear and splined basis functions. To guarantee that the wall grid lay on the geometry surface, the GridTool[15] code was used to project the grid to the original Non-Uniform Rational Bi-cubic Splines (NURBS) data, received from GEOLAB. The most significant change in grid point location was less than 0.0001 inch as a result of the projection. The projected grid was not smoothed any further. The final wall grid was reduced in dimensionality to 121 points in the I-direction and 153 points in the J-direction. This represents a decrease by a factor of five in the number of grid points to be used in the simulation of the inviscid flowfields.

Initial viscous wall grid

Streamwise thinning and redistribution

Circumferential thinning and redistribution

Projection and final smoothing
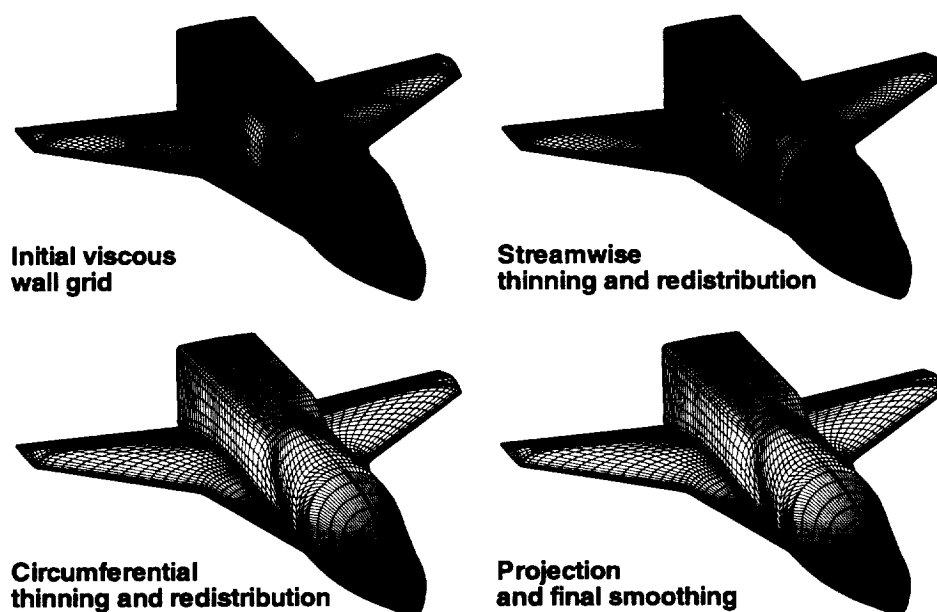
Figure 5.1: Viscous-to-inviscid wall grid conversion.

5.2 Surface Grid Quality

Prior to grid generation, the quality of the created wall grid was assessed with the 2D measures identified in section 3.2. These are presented in appendix C. The globally computed measures for the inviscid grid are listed in figure 5.2 and indicate that there are

GPSG problems in the *I-* and *J-*directions. The values of measures are substantial, but they represent a compromise on the number of points used in the generation of this wall grid. The overall goal of generating the wall surface grid from the viscous wall grid was to eliminate as many points as possible without sacrificing quality and to still adhere to all the requirements in section 1.1. The new requirements along with the original 21, made this problem too restrictive. To save on generation time, grid quality was compromised as agreed to by the customer.

```
Wall Grid Dimensions:  (121 X 153)


    Measure           Minimum          Maximum          Average           Units
    -------           =======          =======          =======          ===============
Orthogonality      0.435205E+02     0.136523E+03     0.905804E+02         (degrees)
Cell Area          0.318267E-02     0.347656E+02     0.560278E+01     (square inches)
I-direct GPSG      0.100000E+01     0.227881E+01     0.107413E+01          (none)
J-direct GPSG      0.100000E+01     0.298205E+01     0.106127E+01          (none)


  Avg. in I of Area Gradients (>1.5)=    1.930330      TOTAL I=         493
  Avg. in J of Area Gradients (>1.5)=    1.691619      TOTAL J=         209
  Minimum orthogonality =     43.52052       degrees.
```

Figure 5.2: Inviscid wall surface grid quality.

The GPSG problem identified on the surface will pose problems as these point-spacing gradients are propagated into the interior of the volume domain. This will result in reduced volume grid quality but a reasonable compromise of all requirements.

5.3 Domain Discretization

Generation of the domain that will encompass the entire flow domain commences with the limits in angle of attack and Mach number extracted from the CFD run matrix in table 2.1. Based on this matrix and with equation 1.1, the shock standoff is computed to be:

$$R_{nose} = 0.533 \text{ feet}$$

$$\text{For Mach} = 3.0: \quad \frac{\rho_2}{\rho_1} = 3.857$$

$$\Delta S_{standoff} = \frac{0.78 \times 0.533 \times 2.0}{3.857} \times 12.0 = 2.587 \quad \text{inches}$$

The computation of the limits for the exit flow domain was based on the method described in section 1.3.1, and resulted in the following quantities for the leeside:

$$\mu = 19.47°$$
$$z_{seed} = 1722.836$$

$$X_{leeside} = 2018 \text{ inches}$$
$$Z_{leeside} = -714 \text{ inches}$$
and for the windside:
$$\theta = 0.64°$$
$$\beta = 19.75°$$

$$X_{windside} = -280 \text{ inches}$$
$$Z_{windside} = -647 \text{ inches}$$

With these values for the exit limits, and these points connected according to the process for domain discretization, the domain for the X34 viscous computation is defined as shown in figure 5.3:

5.4 Block and Face Construction

Identical to the viscous grid domain construction, the inviscid domain grids are generated in order of the symmetry planes, the exit plane, the pole boundary at the nose, and the outer boundary. The process used for each of these surfaces will be discussed in the following sections.

5.4.1 Symmetry Plane Generation

The construction of the faces for the computational block of the inviscid computations for the X34 was accomplished by first generating the symmetry planes. These surfaces were generated by selecting a point distribution on the outer boundary edge that produces nearly orthogonal grid lines at the wall edge and straight grid lines towards the outer boundary edge as shown in figure 5.4. To ensure monotonicity of grid point spacing, the connecting grid lines from the wall to the outer boundary were distributed with a Vinokur[14] function which usually provides cell-to-cell spacings less than 1.5 to meet requirement (2). The dimension of these grid lines was limited to 33 points as this is adequate for volume generation while keeping the overall grid dimensions small enough to fit within existing computer architecture for grid generation.

The symmetry surface grids were initially generated with TFI. The surfaces were then elliptically smoothed with a Poisson solver for 40 iterations with an orthogonal boundary condition at the pole boundary and wall edges and an interpolated angle boundary condition on the outer boundary and exit edges. This produced grid lines that have minimal orthogonality at the outer boundary edge as shown in figure5.4. To improve the straightness of the K-lines, a subface of one cell at the outer boundary was created to maintain the current angle constraints. The interior domain was smoothed with the Poisson solver to convergence with identical boundary conditions, except for the outer boundary, where a slope continuity boundary condition was imposed. The result is a windside surface grid that meets requirements (2), (4), (8), and (12) through (15).

50
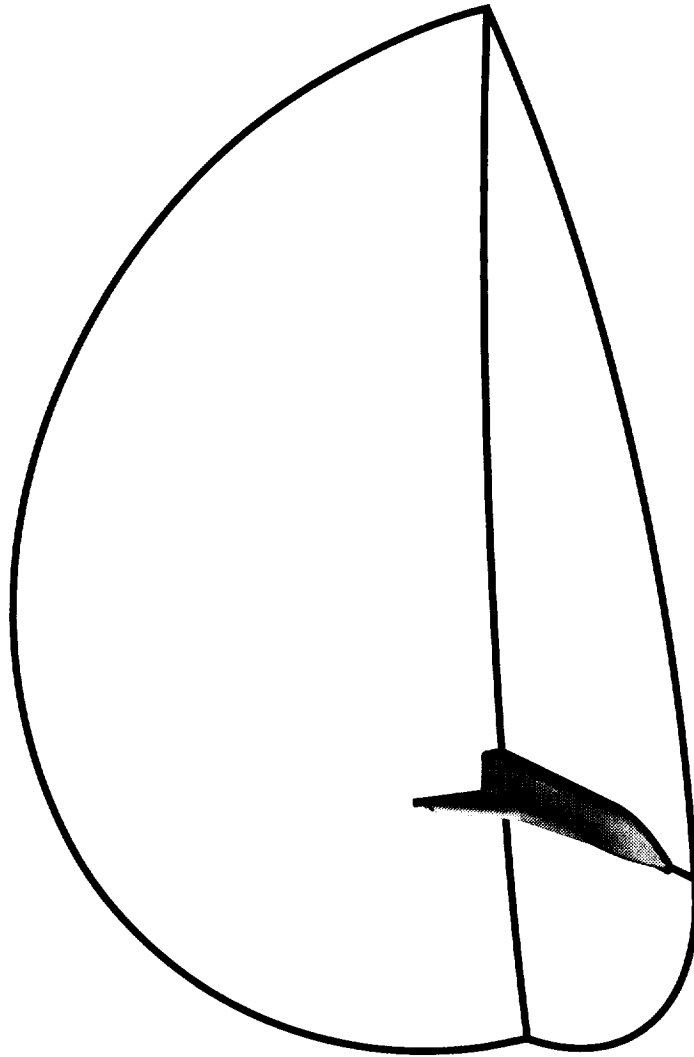
Figure 5.3: Inviscid flow domain definition based on flowfield to be simulated.

5.4.2 Exit Plane Generation

The exit plane was the most complex surface grid to be generated, and was initially generated by using a distribution that copied the wall grid cross-sectional point distribution to the outer boundary edge. This produced a grid that was not adequate for any requirement, and resulted in the redistribution of the outer boundary edge to get nearly straight grid lines at the following key locations on the wall grid:

- Leeside fuselage and wing root intersection.

- Top and bottom of the wing tip.

- Windside fuselage and wing root intersection.
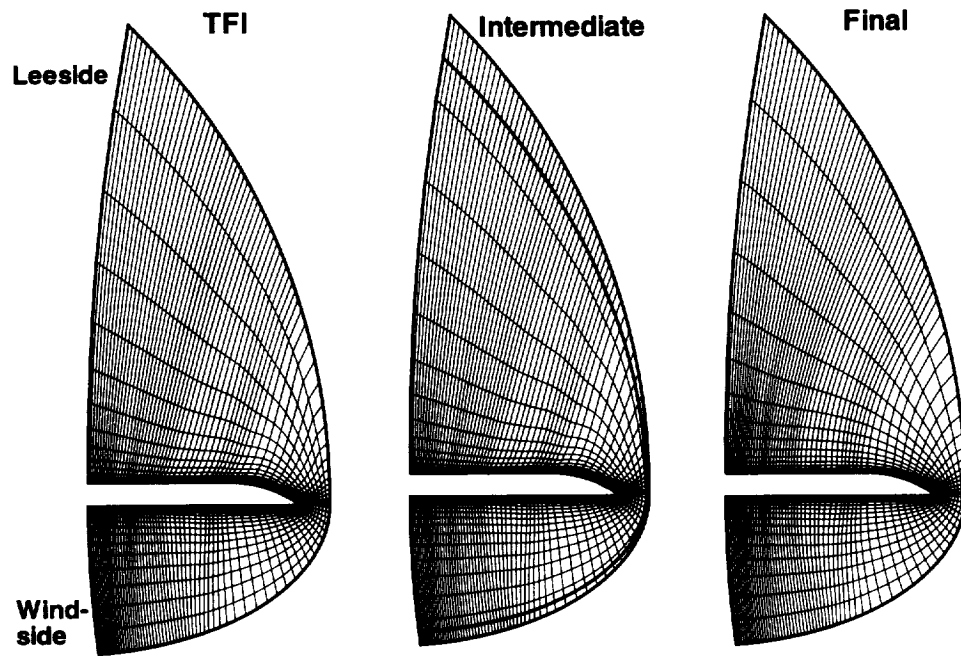
Figure 5.4: Inviscid grid - symmetry surface generation process.

Subfaces were constructed to connect these key geometrical features to the outer domain with grid lines that ensured orthogonality at the wall and nearly straight grid lines near the outer boundary edge. The subfaces were initially generated with TFI again and subsequently smoothed with orthogonality boundary conditions on the symmetry plane and wall edges, interpolated angle boundary conditions on the outer boundary edge, and slope continuity at the subface interfaces. The resulting grid had several problems with the convexities near the wingtip and concavities at the wing root, as shown in figure 5.5.
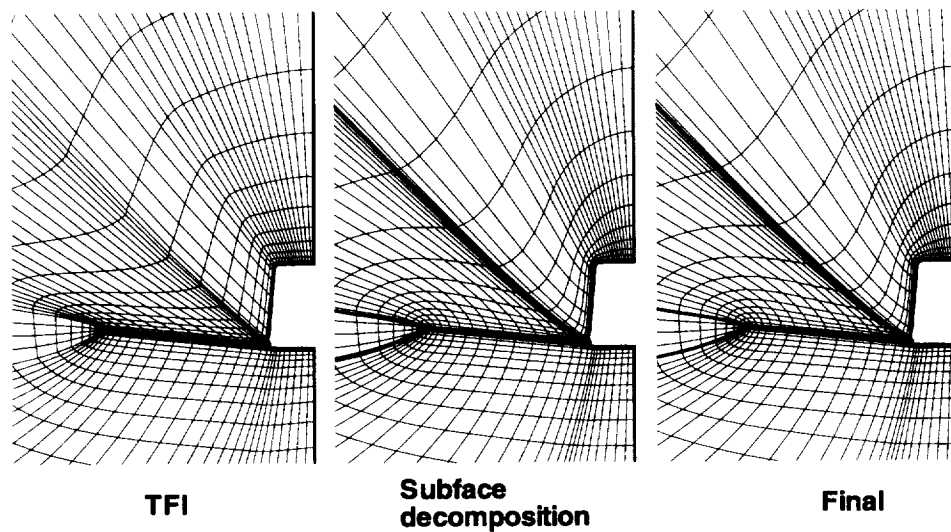
Figure 5.5: Inviscid grid - exit domain initial subface decomposition and generation.

52

These problems were alleviated through surface grid manipulations with the VGM code. The grid was smoothed using HVI on the concave regions and redistributing the grid points in the wingtip region to reduce GPSGs at the interfaces to the undisturbed grid. The final result is an exit plane surface grid that is smooth and adheres to all requirements, as shown in figure 5.5.

5.4.3 Pole and Outer Boundary Generation

The remaining surfaces to be generated were the outer boundary and the pole boundary on the nose. The outer boundary surface was generated with polar TFI with the axis along the Z-coordinate, and the pole grid was generated with standard TFI. All surfaces generated were output in a GRIDGEN face file in preparation for volume grid generation.

5.5 Volume Generation

The inviscid volume grid is generated completely with the 3DMAGGS code in full dimensionality with the boundary conditions in table 4.1. The only change to these boundary conditions for the inviscid grid was the wall orthogonality decay rate, which was 0.40 as compared with the default of 0.45. The GRIDGEN data was converted to the 3DMAGGS data with the PREMAGGS code, and the 3DMAGGS code was executed for 500 iterations using 87 minutes of CPU time on an SGI-R10k to get the initial basis grid for creating the inviscid volume grid. This number of iterations produced a solution-converged grid. However, there were minor problems with grid line skewness in the wingtip region. VGM was subsequently used to improve these regions and generate the final deliverable volume grid. These manipulations resulted in a volume grid illustrated with representative planes shown in figure 5.6.

5.6 Volume Grid Quality

The quality of the delivered volume grid assessed with the measures of table 3.2, was determined with the 3DVOLCHK code. The output from this code is listed in appendix D. Although the area gradients do not reflect the wall grid GPSGs exactly, they do indicate that the volume violates the requirements, as evidenced by the average values of those cell-to-cell scalings greater than the 1.5 maximum. Considering the volume has 583,680 cells, the number of cells in question is significantly less than the overall volume grid. From the surface grid quality assessment in section 5.2, the I- and J-direction GPSG was locally already in violation of the requirements. As stated in the surface quality section, these violations would propagate into the volume, which accounts for the violations here. Although there are local violations of some requirements, all requirements are met globally, and the local violations are insignificant with respect to the entire volume.

I=109
J=93

3DMAGGS
solution

VGM
smoothing
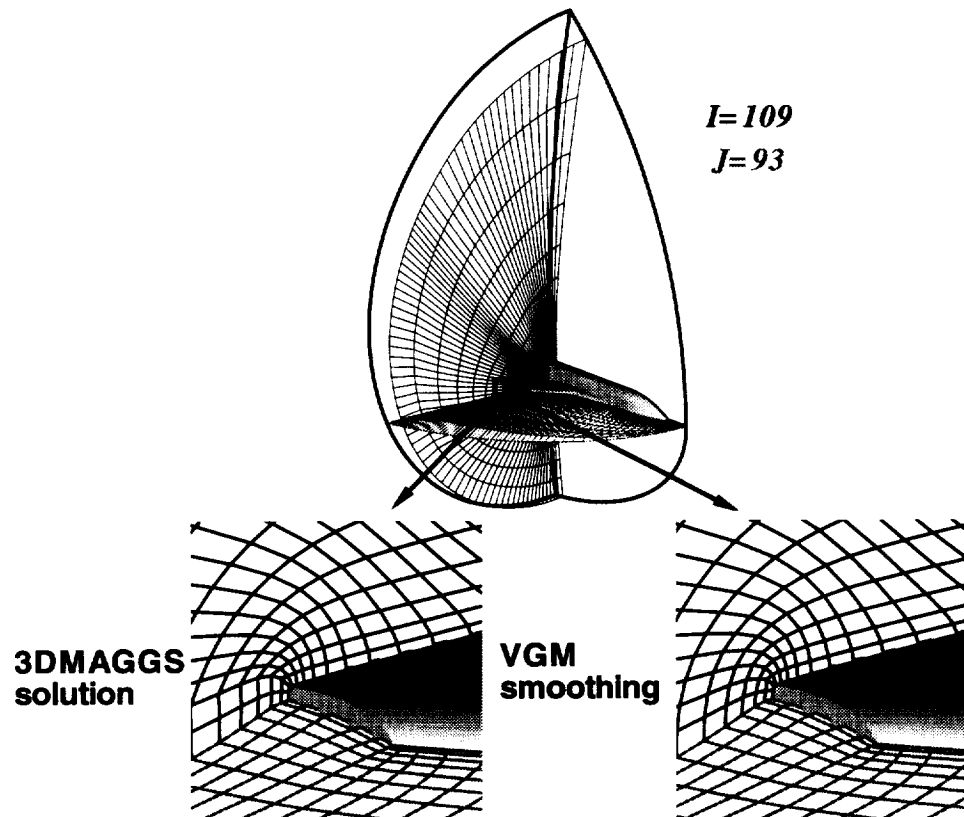
Figure 5.6: Inviscid grid with improved wingtip grid line quality.

Chapter 6

Viscous Grid Parametrics

Generation of the design parametrics for the X34 program is not done as an initial volume grid size based on the equations in section 1.3.1. Rather, these volume grids are constructed with the viscous grid delivered to CFD computations as the starting point or an adapted solution-converged volume grid from CFD simulations. The design parametric is then inserted by a localized insertion process.[16] The process entails the following steps:

(1) Isolate a portion of the volume grid that encompasses the geometrical feature to be modified.

(2) Redistribute the interfaces of the isolated grid to the original volume grid to reduce the clustering in the K-direction.

(3) Construct a new wall surface geometry which reflects the desired parametric change using a CAD tool.

(4) Replace the original surface in the isolated grid with the new surface.

(5) Modify other faces affected by the change in geometry and interface surface grids.

(6) Apply an elliptic solver to the parametric zone.

(7) Redistribute the grid points along the K-lines of the parametric zone to approximate the distribution in the original volume grid.

(8) Insert the parametric zone volume grid back into the original volume grid.

(9) Blend the grid point distributions of the new grid to the original grid at their interfaces, along the K-lines.

Based on the CFD run matrix for the viscous computations in table 2.2, three parametrics are to be generated: two for the 23° angle of attack, which represents a change in elevon and bodyflap orientation, and one for the 15.22° angle of attack. The elevon parametrics are generated differently than the bodyflap deflections. The following sections are divided into two main parts addressing the elevon and bodyflap parametrics. In addition, assumptions or requirements used in the development of these parametric volume grids are identified in the respective section.

6.1 Elevon Parametric

The following sections describe the methods used to generate the elevon parametric for the 23° angle of attack. The elevon parametric is generated by using the original viscous grid delivered for CFD simulations as the starting point. The process to generate the viscous grid used for this elevon is identical to the 15.22° angle of attack. Only the first elevon will be explained in detail.

6.1.1 Parametric Design Change Surface Quality

The parametric design geometry to be inserted into the baseline volume grid was assessed with the quality measures set forth in chapter 3. This analysis is not shown pictorially, but the wall grid was generated identically to the full-body wall grid with the ICEM/CFD software implemented in the GEOLAB. Because ICEM/CFD uses the same procedure, the elevon has nearly identical quality measures to that of the full body. For the region modified for this elevon deflection change, the grid is relatively good quality, except for the spacing gradients in the cross-direction. Again, these are few in number (55 cells compared with nearly 26,000 cells in the parametric design change), but these point spacing problems will propagate onto the volume interior. Otherwise, the surface grid is of high quality as indicated by the nearly orthogonal average measure and the nearly equally spaced GPSG average measure.

6.1.2 Domain Identification

For the viscous volume grid, the design parametric change encompasses the vehicle from the hinge line of the elevon to the end of the wing wake core and from the leeside wing-fuselage root to the windside root. But to generate this grid, steps 1 and 9 require the region to be sufficiently large to offer a blending region from the undisturbed original volume grid to the swapped-in parametric design change. An additional requirement that was introduced prior to the parametric change was the necessity to retain the forebody grid forward of the hinge line. To ensure the forebody region was undisturbed, the region chosen for the changed grid was from the hinge line to the aft body in the streamwise direction and from the leeside outboard corner of the fuselage to the windside symmetry plane. This region, shown in figure 6.1, encompasses the actual geometrical change which is shaded darker than the entire parametric design change region. This region size was chosen as it offers sizable blending regions in the cross directions while still maintaining the forebody volume grid.

6.1.3 Parametric Domain Preparation

The region identified for the parametric design change is initially extracted from the viscous volume grid. To use an elliptic solver for the volume generation, the grid point distributions in the K-direction must be expanded at the interfaces, or the elliptic equations become too stiff to solve[7] efficiently. The grid is expanded iteratively using the VGM code on those faces with the K-index varying as shown in figure 6.2.

The expanded grid point distributions on the interfaces serve as defining domain faces for the volume generation. These faces include the leeside interface, the windside symmetry
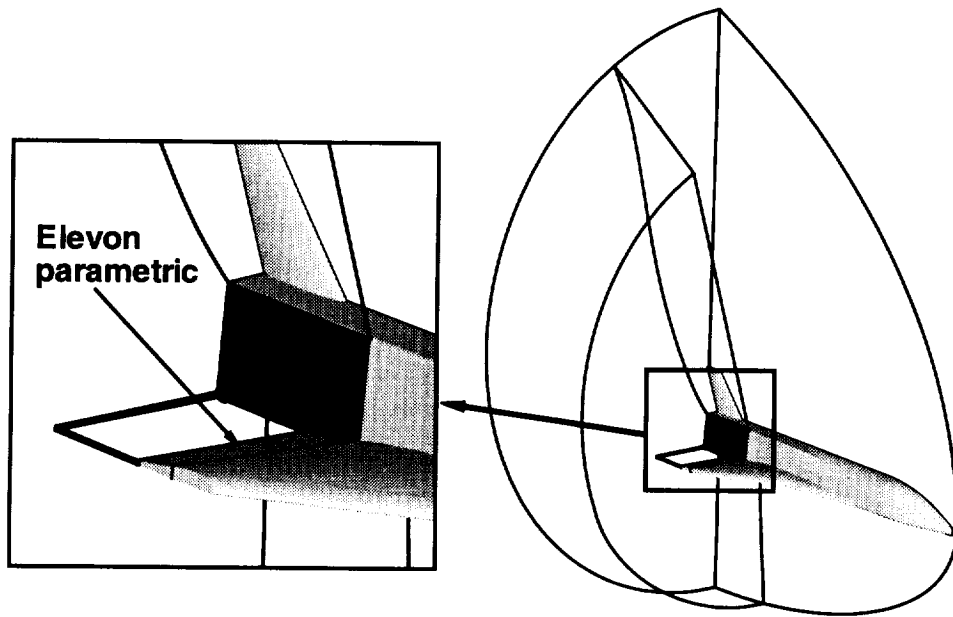
Figure 6.1: Viscous grid design parametric elevon region to be modified.
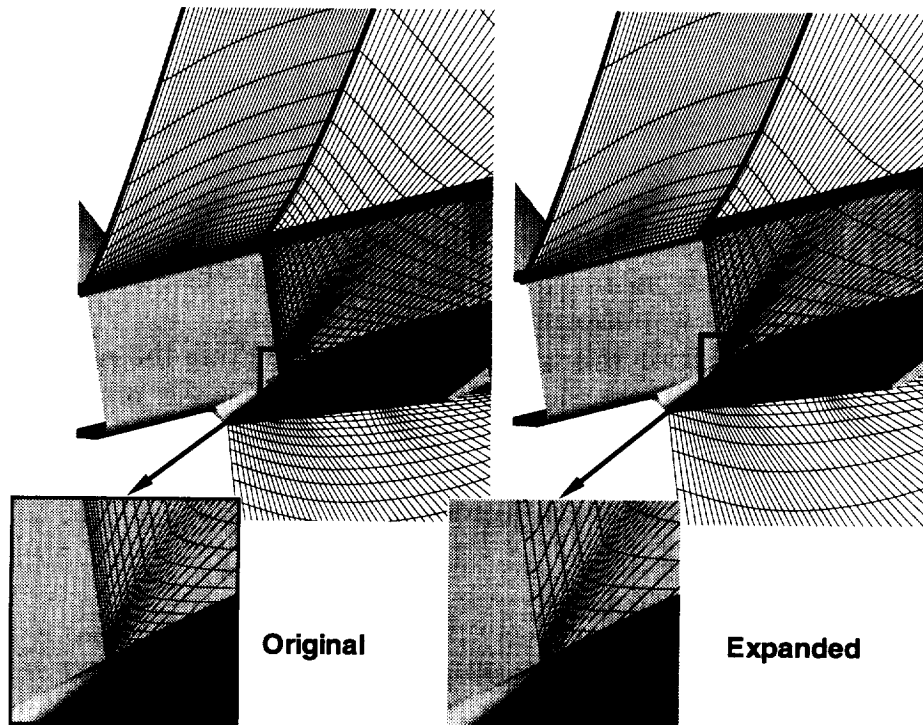
Figure 6.2: Viscous grid elevon design parametric interface K-line clustering expansions.

plane, the inflow interface to the forebody, the exit plane and the outer boundary domain. The design changed is simply accomplished by inserting the grid received from GEOLAB for

the elevon deflection. No more faces need to be generated as these form the full compliment of six block-faces necessary for the zone to be generated.

6.1.4 Volume Generation

The parametric design change volume grid is generated identically to the viscous grid, where an inviscid grid is first created and then converted to the viscous grid. The inviscid grid, or viscous basis grid, is generated with the **3DMAGGS** code with source term controls listed in table 6.1:

Face description	Boundary condition	Decay rate
Inflow interface	Orthogonality	0.40
Exit	Orthogonality	0.40
Leeside interface	Orthogonality	0.30
Windside symmetry	Orthogonality	0.30
Wall	Orthogonality	0.35
Outer boundary	Orthogonality	0.40

Table 6.1: Parametric volume grid generation Poisson solver boundary conditions.

The **GRIDGEN** data was converted to the **3DMAGGS** data with the **PREMAGGS** code and the **3DMAGGS** code was executed for 500 iterations using 60 minutes of SGI-R10k CPU time to get the initial basis grid for creating the inviscid volume grid. This number of iterations produced a solution-converged grid. However, there were minor problems with grid line skewness in the wingtip region. **VGM** was subsequently used to improve these regions and generate the final deliverable volume grid. These manipulations resulted in a volume grid illustrated with representative planes shown in figure 6.3.

The deliverable volume grid was generated by redistributing the parametric zonal grid in the K-direction, inserting it into the originally generated viscous volume grid, and blending the interfaces at the inflow and leeside into the new parametric domain. All these manipulations were performed with the **VGM** code, which resulted in the volume grid with representative I- and J-planes shown in figure 6.4.

6.1.5 Volume Grid Quality

The quality of the delivered volume grid, assessed with the measures of table 3.2, was determined with the **3DVOLCHK** code. The output from this code is listed in appendix E. Although the GPSGs in the volume grid appears to violate the requirements, based on the volume of over 1,000,000 new cells, the number of cells in question is significantly less than the overall volume grid. From the surface grid quality assessment in section 6.1.1, the J-direction GPSG was locally already in violation of the requirements. As explained earlier, these violations propagated into the volume. Although there are local violations of some requirements, all requirements are met globally, and the local violations are insignificant
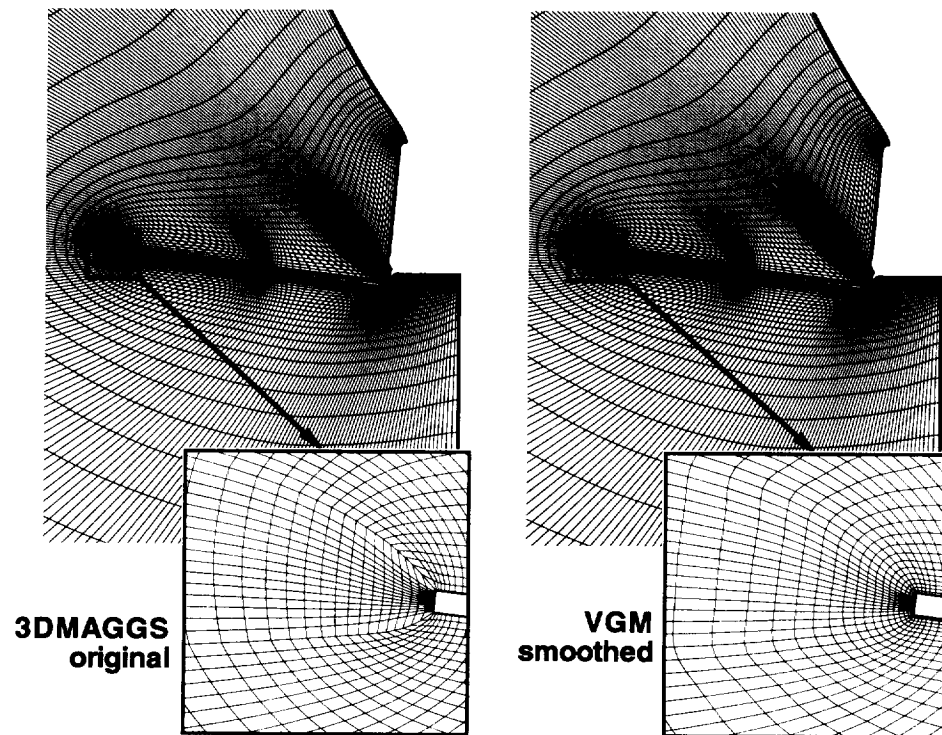
Figure 6.3: Elevon parametric design change volume grid with improved wingtip grid line quality.

with respect to the entire volume. As indicated in section 6.1, two viscous elevon grid parametrics were generated. The quality of the second grid was nearly identical because the process of generation was identical.
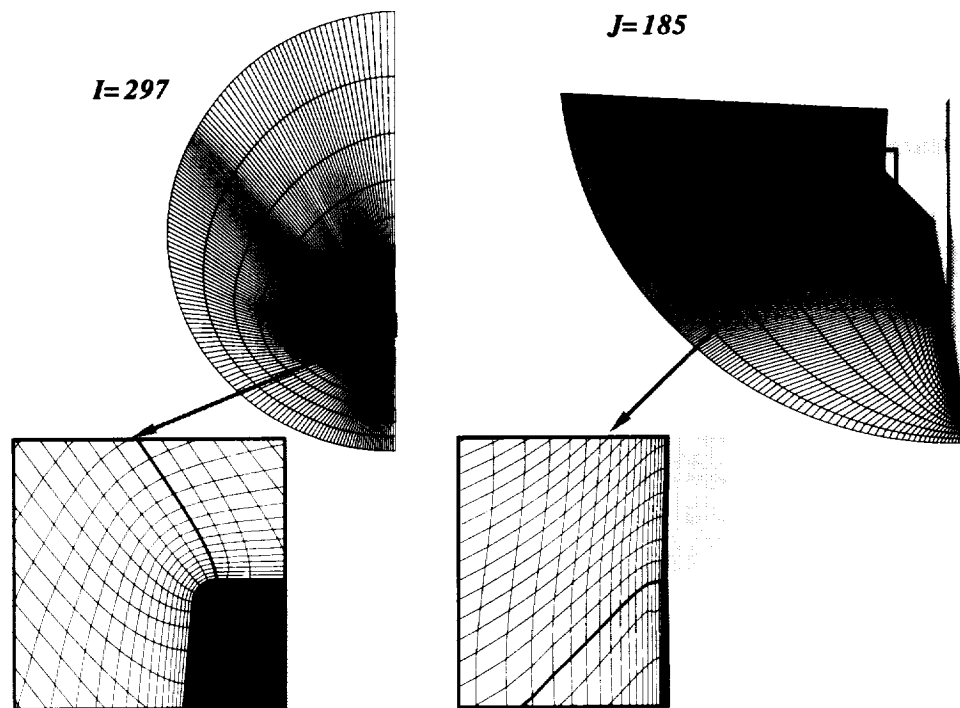
Figure 6.4: Elevon parametric design change volume grid inserted into the original viscous grid.

6.2 Bodyflap Parametric

The following sections describe the methods used to generate the bodyflap parametric for the 23° and 15.22° angles of attack. The bodyflap parametrics are generated from the adapted solution-converged grid from the CFD simulations. Each case then represents a different deliverable. For reasons of document length, only the 0° bodyflap deflection for the 23° angle of attack will be discussed. Each of the remaining volume grids delivered were generated in the same way. The quality assessment of the surface grids that comprise the bodyflap are pictorially illustrated in appendix F.

The bodyflap surface grid is divided into seven separate subfaces to accommodate the LAURA code requirements on application of boundary conditions. The requirements specifically limit the number of boundary conditions to one on a single face. An added complexity is the desire to reduce the number of points in the computation, which is obtained by reducing the grid size on the subface connecting the forebody to the main portion of the bodyflap on the windside as shown in figure 6.5.
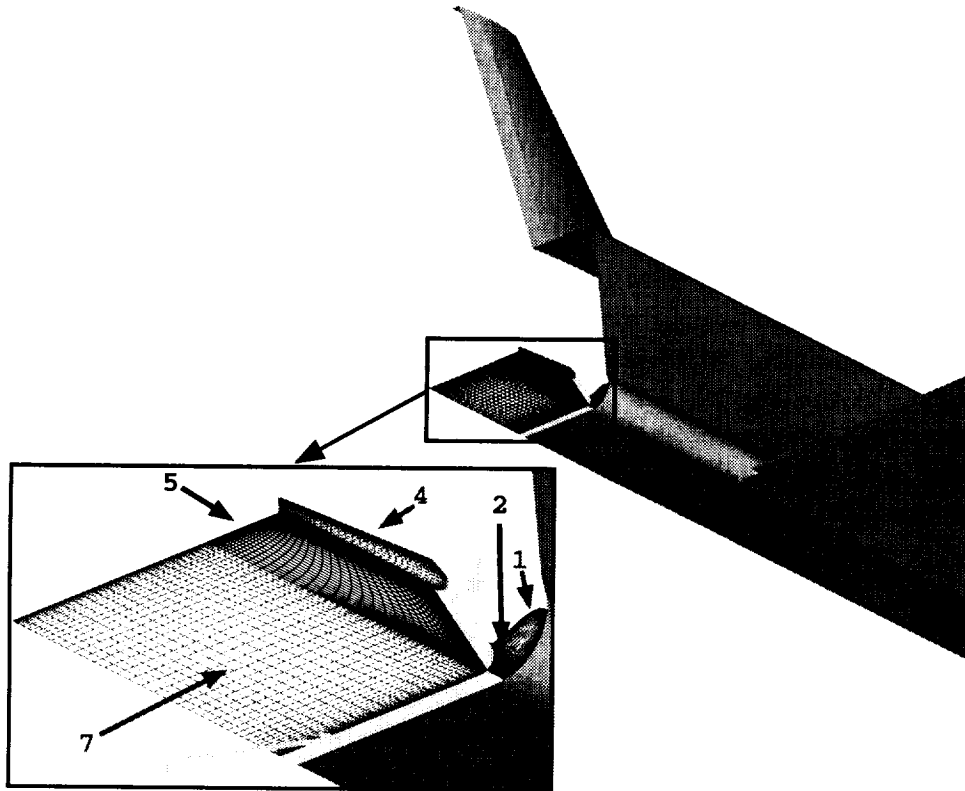
Figure 6.5: Viscous grid design parametric bodyflap decomposition.

Because the bodyflap is discretized so that the notched region, shown in figure 2.6 and the limits on grid dimensions are accommodated through subface dimensionality, the volume grid for this computation becomes extremely complex. The number of blocks to be used is 17, but the grid will be delivered as 4 separate blocks discretized as shown in figure 2.5. For

naming convention, the generated blocks are as follows:

(1) `WIND-WING`: region below the wing wake core abutting the main portion on the bodyflap, interfacing to the notched region, and containing the section of bodyflap aft of the notch

(2) `BODYFLAP`: region below the bodyflap and inboard of the notch region

(3) `WING-WAKE-CORE`: region aft of the forebody wake core and connected to the bodyflap side and the notch region

(4) `NOTCH`: region from the base of the vehicle to the leading edge of the bodyflap and to the remaining `BODYFLAP` and `WING-WAKE-CORE` blocks.

6.2.1 Parametric Design Change Surface Quality

The parametric design geometry to be appended to the baseline volume grid was assessed with the quality measures set forth in chapter 3 and are pictorially shown in appendix F. This grid is in poor condition because it represents a compromise of the topology and all requirements used in the construction. These poor wall grid qualities will propagate onto the volume interior.

6.2.2 Domain Identification and Construction

The viscous volume grid for the bodyflap design parametric is constructed by utilizing the provided wall grids, and extruding the forebody volume grid to construct the remaining surfaces. The extrusion, which is performed with `VGM` is done with the last 30 I-planes to construct projection vectors at select locations along the cross-section. These projected curves, which define the outer boundaries and the `WING-WAKE-CORE` extrusion, are connected to the wall grid and the `WIND-WING` and `BODYFLAP` blocks with straight line point-to-point connections. Generation of the domain for each block is explained in the following three sections for the `WIND-WING` `BODYFLAP` and `WING-WAKE-CORE`The `NOTCH` block was provided by GEOLAB and did not need to be defined or generated but only manipulated as will be explained later.

6.2.2.1 `WIND-WING` Domain Construction

Construction of the `WIND-WING` block is done by extruding cross-sectional points of J=207, 223, and 318 in the aft direction, as shown in figure 6.6. These extruded lines are subsequently connected by lines created by interpolating the amount of coordinate movement in each direction between the extruded lines. The result is an outer boundary definition for the `WIND-WING` block. The interface to the `WING-WAKE-CORE` is constructed by extruding identical J-locations at the interface between the main forebody block and the wing wake block. The exit plane edges at the wingtip are created as another extrusion of the J=207 and 318 planes. The results of these extrusions are shown in figure 6.6, where the dashed, arrow-headed lines indicate the extrusion lines. The dimensions of this block are 81, 121, 65 for the I-, J-, and K-directions, respectively.
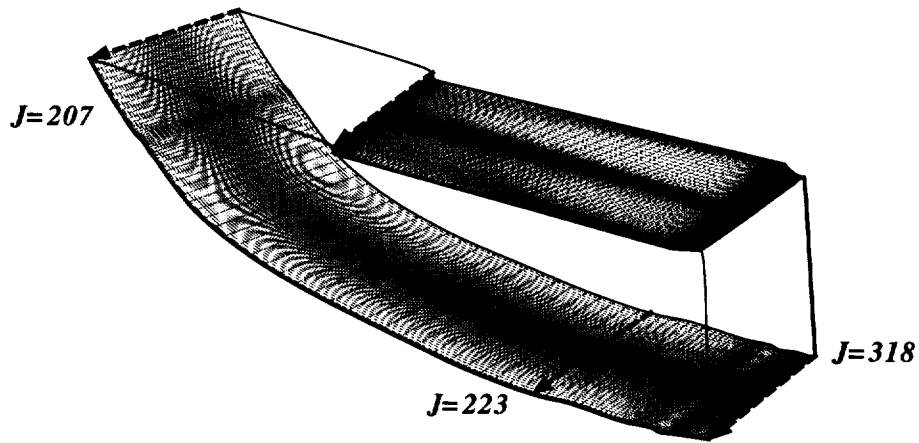
Figure 6.6: WIND-WING extruded boundaries and generated outer domain.

6.2.2.2 BODYFLAP Domain Construction

Construction of the BODYFLAP block is performed similarly to the WIND-WING block by extruding the cross-sectional point of J=369 and the wall point at the windside symmetry-exit planes intersection. The connecting edge with the WIND-WING block is already constructed, so only the windside symmetry plane edges need to be generated. These are generated with straight line connections from the wall grid to the generated projected grid lines. The results of these extrusions are shown in figure 6.7. The dimensions of this block are 65, 33, 65 for the I-, J-, and K-directions, respectively. Note that the I-direction dimension is smaller than the WIND-WING block because this is where the grid dimensionality could be reduced without significant impact on the CFD simulations.

6.2.2.3 WING-WAKE-CORE Domain Construction

Construction of the WING-WAKE-CORE edges is already complete with the generation of the WIND-WING block and the NOTCH block delivered by GEOLAB. To construct the domain, the edges are extracted on the basis of respective interfaces to the various other blocks, as shown in figure 6.8. The dimensions of this block are 81, 17, and 121 for the I-, J-, and K-directions, respectively.

6.2.3 Parametric Domain Preparation

The surface grids required to be generated for each of the bodyflap volume grids are initially generated in the VGM code with 2DTFI. The construct of the edges within the VGM framework enables this generation to be done in a simple and efficient step. The cross-directional interfaces between the three generated blocks are subsequently smoothed with GRIDGEN2D to obtain slope continuity across the block boundaries. Finally, VGM is used to improve grid quality in convex regions and at the interfaces where GRIDGEN2D was unable to do so. Details of the methods used to generate these grids are explained in the following sections.

63
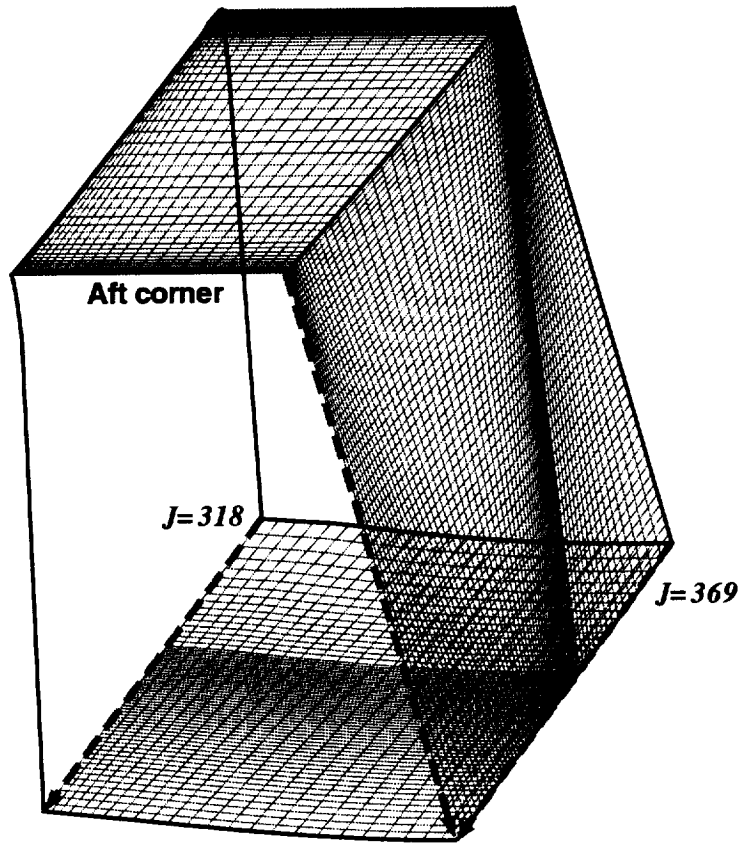
Figure 6.7: BODYFLAP extruded boundaries and generated outer domain.
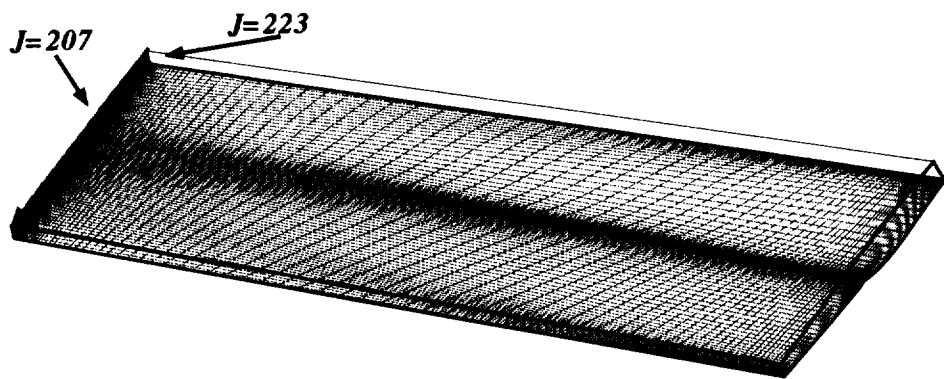
Figure 6.8: WING-WAKE-CORE extruded boundaries and generated outer domain.

6.2.3.1 WIND-WING Domain Preparation

The only face that required the use of the GRIDGEN2D software in the generation of the domain faces for the WIND-WING block was the exit plane. At the exit plane, the interface with the BODYFLAP block must be slope continuous with the WIND-WING block and nearly cell-to-cell continuous. The slope continuity is produced by extracting the exit faces of both blocks, solving them together while holding the interface and the BODYFLAP grid fixed, and inserting the new grids back into there respective block locations. The exit surface grid quality is then improved with the VGM code for the pseudo wingtip region as shown in figure 6.9.
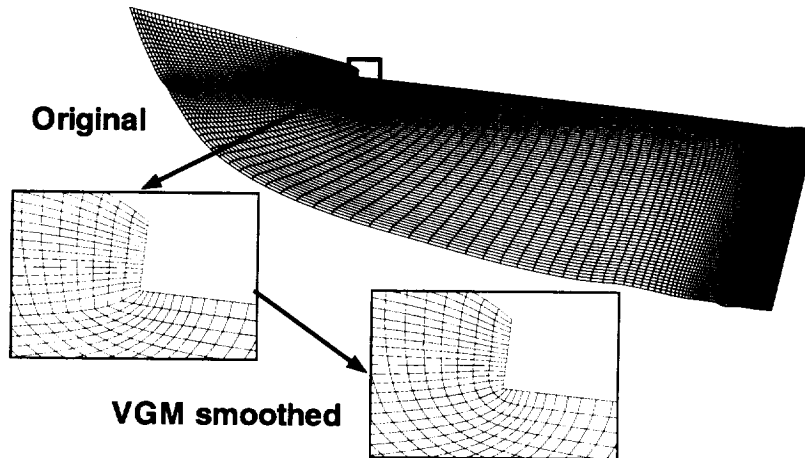
Figure 6.9: WIND-WING exit plane generation across multiple blocks.

6.2.3.2 BODYFLAP Domain Preparation

All surface grids in the BODYFLAP block were initially generated within VGMThe grid exhibited good quality, except at the windside symmetry plane where the grid lines were not completely orthogonal to the wall. The orthogonal condition was generated with the GRIDGEN2D code with interpolated angle boundary conditions at all other edges. The result is a set of domain surfaces that are of high quality while adhering to the geometry and all requirements, as shown in figure 6.10.

6.2.3.3 WING-WAKE-CORE Domain Preparation

Generation of the surface grids that define the block domain of the WING-WAKE-CORE volume were generated entirely from VGM 2DTFI and extractions of delivered data from GE-OLAB. The elliptic solver GRIDGEN2D was not needed for any of these faces. Representative surface grids of this block are shown in volume figures.
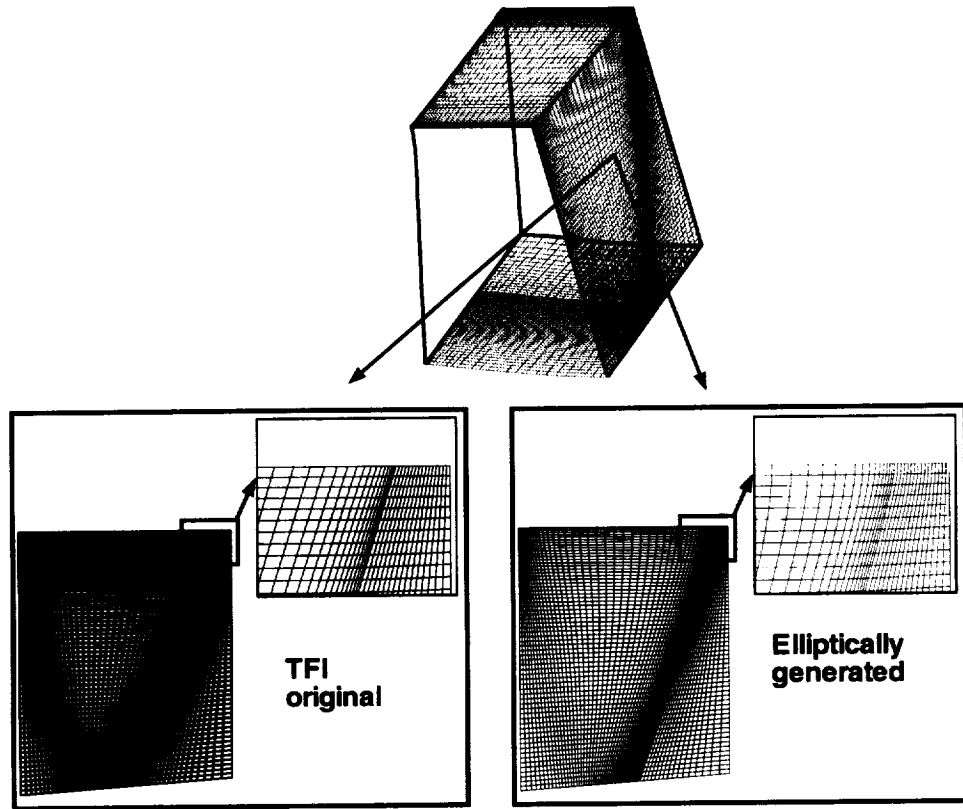
Figure 6.10: **BODYFLAP** symmetry plane generation-grid improvement.

6.2.4 Volume Generation

The bodyflap parametric design change volume grids are initially generated with 3DTFI and subsequently smoothed to obtain good orthogonality at the wall grids while maintaining some slope continuity at the interfaces. For the set of blocks at hand, only the WIND-WING and WING-WAKE-CORE blocks required elliptic volume generation because of the pseudo wingtip region and the bodyflap side, respectively. These blocks were generated with the 3DMAGGS code with the source term controls listed in table 6.2:

Face description	Boundary condition	Decay rate
Inflow interface	Orthogonality	0.40
Exit	Orthogonality	0.40
Leeside interface	Orthogonality	0.30
Windside symmetry	Orthogonality	0.30
Wall	Orthogonality	0.35
Outer boundary & Wingtip	Orthogonality	0.40

Table 6.2: Poisson solver boundary conditions for the bodyflap blocks.

66

The 3DMAGGS code was executed for 200 iterations to obtain a solution-converged grid for each block. The quality of the WIND-WING elliptically generated grid was subsequently improved by regenerating the wingtip region with 3DTFI and the interface region to the BODYFLAP block with 3DTFI. The resulting grid is shown in figure 6.11 with the representative I-plane and accompanying bodyflap blocks.
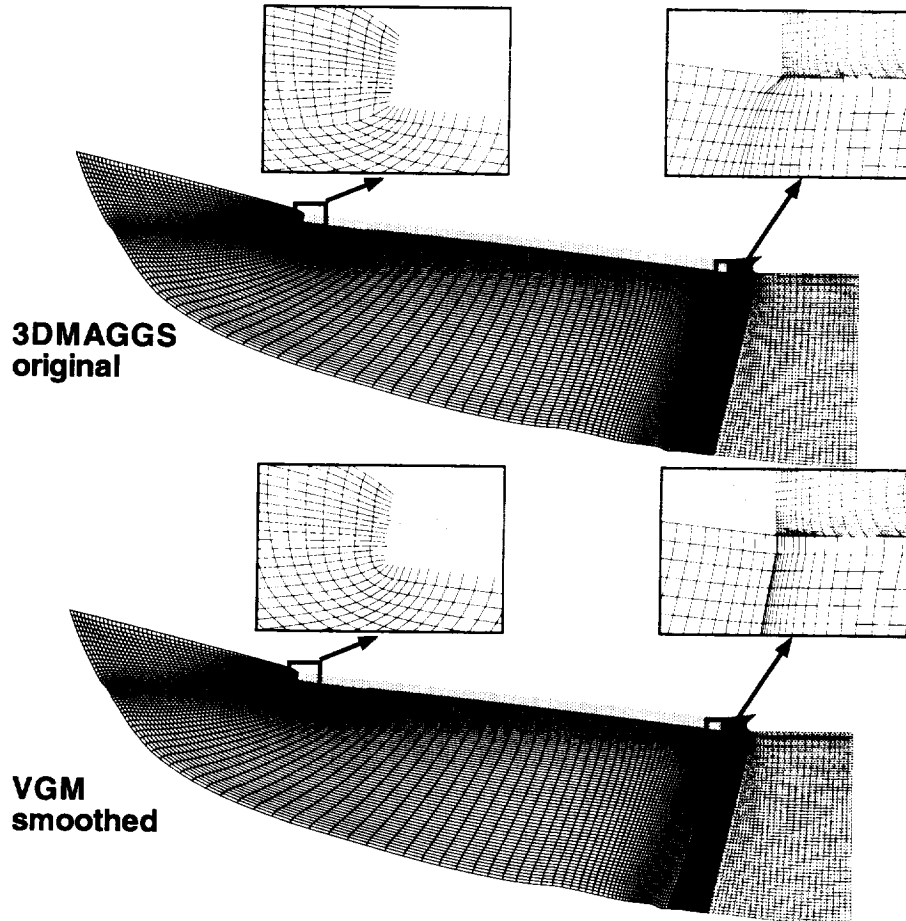
Figure 6.11: Bodyflap-wake parametric design change volume grid with improved wingtip grid line quality.

To obtain slope continuity between the upstream forebody and downstream blocks, with respect to the interface to the base (i.e., wake) region, the K-line distribution from the upstream block was copied into the downstream block. The final delivered grid was constructed by grouping the various wake blocks in conjunction with feeder blocks from the forebody region. The feeder blocks are single-cell slabs of the exit plane of the forebody blocks that connect to the downstream blocks and provide the initial boundary conditions for the CFD simulations. The blocks and the slope continuity are shown in figure 6.12.
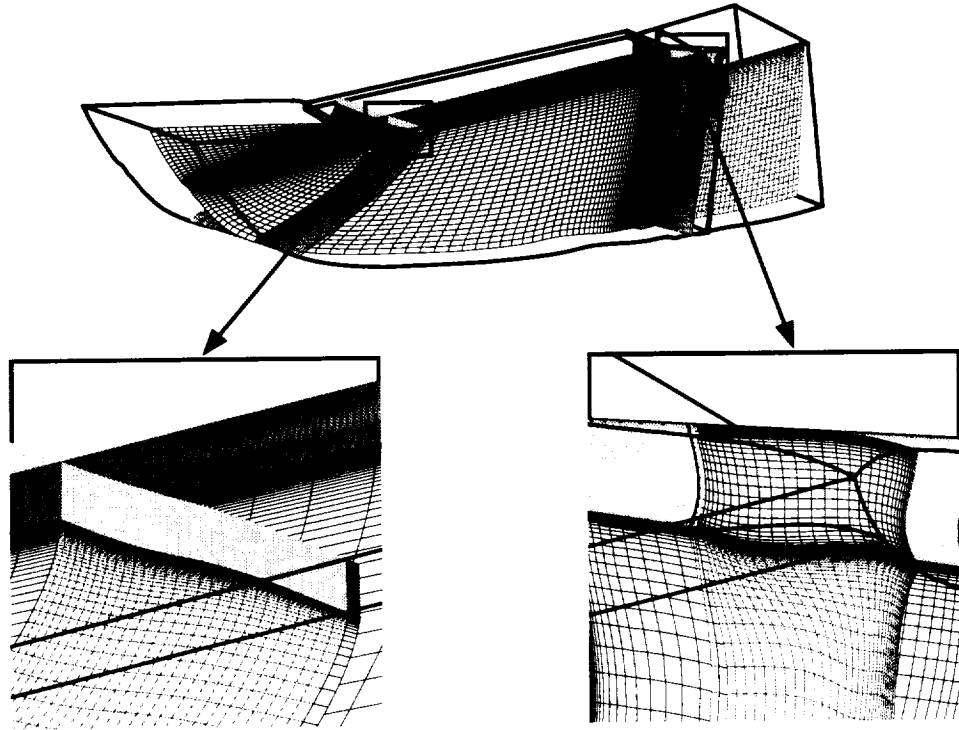
Figure 6.12: Delivered bodyflap-wake parametric design change volume grid.

6.2.5 Volume Grid Quality

The quality of the delivered volume grid, assessed with the measures of table 3.2, was determined with the 3DVOLCHK code. The output from this code is listed in appendix G. Although the GPSGs in the volume grids appear to violate the requirements, this set of blocks represents a compromise of all the requirements used in the development. From the surface grid quality assessment in section 6.2.1, the J-direction GPSG was locally already in violation of the requirements. As indicated earlier, these violations propagated into the volume, and accounts for the violations here. Although there are local violations of some requirements, all requirements are met globally, and the local violations are insignificant with respect to the entire volume.

68

Chapter 7

Inviscid Grid Parametrics

Generation of the inviscid design parametrics for the X34 program is done with an inviscid grid after a bow shock adapted solution-converged volume grid from CFD simulations is obtained. The design parametric is then inserted using a localized insertion process.[16] The process entails similar steps as the viscous elevon parametrics by using the steps in section 6 to insert the vehicle design parametric and then using the steps in section 5.1 to reconstruct a similar grid of the inviscid wall grid design parametric.

Based on the CFD run matrix for the inviscid computations in table 2.1, three parametrics are generated: case numbers 2, 3 and 6. The following sections address the generation of the elevon for case number 2, as the process is identical for subsequent design parametrics.

7.1 Parametric Design Change Surface Quality

The parametric design geometry to be inserted into the solution-converged volume grid was assessed with the quality measures set forth in chapter 3. Because the methods used to develop the wall grid of the elevon design parametrics were identical to the original undeflected elevon case, the wall grids are nearly identical in grid quality. For the region modified for this elevon deflection change, the grid is relatively good quality, except for the spacing gradients. Again, these gradients result from the compromises made in the development of the wall grid as indicated in section 5.1. Aside from the spacing gradient problems, the remaining measures fall in line with the requirements and are of high quality as indicated by the nearly orthogonal average measure and the nearly equally spaced GPSG average measure.

7.2 Domain Identification

For the inviscid volume grid, the design parametric change encompasses the vehicle from the hinge line of the elevon to the trailing edge of the wing and from the leeside wing-fuselage root to the windside root. But to generate this grid, steps 1 and 9 of the parametric volume grid generation require the region to be sufficiently large to offer a blending region from the undisturbed original volume grid to the swapped-in parametric design change. Similarly to the viscous elevon parametrics, an additional necessary requirement was introduced prior to

the parametric change to retain the forebody grid forward of the hinge line. To ensure the forebody region was undisturbed, the region chosen for the changed grid was from the hinge-line to the aft body in the streamwise direction and from the leeside outboard corner of the fuselage to the windside symmetry plane. This region, shown in figure 7.1, encompasses the actual geometrical change which is shaded darker than the entire parametric design change region. This region size was chosen as it offers large blending regions in the cross directions while still maintaining the forebody volume grid.
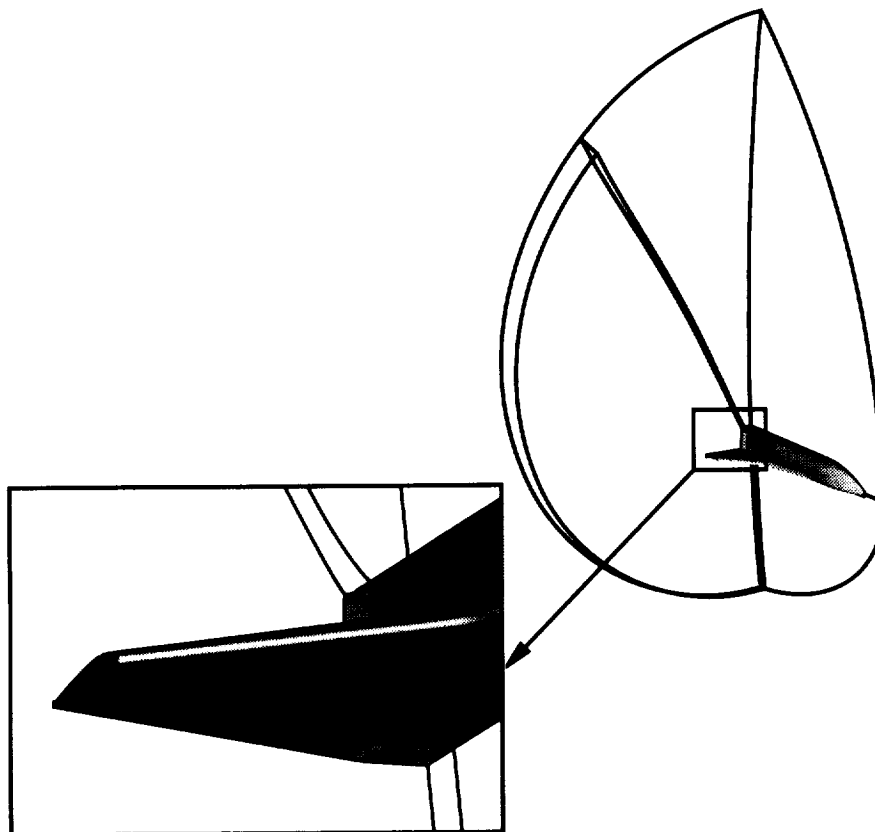
Figure 7.1: Inviscid grid design parametric elevon region to be modified.

7.3 Parametric Domain Preparation

The identified region for the parametric design change is initially extracted from the inviscid solution-converged and adapted volume grid. Although the computations were inviscid, the LAURA code ALiGN-SHocK procedure created near wall clusterings that were not conducive toward elliptic volume generation. To employ an elliptic solver for the volume generation, the grid point distributions in the K-direction must be expanded at the interfaces, or the elliptic equations become too stiff to solve[7] efficiently. The grid is expanded iteratively with the VGM code on those faces with the K-index varying as shown in figure 7.2.

The expanded grid point distributions on the interfaces serve as defining domain faces
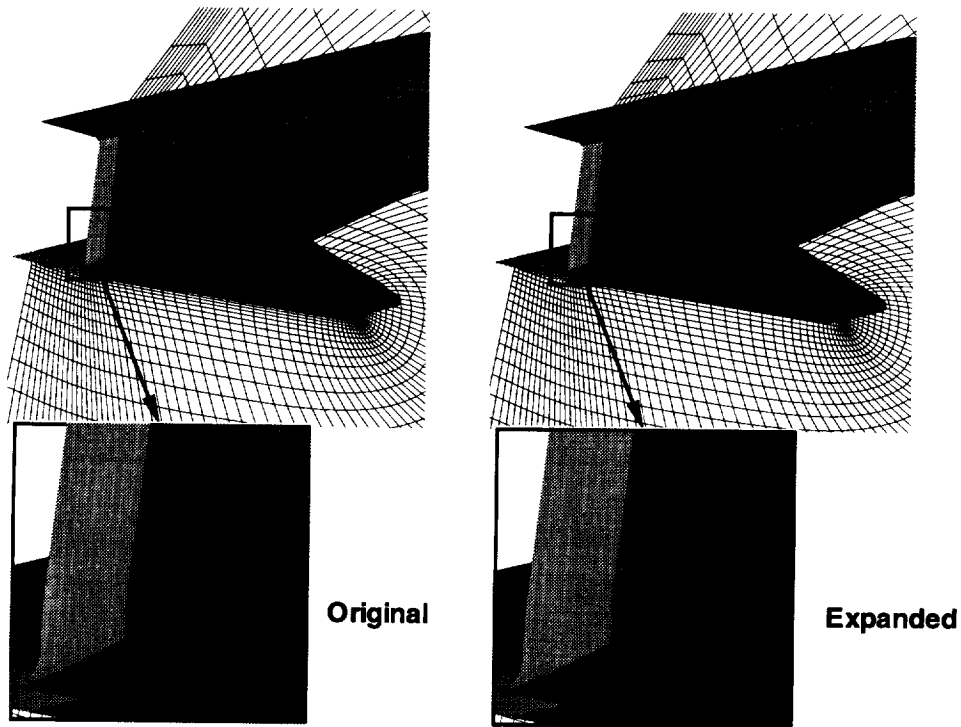
Figure 7.2: Inviscid grid elevon design parametric interface K-line clustering expansions.

for the volume generation. These faces include the leeside interface, the windside symmetry plane, the inflow interface to the forebody, the exit plane, and the outer boundary domain. The design change was accomplished by inserting, into the wall grid, the grid generated with the procedure outlined in section 7, into the wall grid. No more faces need to be generated as these form the full compliment of six block faces for the zone to be generated.

7.4 Volume Generation

The parametric design change volume grid is generated identically to the inviscid grid with 3DMAGGS coupled with the VGM code, which was necessary to improve grid quality were necessary as explained in section 5.5. The only change to the process was the weakening of the orthogonality source terms from the leeside interface to the original volume grid, from 0.35 to 0.45 in decay rate. The GRIDGEN data was converted to the 3DMAGGS data with the PREMAGGS code, and the 3DMAGGS code was executed for 500 iterations using 60 minutes of SGI-R10k CPU time to get the initial basis grid for creating the inviscid volume grid. Although the resultant grid was solution-converged, there were minor problems with grid line skewness in the wingtip region. The VGM code was subsequently used to improve these regions and generate the final deliverable volume grid. These manipulations resulted in a volume grid with representative planes shown in figure 7.3.

The deliverable volume grid was generated by copying the distributions from the original volume grid into the parametric zonal grid in the K-direction, inserting it into the originally generated viscous volume grid, and blending the interfaces at the inflow and leeside into the
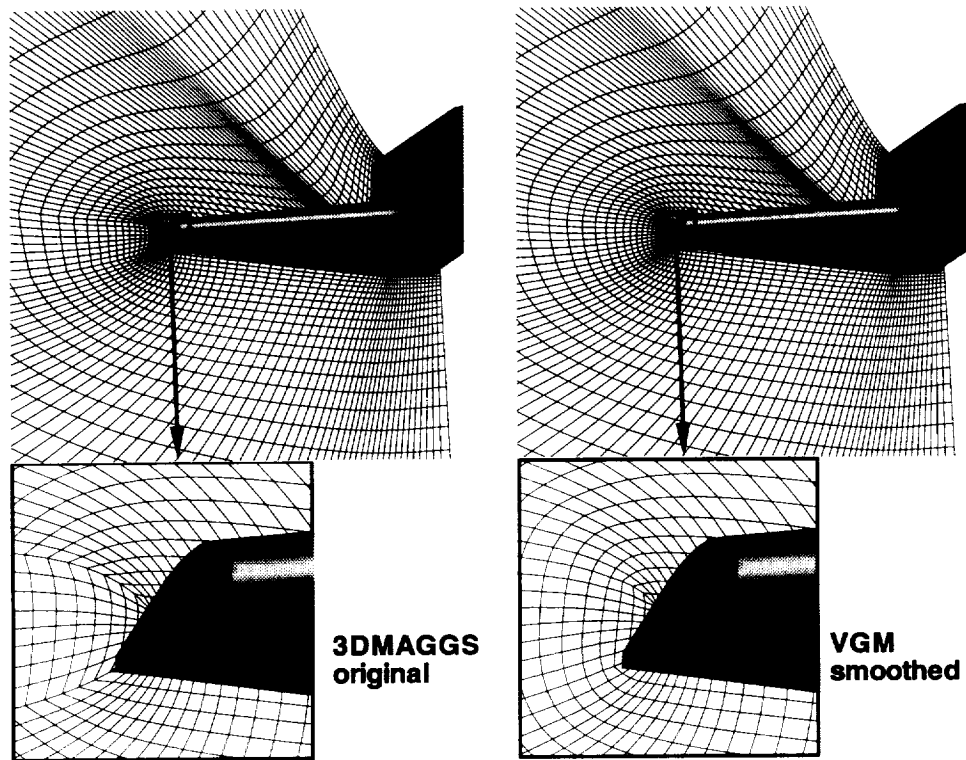
Figure 7.3: Elevon parametric design change volume grid with improved wingtip grid-line quality.

new parametric domain. All these manipulations were performed with the VGM code which resulted in the volume grid shown with representative I- and J-planes in figure 7.4.

7.5 Volume Grid Quality

The quality of the delivered volume grid, assessed using the measures of table 3.2, was determined with the 3DVOLCHK code. The output from this code is listed in appendix H. Although the GPSGs in the volume grid appear to violate the requirements, based on the volume of 1,650,688 new cells, the number of cells in question is significantly less than the overall volume grid. From the surface grid quality assessment in section 7.1, the J-direction GPSG was locally already in violation of the requirements. As indicated, these violations would propagate into the volume, which accounts for the violations here. Although there are local violations of some requirements, all requirements are met globally, and the local violations are insignificant with respect to the entire volume. As indicated in section 6.1, two viscous elevon grid parametrics were generated. The quality of the second grid was nearly identical because the process of generation was identical.

I=117   J=93
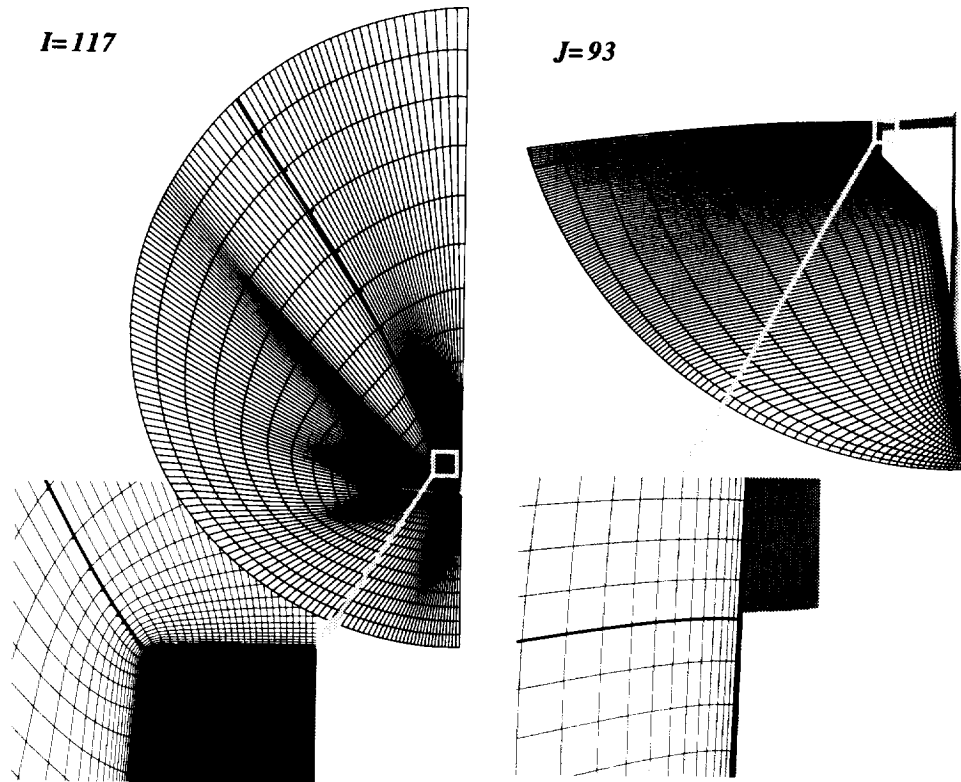
Figure 7.4: Elevon parametric design change volume grid inserted into the original inviscid grid.

Chapter 8

Topological Variations

Throughout the development of the parametric design changes for the X34 vehicle, the ease of boundary condition implementation with the LAURA code raised issues of proper or improper topologies. The topologies initially chosen and illustrated in section 2.2 generate the best volume grid, which is the most difficult process of grid generation. During the computations of the X34 CFD simulations, a requirement to evaluate the effect of turbulent boundary layers was invoked. This requirement resulted in the majority of all topological changes to the grids and are explained in this chapter. The first two sections of this chapter describe the topology changes to the main forebody grids and the bodyflap volume grids resulting from the requirement to model wall-bounded turbulence. A third section is added to explain improvements to grid resolution that were required to properly compute temperature profiles in the bodyflap region.

8.1 Elevon Topology Modification

The requirement to use turbulence modeling invokes requirement (16). Requirement (16) specifically states that to perform turbulence modeling, the boundary layer gradients are modeled in the K-direction only and, specifically, at the minimum index end (i.e., $K = 1$). To implement this new requirement on grid topology, the computational orientation of the wake blocks had to be modified, and resolution of the near-wall gradients had to be provided. As shown in figure 8.1, the topology of the wing wake for the elevon was changed from a J-direction emanating from the wall to a K-direction index, which required a reversal in the original K-direction to maintain a right-handed coordinate system.

The improved resolution was created by increasing the number of points at the wall in the new K-direction from 1 cell of the wake grid at the wall to 16 cells. These cells were redistributed at the wall so that the cell heights on the leeside and windside of the wing at the trailing edge were identically matched on the side of the fuselage. This redistribution produced the following problems:

- Crossflow gradients from 1 cell on the windside and leeside were mated to 16 cells on the side of the fuselage.

- The grid line curvature in the new J-direction was inadequate and of poor quality.
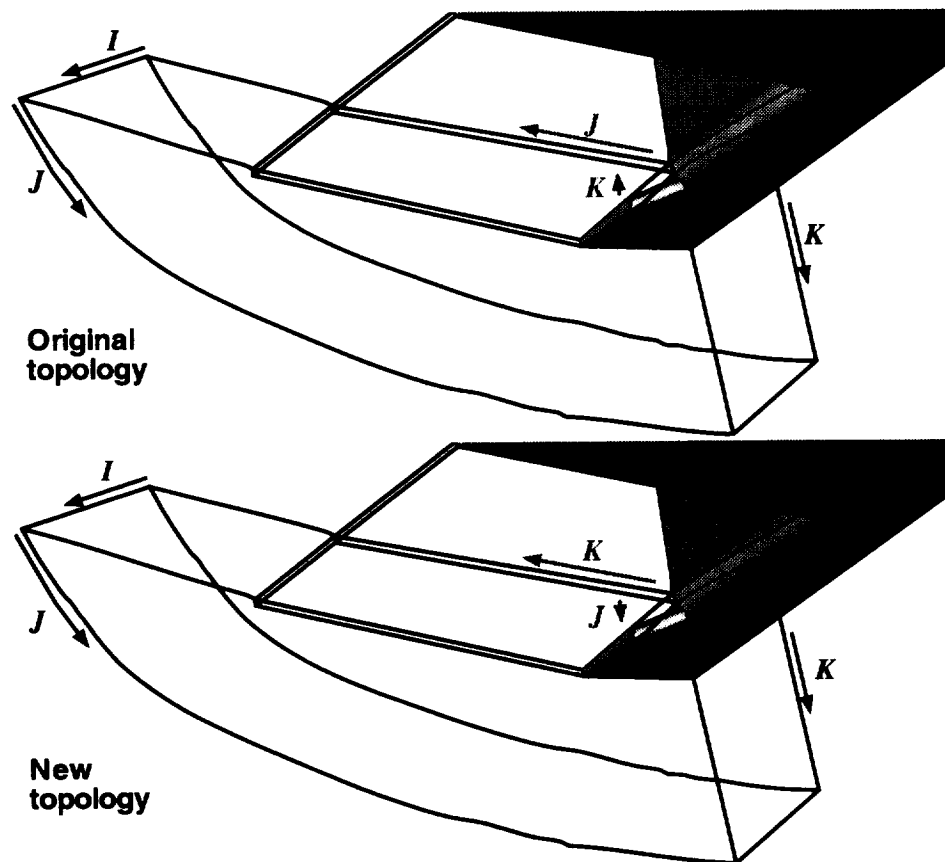
Figure 8.1: Original and new topolgies in the wing wake regions to enable wall-based turbulence modeling.

The LAURA code provides an ordered subset matching boundary condition for explicit purposes of improving grid resolution in regions such as the wing wake, but the resolution changes should only be done where flowfield gradients are insignificant. This caveat required several additional changes to be applied to the wake and forebody regions of the main volume grid to correct the previously mentioned problems. The first change increased the grid dimensionality in the new J-direction as well as the clustering in this direction to both ends so that the cells at the limits would approach squares in a cross-sectional view as shown in figure 8.2.

The clustering of the wake in the new J-direction was performed at the fuselage and blended to an equally spaced region at the pseudo wingtip. This provided the necessary resolution at the interface of the wake from the leeside to the windside at the fuselage, while offering an ordered subset connection at the wing-tip region. The second change redimensioned and stretched the single cells in the J-direction of the main block that connects to the new cells at the wake block and added mirrored cells on the fuselage to reduce the significant changes in GPSGs. The new topology, shown in figure 8.3, corrected all the problems of grid quality and enabled the implementation of requirement (16).
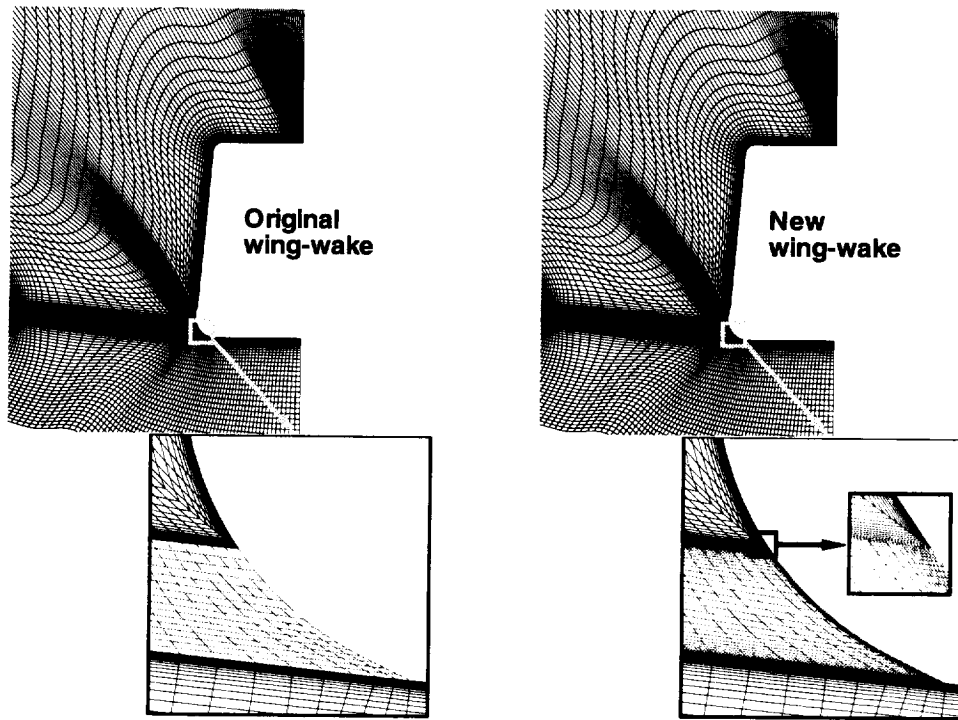
Figure 8.2: Improved grid resolution in the wing wake of the main volume grid.
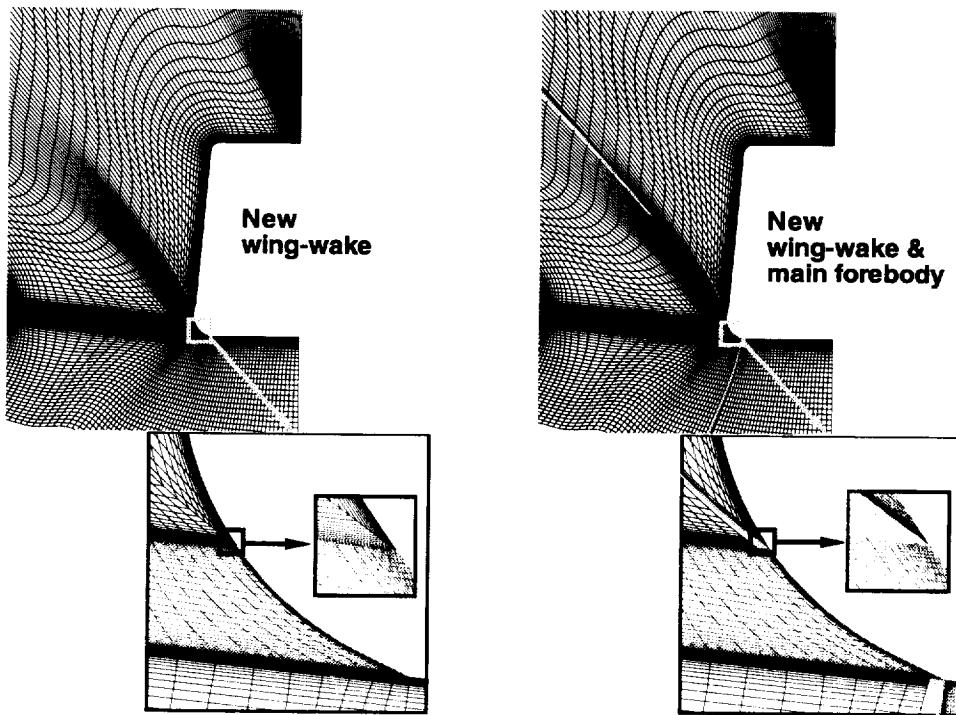
Figure 8.3: Improved grid resolution in the forebody of the main volume grid.

8.2 Bodyflap Topology Modification

Three topologies were used for the modeling of the bodyflap region. The original, as shown in figure 2.5, was first modified to provide consistency to the forebody blocks and then modified again to reduce the number of blocks in the decomposition required by the LAURA for the application of single-boundary conditions to a block face. Consistency of block-to-block matching between the forebody blocks and the bodyflap blocks was implemented by performing identical manipulations as those done in the wing wake and forebody blocks, on the connecting bodyflap blocks. The results of these manipulations are illustrated in figure 8.4
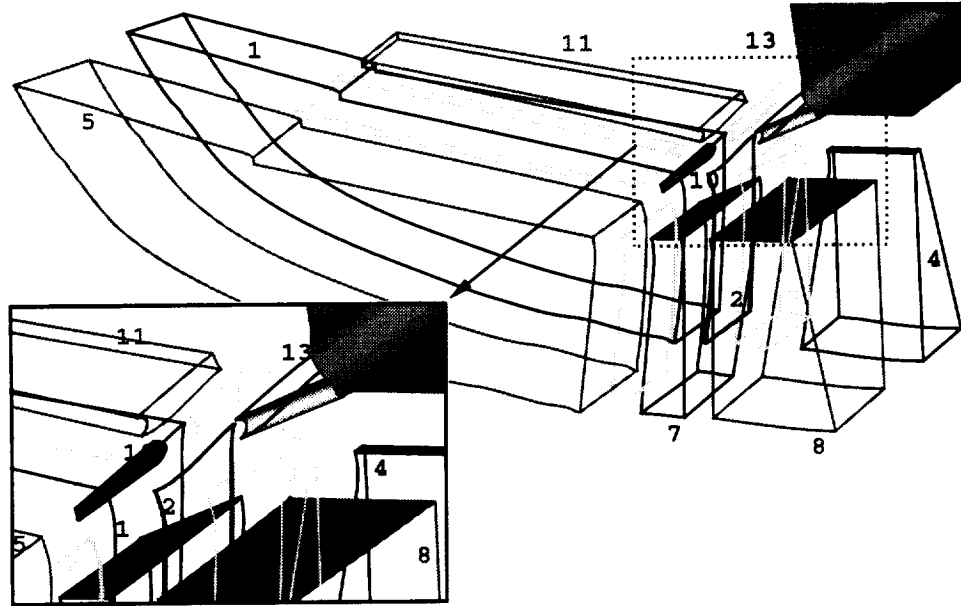
Figure 8.4: Consistency topological modifications from the forebody to the bodyflap blocks.

Notice that the decomposition of blocks for the new bodyflap wake regions has increased the number of blocks from 4 to 13, which is a result of the LAURA requirement of one boundary condition per block face. This decomposition was time consuming to implement in the LAURA code because of the number of blocks. The number of blocks in this decomposition was reduced by changing the topology a third time through increasing the grid density (i.e., densification) of the windside blocks to be identical to the upstream forebody blocks. This was augmented by the densification of the streamwise direction in the BODYFLAP block to be identical to the WIND-WING block, which enabled the combination of cross-direction blocks into a single block. The result of these manipulations is shown in figure 8.5, and the 13 blocks were condensed into a total of 6.
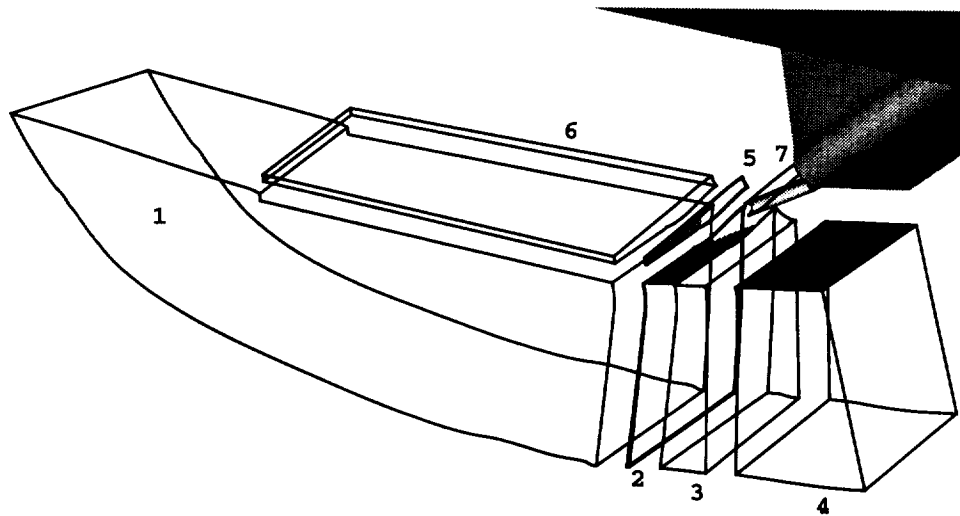
Figure 8.5: Increased density of grid points of the bodyflap blocks to reduce the number of blocks in the decomposition.

8.3 Modeling Improvements for the Bodyflap NOTCH

One of the most difficult regions to generate a grid, was the NOTCH block of the bodyflap. This region is small but poses difficulties when attempting to generate a grid that adheres to requirements (5), (11), (12), (14), (18), (19), and especially, (8) and (16). For the original topology, the cell sizes at the wall were not conducive to accurate predictions of heating at the wall. The accuracy was improved by increasing the dimensionality of the grid in the I- and K-directions by a factor of 8 in each direction for a total of 64 times the original grid dimension. This densification produced negative volumes because of the skewness of the NOTCH grid face at the base of the vehicle as shown in figure 8.6.
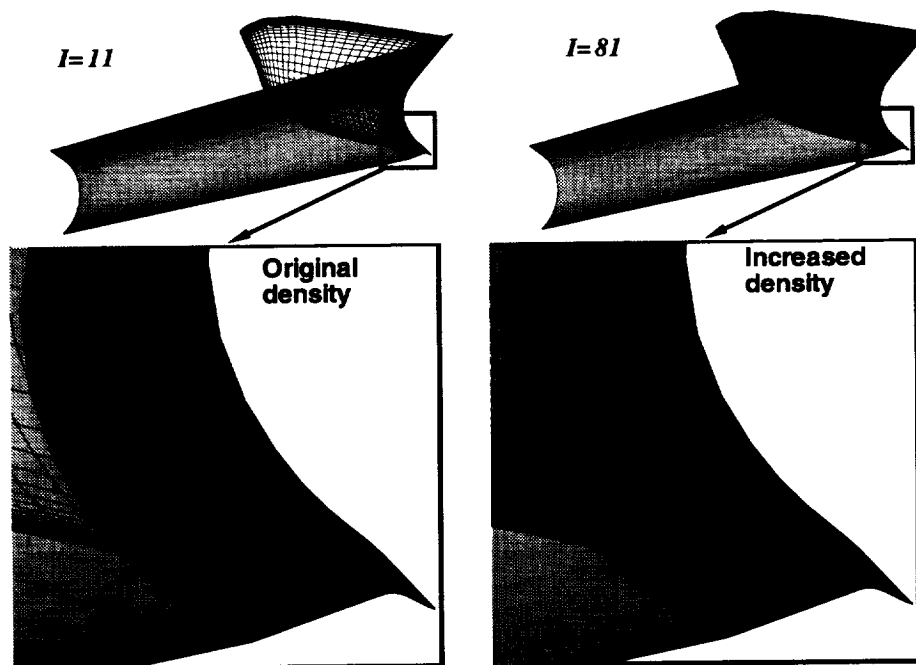
Figure 8.6: Densification of the NOTCH bodyflap block to improve thermal environment modeling.

The negative volumes were removed by regenerating the NOTCH grid face that comprises the base of the vehicle with the GRIDGEN2D elliptic solver, regenerating the grid with VGM's 3DTFI, and redoing the densification. With orthogonal boundary conditions used at all edges of the base face, the grid lines became less skewed and were easily manipulated to obtain the required wall cell spacing for improved thermodynamic modeling. The resulting grid is shown in figure 8.6.

Chapter 9

Summary

This report identifies the surface and volume grids generated for the X34 during the first half of 1997. Thirty-six volume grids were generated for this program in this time by the methods explained in previous chapters. The CFD run matrices identifying the volume grids generated were just the basis. Throughout the evolution process, the ALiGN-SHocK routine of LAURA was used to improve grid point usage efficiency by placing points to adequately model the boundary layer for the viscous computations and capture near wall flowfield gradients in inviscid computations, as well as capture the outer domain bow shock for each flow type. During these improvements, the production of negative volumes was prevalent, which resulted in the regeneration of certain regions to continue the flow solution process. Tables 9.1 and 9.2 highlight all the volume grids, as well as the time to generate each for the inviscid and viscous computations, respectively:

Case number	Generation time (wallclock hrs.)	Modification number	Description of solved problem
1,4,5,7	10.0	0	Initial volume grid based on viscous wall grid
1,4,5,7	0.3	1	Switch from single to multiple block format
1,4,5,7	17.0	2	Rebuilt wall grid from VGM redistributions
3	4.5	0	$-10°$ deflected elevon
3	8.0	1	$-10°$ deflected elevon w/rebuilt wall grid
6	4.1	0	$-10°$ deflected elevon
6	7.5	1	$-10°$ deflected elevon w/rebuilt wall grid
2	4.5	0	$+10°$ deflected elevon
2	4.1	1	$+10°$ deflected elevon w/rebuilt wall grid

Table 9.1: Actual inviscid volume grids generated and delivered for the X34 program.

Case number	Generation time (wallclock hrs.)	Modification number	Description of solved problem
1,3	10.3	0	Initial volume grid*
1	4.0	1	Improved wing wake topology*
1	0.7	2	Negative volume removal from improved wing wake topology*
1	4.0	3	Improved K-lines for thermal modeling*
1	1.6	4	Wake adaption of improved wing wake*
1	22.1	5	Solution-adapted grid w/bodyflap
1	0.2	6	Solution-adapted grid w/bodyflap (single-block files)
1	0.2	7	Solution-adapted grid w/bodyflap (feeder blocks omitted)
1	0.5	8	Solution-adapted grid w/bodyflap (improved block interfaces)
1	0.9	9	Solution-adapted grid w/bodyflap (intermediate topology change)
1	1.5	10	Solution-adapted grid w/bodyflap (final topology change)
1	0.8	11	Improved NOTCH dimensionality
1	0.8	12	Negative volume removal from improved NOTCH dimensionality
2	5.5	0	Solution-adapted grid w/deflected elevon
2	2.5	1	Solution-adapted grid w/deflected bodyflap
2	3.0	2	Solution-adapted grid w/deflected bodyflap (final topology change)
3	2.7	1	Improved wing wake topology*
3	0.5	2	Negative volume removal from improved wing wake topology*
3	3.0	3	Improved K-lines for thermal modeling*
3	8.5	4	Solution-adapted grid w/bodyflap
3	0.2	5	Solution-adapted grid w/bodyflap (feeder blocks omitted)
3	0.7	6	Solution-adapted grid w/bodyflap (intermediate topology)
3	1.5	7	Solution-adapted grid w/bodyflap (final topology)
3	0.7	8	Improved NOTCH dimensionality
3	0.8	9	Negative volume removal from improved NOTCH dimensionality
4	0.9	0	+10° deflected elevon*
4	0.4	1	+10° deflected elevon* (improved wing wake topology)

* Bodyflap not included in volume grid.

Table 9.2: Actual viscous volume grids generated and delivered for the X34 program.

Appendix A

Viscous Grid Surface Quality Measures

As identified in section 3.2, the quality measures for the inviscid surface grid used for all computations are shown in figures A.1 - A.9, representing the GPSGs in the ξ-, and η-directions, the aspect ratios of the cells, the cell areas, grid orthogonality, and the surface derivatives. These measures are included to aid in possible identification of solution errors and issues with the CFD simulations.
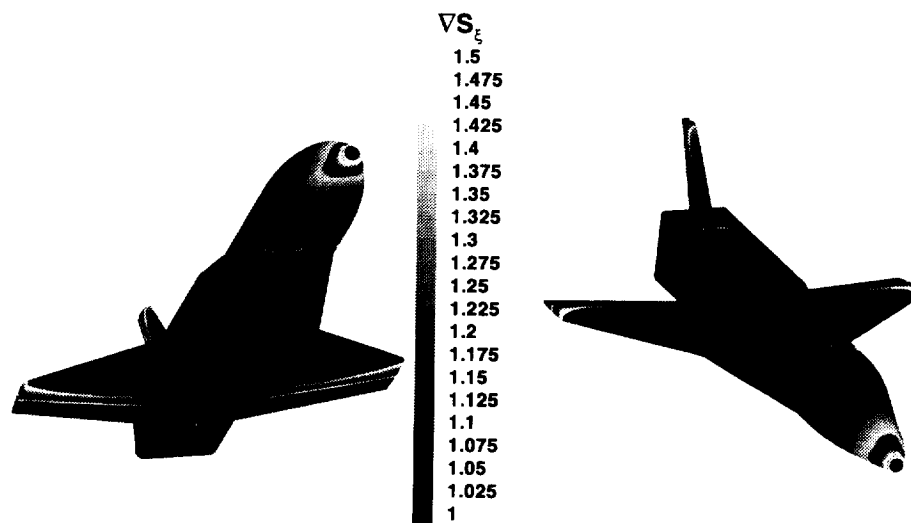
Figure A.1: Grid-point-spacing gradients in the I-direction.
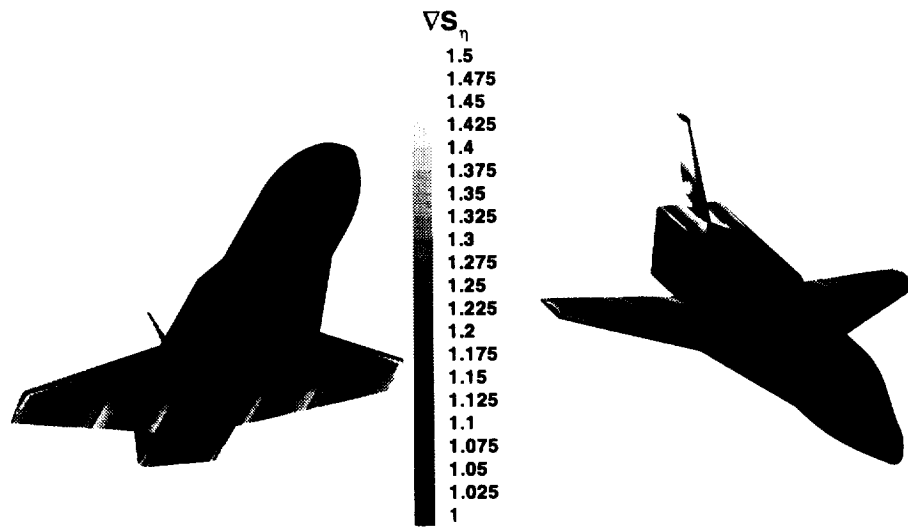
Figure A.2: Grid-point-spacing gradients in the J-direction.
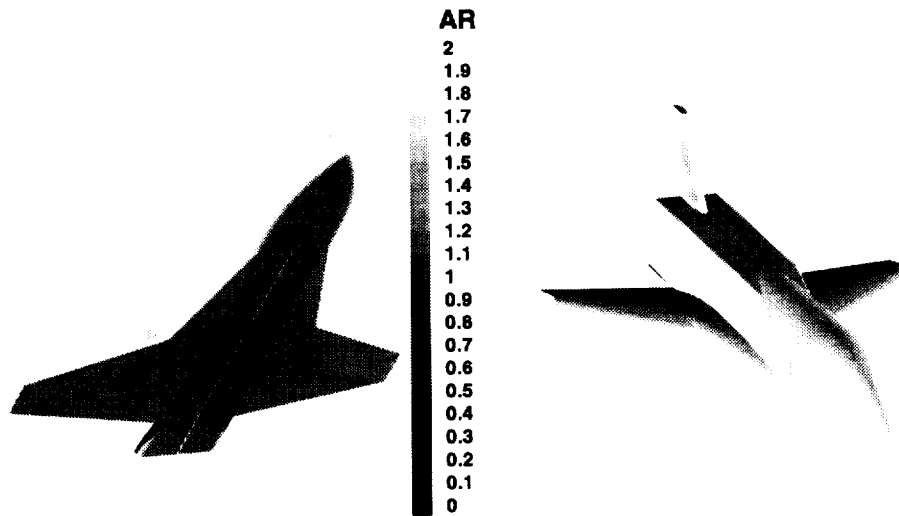
Figure A.3: Cell aspect ratio for viscous computational grid.
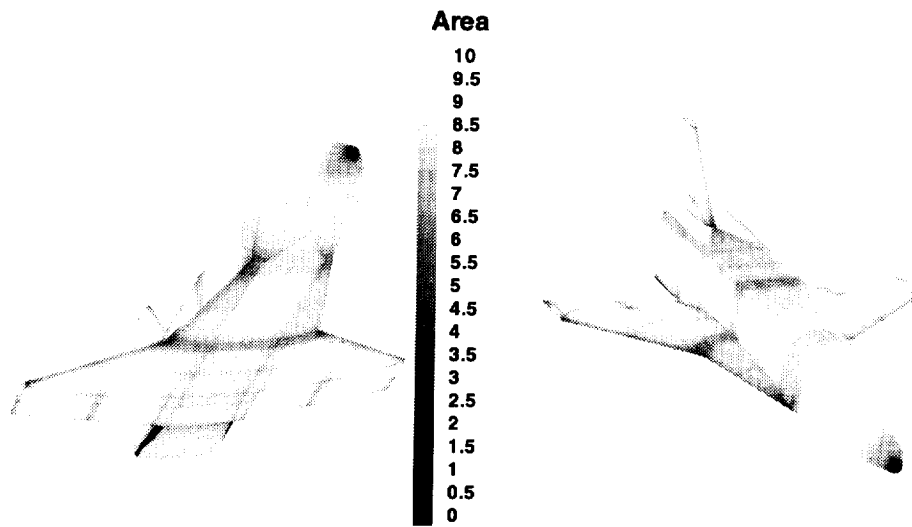
Figure A.4: Cell area for viscous computational grid.
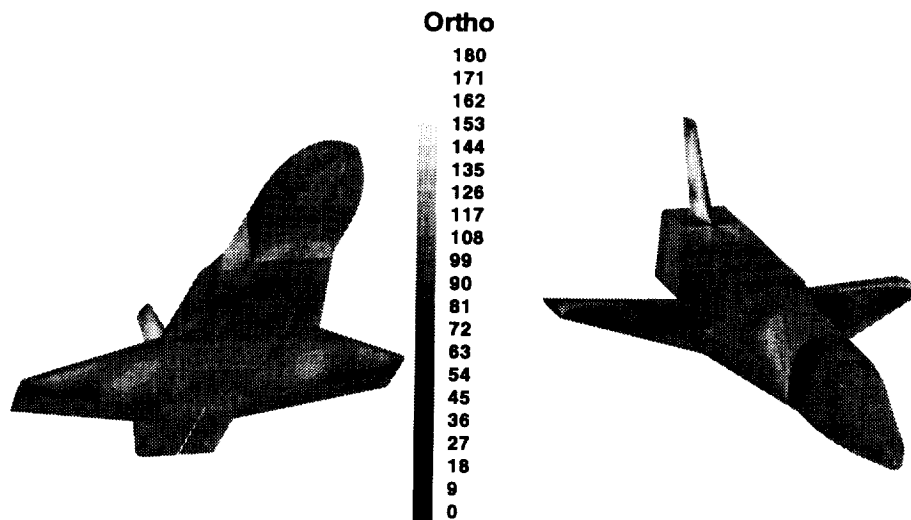
Figure A.5: Orthogonality of grid line intersections in the viscous wall grid.
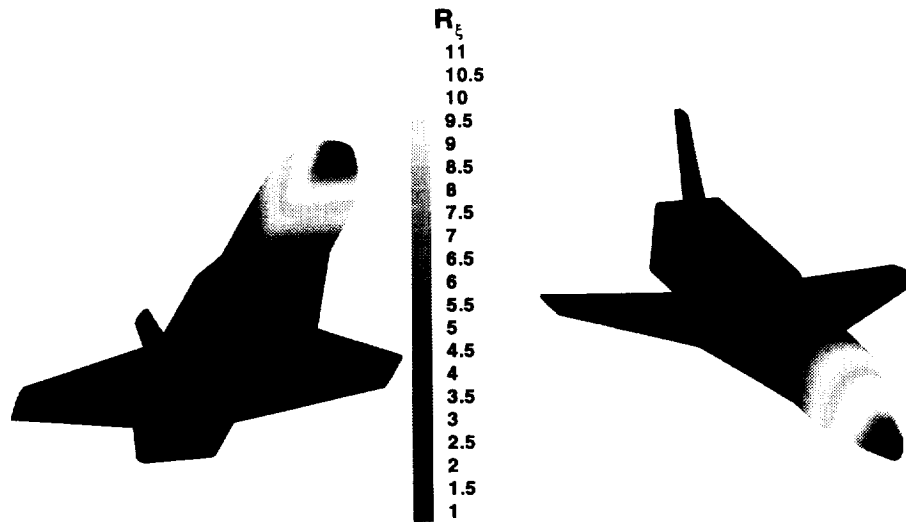
Figure A.6: First derivative of coordinates modeling the wall for viscous computations in the I-direction.
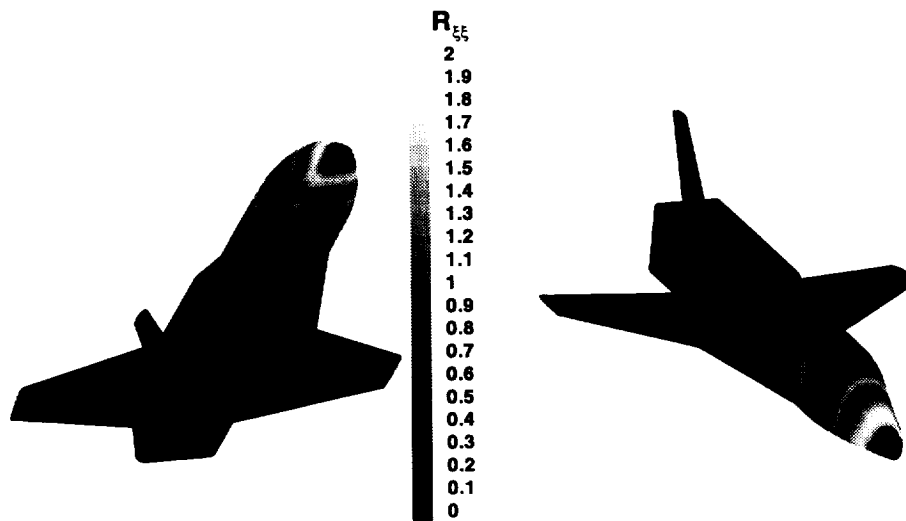
Figure A.7: Second derivative of coordinates modeling the wall for viscous computations in the I-direction.

R_η
15
14.25
13.5
12.75
12
11.25
10.5
9.75
9
8.25
7.5
6.75
6
5.25
4.5
3.75
3
2.25
1.5
0.75
0
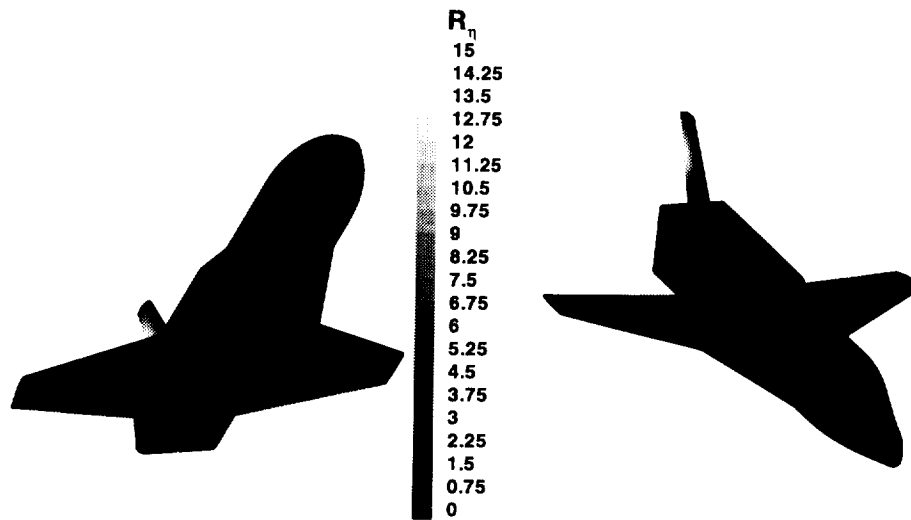
Figure A.8: First derivative of coordinates modeling the wall for viscous computations in the J-direction.

$R_{\eta\eta}$
1
0.95
0.9
0.85
0.8
0.75
0.7
0.65
0.6
0.55
0.5
0.45
0.4
0.35
0.3
0.25
0.2
0.15
0.1
0.05
0
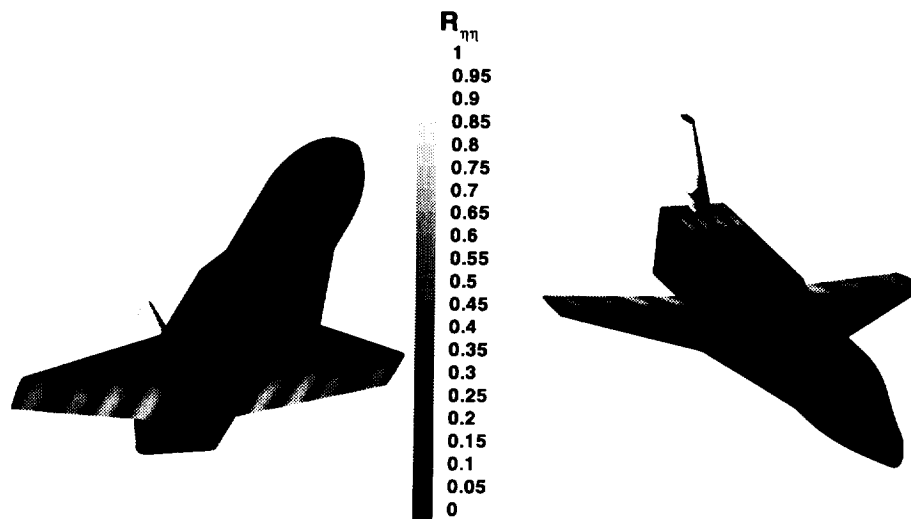
Figure A.9: Second derivative of coordinates modeling the wall for viscous computations in the J-direction.

Appendix B

Viscous Volume Grid Quality Measures

The quality measures of the viscous volume grid delivered for CFD simulations is shown in figure B.1:

```
Block: MAIN (369 X 305 X 65)
       Measure                      Minimum         Maximum         Average
       =======                      =======         =======         =======
       Volume                   0.122428E-03    0.836847E+04    0.912598E+02
       Aspect Ratio             0.970958E+00    0.879803E+01    0.152414E+01
       IJ Orthogonality         0.247106E+00    0.100000E+01    0.947846E+00
       JK Orthogonality         0.134447E+00    0.100000E+01    0.847578E+00
       IK Orthogonality         0.198196E+00    0.100000E+01    0.872895E+00
        Avg. Area Gradients in I =   1.5644300   TOTAL #of I =11474
        Avg. Area Gradients in J <   1.5000000   TOTAL #of J =    0
        Avg. Area Gradients in K =   1.5144236   TOTAL #of K = 1443

Block: WINGE-WAKE (73 X 81 X 17)
       Measure                      Minimum         Maximum         Average
       =======                      =======         =======         =======
       Volume                   0.387246E-02    0.100374E+01    0.252296E+00
       Aspect Ratio             0.101617E+01    0.277706E+01    0.169547E+01
       IJ Orthogonality         0.694641E+00    0.999996E+00    0.877922E+00
       JK Orthogonality         0.107066E+00    0.100000E+01    0.926222E+00
       IK Orthogonality         0.915762E+00    0.100000E+01    0.981000E+00
        Avg. Area Gradients in I <   1.5000000   TOTAL #of I =    0
        Avg. Area Gradients in J <   1.5000000   TOTAL #of J =    0
        Avg. Area Gradients in K <   1.5000000   TOTAL #of K =    0
```

Figure B.1: Viscous volume grid quality measures.

Appendix C

Inviscid Grid Surface Quality Measures

As identified in section 3.2, the quality measures for the inviscid surface grid used for all computations are shown in figures C.1 - C.9, representing the GPSGs in the ξ-, and η-directions, the aspect ratios of the cells, the cell areas, grid orthogonality, and the surface derivatives.
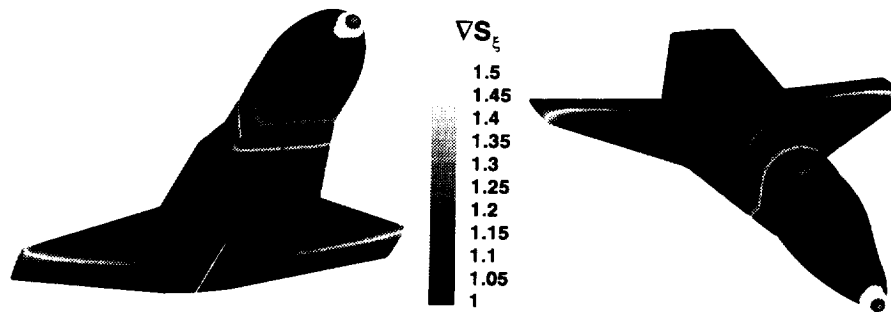
Figure C.1: Grid-point-spacing gradients in the I-direction.

Most importantly, the wall grid quality, as computed by the GRIDQUAL code, identified several issues that needed attention. The computed measures listed in figure 5.2 indicate GPSG problems in the I-direction and highly skewed cells on the surface.
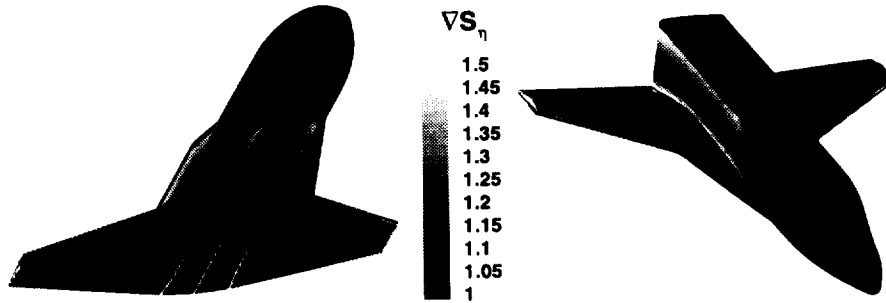
Figure C.2: Grid-point-spacing gradients in the J-direction.
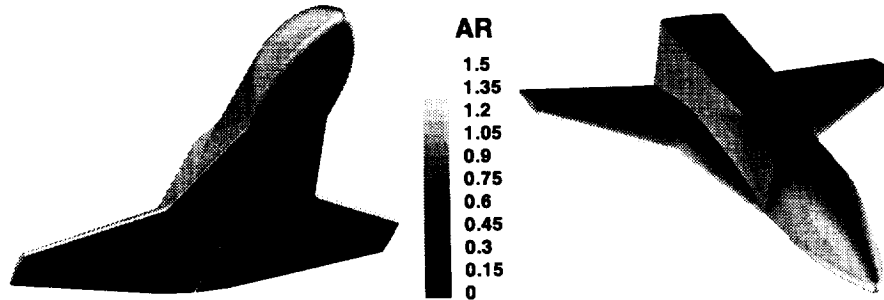
Figure C.3: Cell aspect ratio for inviscous computational grid.

Area

10
9.5
9
8.5
8
7.5
7
6.5
6
5.5
5
4.5
4
3.5
3
2.5
2
1.5
1
0.5
0
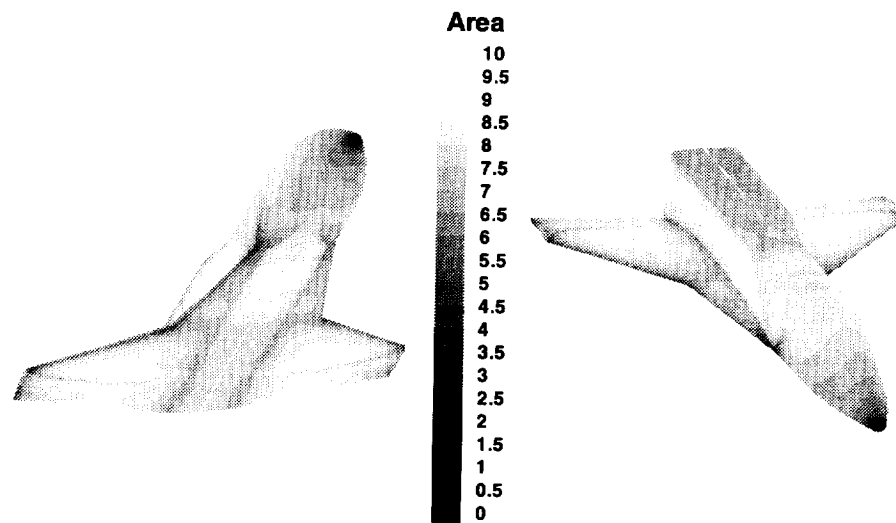
Figure C.4: Cell area for inviscid computational grid.

Ortho

180
171
162
153
144
135
126
117
108
99
90
81
72
63
54
45
36
27
18
9
0
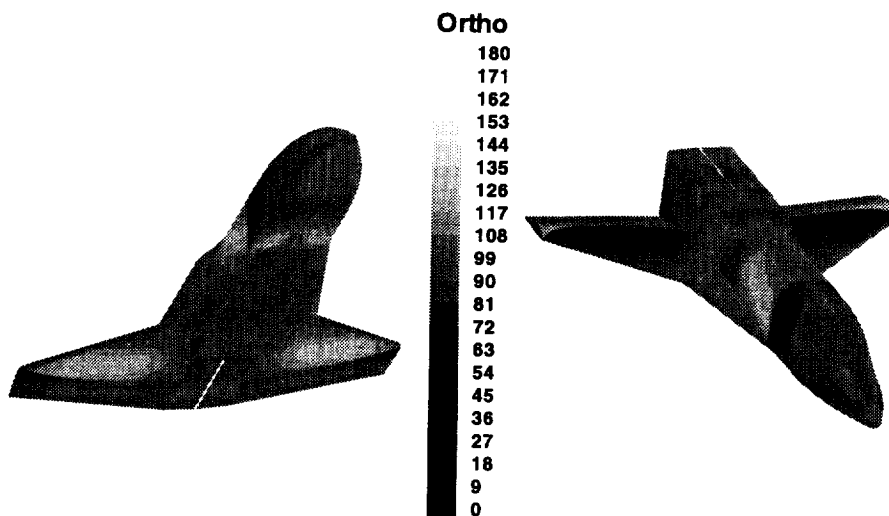
Figure C.5: Orthogonality of grid line intersections in the inviscid wall grid.

93
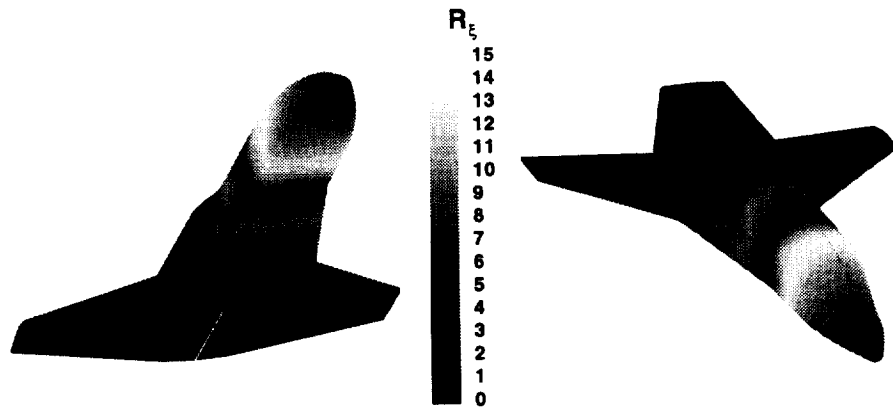
Figure C.6: First derivative of coordinates modeling the wall for inviscid computations in the I-direction.
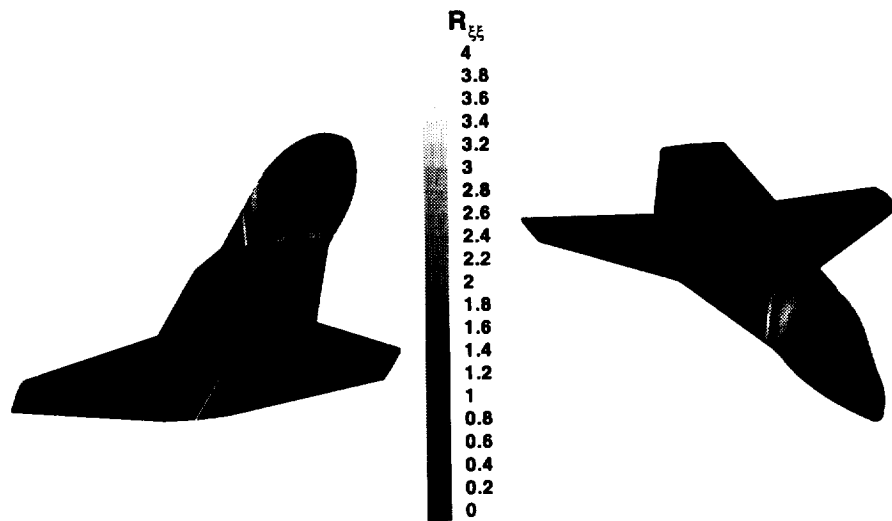
Figure C.7: Second derivative of coordinates modeling the wall for inviscid computations in the I-direction.
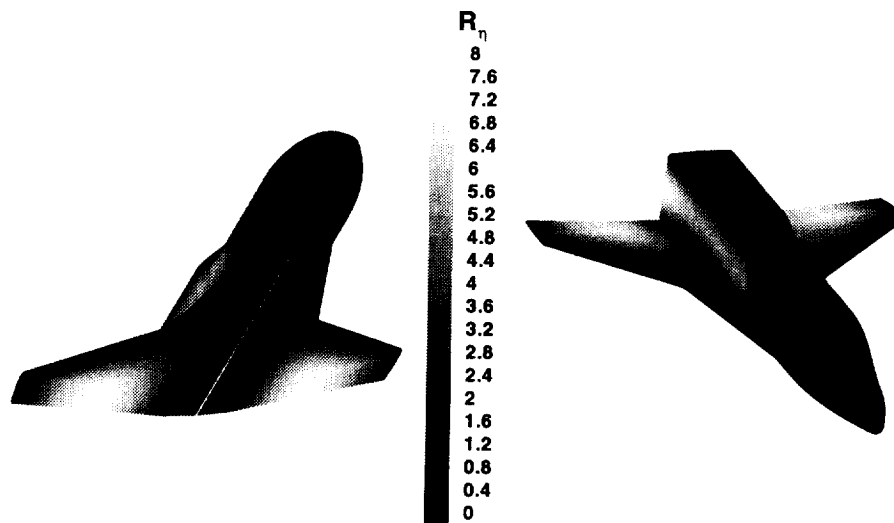
Figure C.8: First derivative of coordinates modeling the wall for inviscid computations in the J-direction.
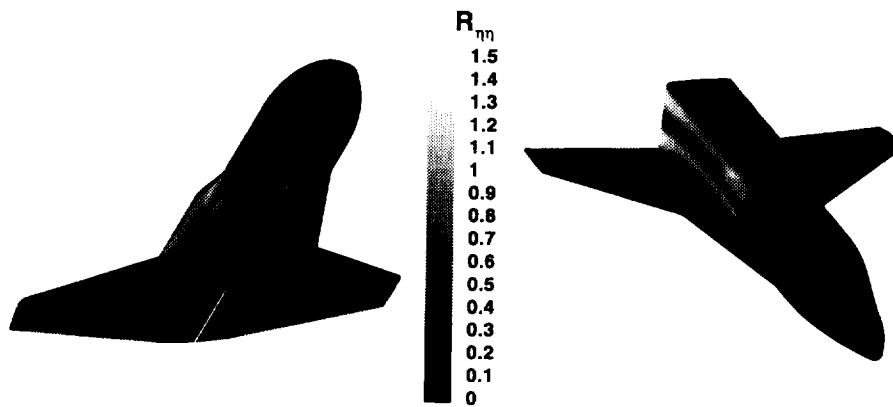
Figure C.9: Second derivative of coordinates modeling the wall for inviscid computations in the J-direction.

Appendix D

Inviscid Volume Grid Quality Measures

The quality measures of the inviscid volume grid delivered for CFD simulations is shown in figure D.1:

```
Block: MAIN (121 X 153 X 33)
        Measure                  Minimum       Maximum        Average
        =======                  =======       =======        =======

        Volume               0.153681E-01   0.258163E+05   0.791617E+03
        Aspect Ratio         0.843276E+00   0.534970E+01   0.142400E+01
        IJ Orthogonality     0.413680E+00   0.100000E+01   0.923471E+00
        JK Orthogonality     0.261945E+00   0.100000E+01   0.844115E+00
        IK Orthogonality     0.371957E+00   0.100000E+01   0.878601E+00

        Avg. Area Gradients in I =  1.7159985   TOTAL #of I = 2882
        Avg. Area Gradients in J <  1.5000000   TOTAL #of J =    0
        Avg. Area Gradients in K =  1.6212567   TOTAL #of K = 2351
```

Figure D.1: Inviscid volume grid quality measures.

Appendix E

Viscous Elevon Volume Grid Quality Measures

The quality measures of the viscous volume grid for the elevon parametric design change delivered for CFD simulations is shown in figure E.1:

```
Block: MAIN (369 X 305 X 65)
       Measure                    Minimum         Maximum         Average
       =======                    =======         =======         =======
       Volume                     0.122428E-03    0.836847E+04    0.912588E+02
       Aspect Ratio               0.977651E+00    0.879803E+01    0.152454E+01
       IJ Orthogonality           0.247106E+00    0.100000E+01    0.946569E+00
       JK Orthogonality           0.165632E+00    0.100000E+01    0.845621E+00
       IK Orthogonality           0.198196E+00    0.100000E+01    0.871012E+00
        Avg. Area Gradients in I =   1.5642824   TOTAL #of I =11557
        Avg. Area Gradients in J <   1.5000000   TOTAL #of J =    0
        Avg. Area Gradients in K =   1.5191799   TOTAL #of K = 1551

Block: WINGE-WAKE (73 X 81 X 17)
       Measure                    Minimum         Maximum         Average
       =======                    =======         =======         =======
       Volume                     0.288446E-02    0.100509E+01    0.253113E+00
       Aspect Ratio               0.982280E+00    0.269214E+01    0.171420E+01
       IJ Orthogonality           0.696308E+00    0.999998E+00    0.871172E+00
       JK Orthogonality           0.100738E-02    0.100000E+01    0.939044E+00
       IK Orthogonality           0.781973E+00    0.999989E+00    0.876586E+00
        Avg. Area Gradients in I <   1.5000000   TOTAL #of I =    0
        Avg. Area Gradients in J =   1.5733669   TOTAL #of J =    5
        Avg. Area Gradients in K <   1.5000000   TOTAL #of K =    0
```

Figure E.1: Viscous volume grid quality measures for the elevon parametric design change.

Appendix F

Viscous Grid Bodyflap Surface Quality Measures

As identified in section 3.2, the quality measures for the viscous surface grid that represents the bodyflap used for all computations are shown in figures F.1, - F.9, representing the GPSGs in the ξ-, and η-directions, the aspect ratios of the cells, the cell areas, grid orthogonality, and the surface derivatives.
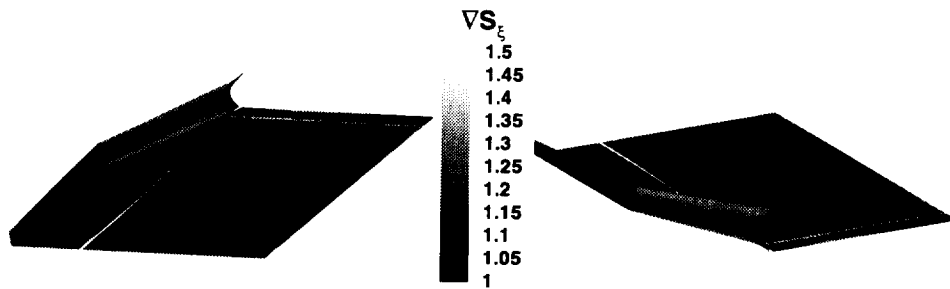
Figure F.1: Grid-point-spacing gradients in the I-direction.
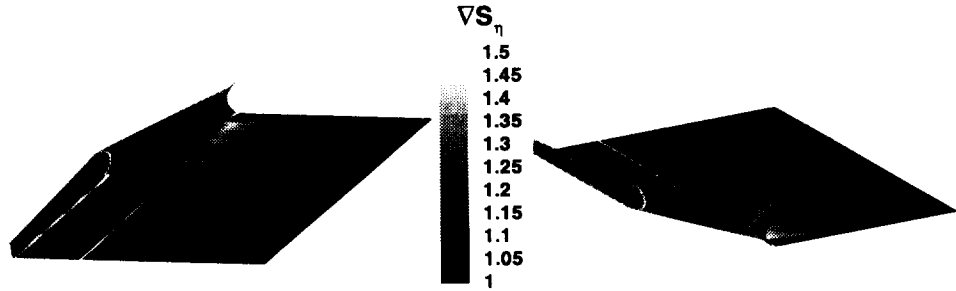
Figure F.2: Grid-point-spacing gradients in the J-direction.
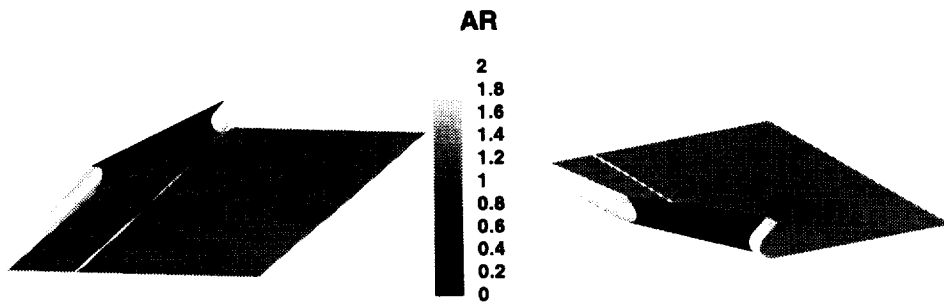
Figure F.3: Cell aspect ratio for inviscid computational grid.
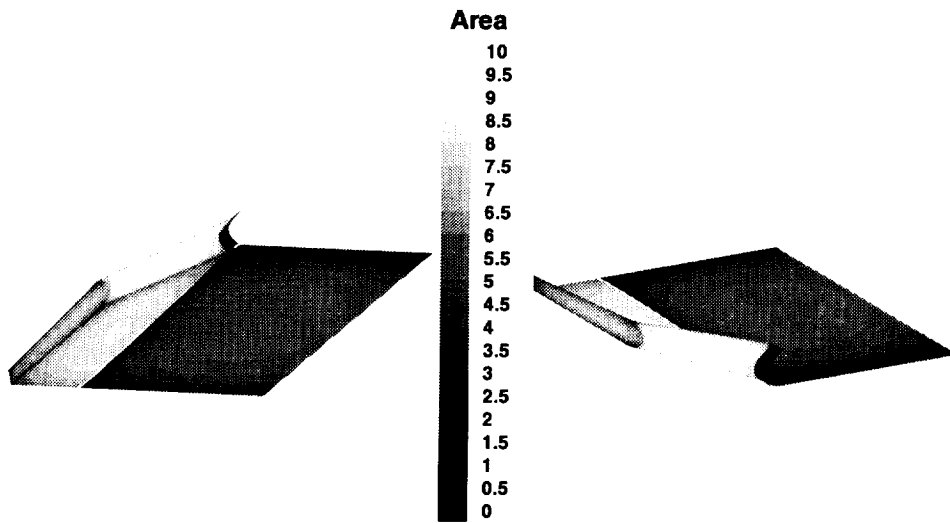
Figure F.4: Cell area for inviscid computational grid.
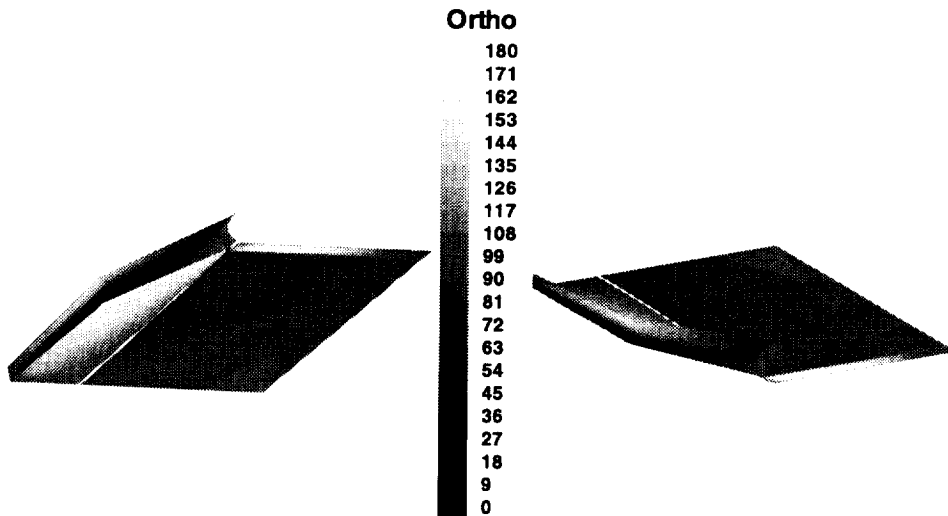
Figure F.5: Orthogonality of grid line intersections in the inviscid wall grid.
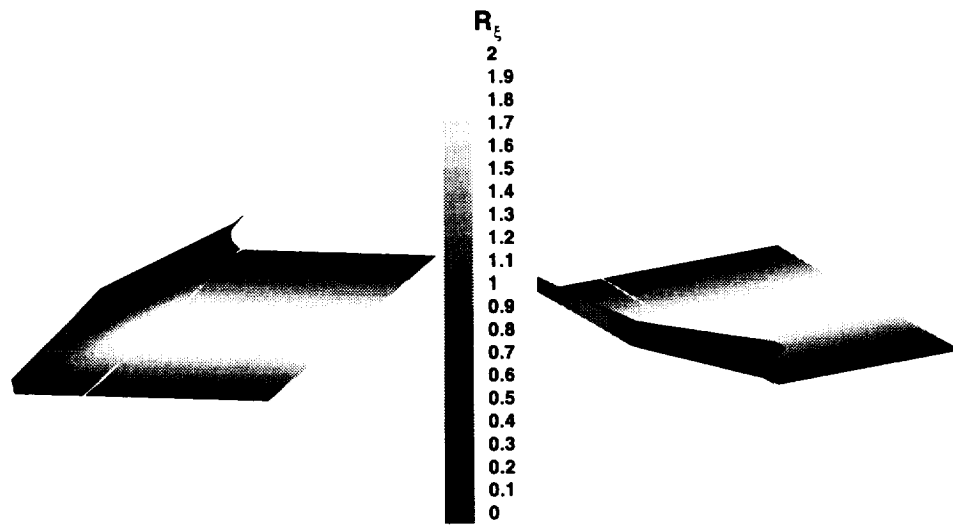
Figure F.6: First derivative of coordinates modeling the wall for inviscid computations in the I-direction.
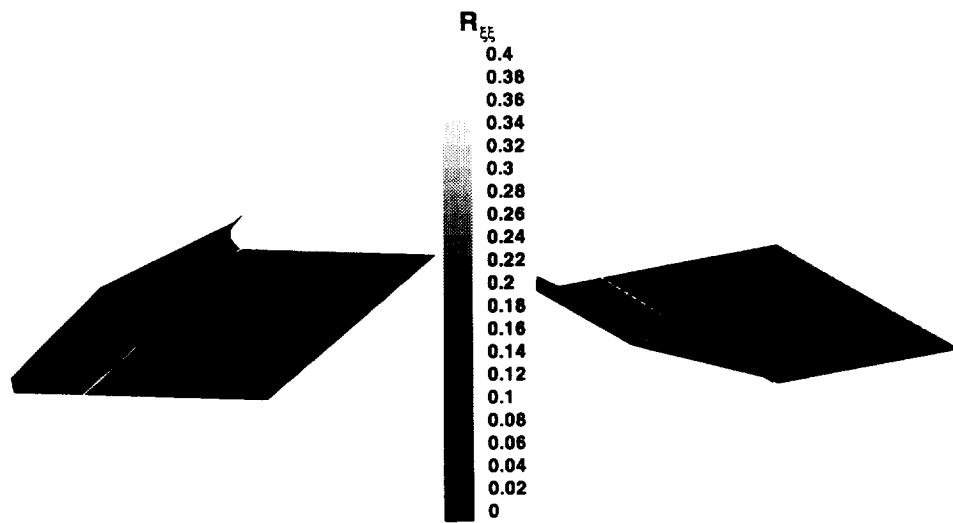
Figure F.7: Second derivative of coordinates modeling the wall for inviscid computations in the I-direction.
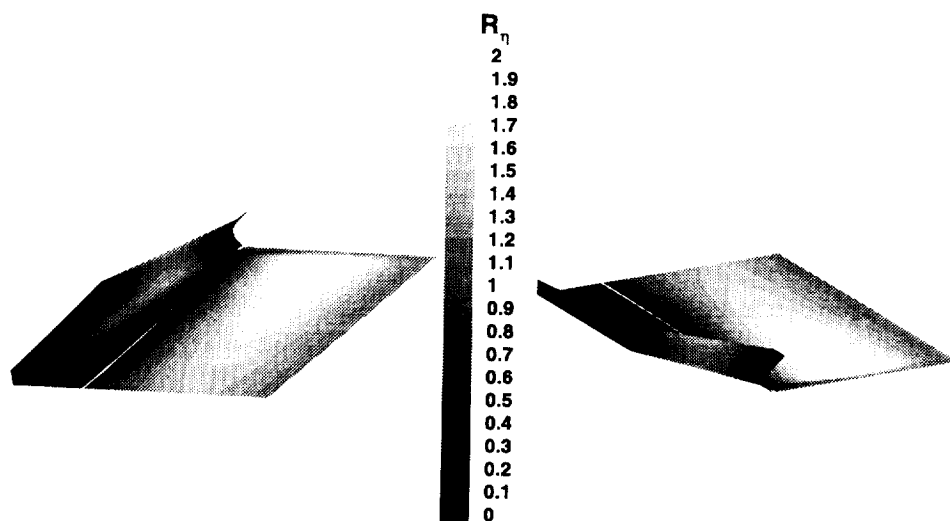
Figure F.8: First derivative of coordinates modeling the wall for inviscid computations in the J-direction.
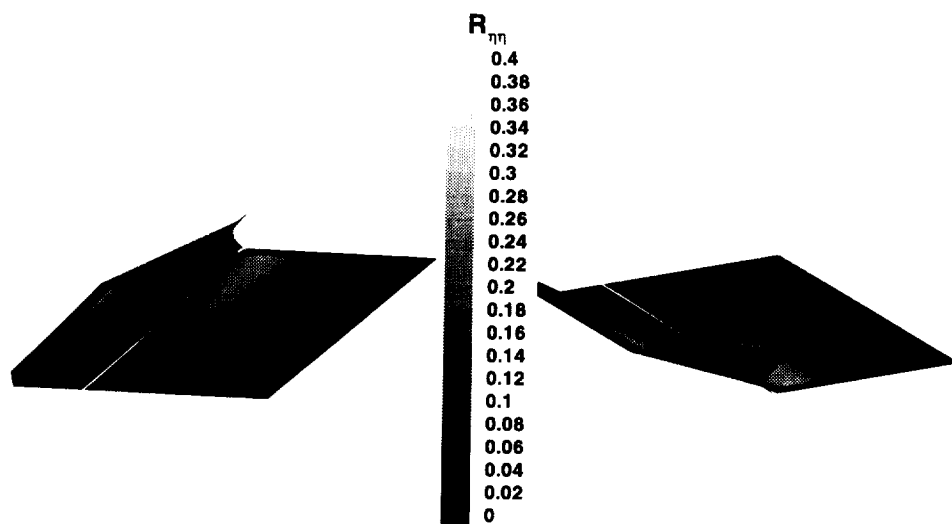
Figure F.9: Second derivative of coordinates modeling the wall for inviscid computations in the J-direction.

Most importantly, the wall grid quality measures, as computed by the GRIDQUAL code, identified several issues that needed attention. The computed measures listed in Figs. F.10 are for five individual surfaces that comprise the bodyflap wall, and the quantities indicate GPSG problems in the I-direction and highly skewed cells on the flap outboard surface and the flap interface to the fuselage.

```
Surface: Flap Outboard, Aft of NOTCH; (49 X 45)


          Measure        Minimum        Maximum        Average
          -------        =======        =======        =======
          Orthogonality  0.899958E+02   0.158729E+03   0.130447E+03
          Cell Area      0.149965E-03   0.756983E+00   0.158072E+00
          I-direct GPSG  0.100041E+01   0.119834E+01   0.107701E+01
          J-direct GPSG  0.100004E+01   0.189056E+01   0.112312E+01


          Avg. in I of Area Gradients (>1.5)= 0.000000  TOTAL I= 0
          Avg. in J of Area Gradients (>1.5)= 1.775931  TOTAL J= 36
          Largest Grid-Point-Spacing-Gradient in I:   1.198344
          Largest Grid-Point-Spacing-Gradient in J:   1.890557
          Minimum orthogonality =    89.99584      degrees.


Surface: Flap Inboard; (65 X 25)


          Measure        Minimum        Maximum        Average
          -------        =======        =======        =======
          Orthogonality  0.826129E+02   0.162468E+03   0.974351E+02
          Cell Area      0.993658E-02   0.361146E+01   0.861206E+00
          I-direct GPSG  0.100000E+01   0.255983E+01   0.109598E+01
          J-direct GPSG  0.100000E+01   0.144489E+01   0.101232E+01


          Avg. in I of Area Gradients (>1.5)= 2.053857  TOTAL I= 24
          Avg. in J of Area Gradients (>1.5)= 0.000000  TOTAL J= 0
          Largest Grid-Point-Spacing-Gradient in I:   2.559834
          Largest Grid-Point-Spacing-Gradient in J:   1.444889
          Minimum orthogonality =    82.61292      degrees.
```

Figure F.10: Viscous bodyflap surface grid quality measures.

Although these measures seem to be extreme, the averages are within the allowables identified by the requirements. Because the volume grids are based on these surface grids, the volumes will not have higher quality; hence, these measures serve as maximum limits on the quality of the generated volume grids.

Surface: NOTCH Inboard Leading Edge; (33 X 49)

Measure	Minimum	Maximum	Average
Orthogonality	0.893840E+02	0.101035E+03	0.911412E+02
Cell Area	0.544333E-03	0.406041E-01	0.113190E-01
I-direct GPSG	0.100000E+01	0.119699E+01	0.940196E+00
J-direct GPSG	0.100042E+01	0.125908E+01	0.115251E+01

Avg. in I of Area Gradients (>1.5)= 0.000000 TOTAL I= 0
Avg. in J of Area Gradients (>1.5)= 0.000000 TOTAL J= 0
Largest Grid-Point-Spacing-Gradient in I: 1.196989
Largest Grid-Point-Spacing-Gradient in J: 1.259080
Minimum orthogonality =   89.38400   degrees.

Surface: NOTCH Outboard Leading Edge; (49 X 45)

Measure	Minimum	Maximum	Average
Orthogonality	0.270781E+02	0.144748E+03	0.861268E+02
Cell Area	0.142105E-04	0.480170E+00	0.467106E-01
I-direct GPSG	0.100479E+01	0.126190E+01	0.115224E+01
J-direct GPSG	0.100001E+01	0.191093E+01	0.116200E+01

Avg. in I of Area Gradients (>1.5)= 0.000000 TOTAL I= 0
Avg. in J of Area Gradients (>1.5)= 1.900446 TOTAL J= 48
Largest Grid-Point-Spacing-Gradient in I: 1.261898
Largest Grid-Point-Spacing-Gradient in J: 1.910931
Minimum orthogonality =   27.07807   degrees.

Figure F.10: Continued.

107

Surface: Bodyflap Tip; (49 X 49)

Measure	Minimum	Maximum	Average
-------	=======	=======	=======
Orthogonality	0.146187E+02	0.150420E+03	0.878733E+02
Cell Area	0.125684E-03	0.362130E+00	0.337552E-01
I-direct GPSG	0.100060E+01	0.128911E+01	0.106674E+01
J-direct GPSG	0.100000E+01	0.125938E+01	0.115247E+01

Avg. in I of Area Gradients (>1.5)= 0.000000   TOTAL I= 0
Avg. in J of Area Gradients (>1.5)= 0.000000   TOTAL J= 0
Largest Grid-Point-Spacing-Gradient in I: 1.289106
Largest Grid-Point-Spacing-Gradient in J: 1.259377
Minimum orthogonality =   14.61871   degrees.

Figure F.10: Concluded.

Appendix G

Viscous Bodyflap Volume Grid Quality Measures

The quality measures of the viscous volume grid for the bodyflap parametric design change delivered for CFD simulations is shown in figure G.1:

```
Block: WIND-WING (81 X 156 X 65)
       Measure                  Minimum        Maximum        Average
       =======                  =======        =======        =======
       Volume              0.212050E-06   0.109942E+02   0.502898E+00
       Aspect Ratio        0.994197E+00   0.267154E+02   0.267528E+01
       IJ Orthogonality    0.130819E+00   0.100000E+01   0.820870E+00
       JK Orthogonality    0.230187E+00   0.100000E+01   0.830539E+00
       IK Orthogonality    0.406762E+00   0.100000E+01   0.899513E+00
        Avg. Area Gradients in I <   1.5000000   TOTAL #of I =    0
        Avg. Area Gradients in J =   2.5615823   TOTAL #of J =  180
        Avg. Area Gradients in K <   1.5000000   TOTAL #of K =    0

Block: BODYFLAP (65 X 25 X 65)
       Measure                  Minimum        Maximum        Average
       =======                  =======        =======        =======
       Volume              0.191751E-04   0.797556E+01   0.892855E+00
       Aspect Ratio        0.995208E+00   0.323088E+02   0.436328E+01
       IJ Orthogonality    0.187797E+00   0.100000E+01   0.902461E+00
       JK Orthogonality    0.687202E+00   0.100000E+01   0.963376E+00
       IK Orthogonality    0.647583E+00   0.100000E+01   0.910638E+00
        Avg. Area Gradients in I =   2.0203881   TOTAL #of I = 1649
        Avg. Area Gradients in J <   1.5000000   TOTAL #of J =    0
        Avg. Area Gradients in K <   1.5000000   TOTAL #of K =    0
```

Figure G.1: Viscous volume grid quality measures for the bodyflap parametric design change.

```
Block: WING-WAKE-CORE (81 X 49 X 96)
        Measure             Minimum        Maximum         Average
        =======             =======        =======         =======
        Volume          0.298077E-06   0.820863E+00    0.408415E-01
        Aspect Ratio    0.996010E+00   0.131296E+02    0.286878E+01
        IJ Orthogonality 0.110474E+00  0.100000E+01    0.915555E+00
        JK Orthogonality 0.571573E+00  0.100000E+01    0.958863E+00
        IK Orthogonality 0.249454E+00  0.999998E+00    0.870008E+00

        Avg. Area Gradients in I =  1.7747709  TOTAL #of I =  514
        Avg. Area Gradients in J <  1.5000000  TOTAL #of J =    0
        Avg. Area Gradients in K =  5.9358592  TOTAL #of K = 4072

Block: NOTCH (33 X 49 X 45)
        Measure             Minimum        Maximum         Average
        =======             =======        =======         =======
        Volume          0.375818E-07   0.104742E+00    0.452426E-02
        Aspect Ratio    0.100247E+01   0.389977E+02    0.367607E+01
        IJ Orthogonality 0.216592E+00  0.100000E+01    0.781203E+00
        JK Orthogonality 0.205945E-01  0.999997E+00    0.681977E+00
        IK Orthogonality 0.117033E+00  0.100000E+01    0.577866E+00

        Avg. Area Gradients in I <  1.5000000  TOTAL #of I =    0
        Avg. Area Gradients in J <  1.5000000  TOTAL #of J =    0
        Avg. Area Gradients in K =  1.7756499  TOTAL #of K = 2169
```

Figure G.1: Concluded.

Appendix H

Viscous Bodyflap Volume Grid Quality Measures

The quality measures of the inviscid volume grid for the elevon parametric design change delivered for CFD simulations is shown in figure H.1:

```
Block: MAIN (121 X 153 X 33)

        Measure                 Minimum         Maximum         Average
        =======                 =======         =======         =======
        Volume              0.153436E-01    0.438427E+04    0.227153E+03
        Aspect Ratio        0.929189E+00    0.528678E+01    0.132412E+01
        IJ Orthogonality    0.478912E+00    0.100000E+01    0.927022E+00
        JK Orthogonality    0.286556E+00    0.100000E+01    0.853977E+00
        IK Orthogonality    0.440465E+00    0.100000E+01    0.904695E+00

        Avg. Area Gradients in I =  1.7206075  TOTAL #of I = 3265
        Avg. Area Gradients in J <  1.5000000  TOTAL #of J =    0
        Avg. Area Gradients in K =  1.6402928  TOTAL #of K = 1684
```

Figure H.1: Inviscid volume grid quality measures for the elevon parametric design change.

References

[1] P. A. Gnoffo, "An Upwind–Biased Point–Implicit Relaxation Algorithm for Viscous, Compressible Perfect–Gas Flows," NASA Technical Paper 2953, February 1990.

[2] B. K. Soni, "Two– and Three-Dimensional Grid Generation for Internal Flow Applications of Computational Fluid Dynamics," AIAA Paper 85–1526, 1985.

[3] J. P. Steinbrenner, J. R. Chawner, and C. L. Fouts, "The GRIDGEN 3D Multiple Block Grid Generation System," Wright Research and Development Center Report WRDC–TR–90–3022, October 1989.

[4] S. J. Alter and K. J. Weilmuenster, "The Three–Dimensional Multi–block Advanced Grid Generation System (3DMAGGS)," NASA TM–108985, April 1993.

[5] K. A. Hoffmann, *Computational Fluid Dynamics for Engineers*. Austin, Texas: Engineering Education System^{TM}, 1st ed., 1989.

[6] S. J. Alter, "The Volume Grid Manipulator (VGM): A Grid Reusability Tool," NASA CR–4772, April 1997.

[7] S. J. Alter and K. J. Weilmuenster, "Single Block Three-Dimensional Volume Grids About Complex Aerodynamic Vehicles," NASA TM–108986, November 1993.

[8] J. D. Anderson, *Modern Compressible Flow with Historical Perspective*. New York, NY: McGraw-Hill Book Company, Inc., 1st ed., 1982.

[9] S. J. Alter, "Complex Grid Generation Through the Use of Grid Reusability," AIAA paper 97–1987, June 1997.

[10] H. H. Hamilton II, F. A. Greene, and F. R. DeJarnette, "Approximate Method for Calculating Heating Rates on Three-Dimensional Vehicles," in *Journal of Spacecraft and Rockets* (E. V. Zoby, ed.), vol. 31, pp. 345–354, 1994.

[11] G. E. Farin, "NURBS for Curve and Surface Design," tech. rep., Philadelphia, Pennsylvania, 1991.

[12] W. Kordulla and M. Vinokur, "Efficient Computation of Volume in Flow Predictions," *AIAA Journal*, vol. 21, pp. 917–918, June 1983.

[13] D. A. Anderson, J. C. Tannehill, and R. H. Pletcher, *Computational Fluid Dynamics and Heat Transfer*. Bristol, London: Hemisphere Publishing Co., 1st ed., 1984.

[14] M. Vinokur, "On One-Dimensional Stretching Functions for Fininte-Difference Calculations," NASA CR–3313, 1993.

[15] J. A. Samareh, "GridTool: A Surface Modeling and Grid Generation Tool," in *Surface Modeling, Grid Generation, and Related Issues in Computational Fluid Dynamic (CFD) Solutions* (Y. K. Choo, ed.), vol. CP–3143, pp. 821–831, NASA, May 1995.

[16] S. J. Alter and F. M. Cheatwood, "Elliptic Volume Grid Generation for Viscous Computations in Parametric Design Studies," AIAA Paper 96–1999, June 1996.

REPORT DOCUMENTATION PAGE

1. AGENCY USE ONLY (Leave blank)	2. REPORT DATE November 1997	3. REPORT TYPE AND DATES COVERED Contractor Report

4. TITLE AND SUBTITLE

Surface Modeling and Grid Generation of Orbital Sciences X34 Vehicle (Phase I)

5. FUNDING NUMBERS

C NAS1-96014
WU 242-80-01-01

6. AUTHOR(S)

Stephen J. Alter

7. PERFORMING ORGANIZATION NAME(S) AND ADDRESS(ES)

Lockheed Martin Engineering & Sciences Company
Langley Program Office
M/S 371, NASA Langley Research Center
Hampton, VA 23681

8. PERFORMING ORGANIZATION REPORT NUMBER

9. SPONSORING/MONITORING AGENCY NAME(S) AND ADDRESS(ES)

National Aeronautics and Space Administration
Langley Research Center
Hampton, VA 23681-0001

10. SPONSORING/MONITORING AGENCY REPORT NUMBER

NASA/CR-97-206243

11. SUPPLEMENTARY NOTES

Langley Technical Monitor: K. James Weilmuenster

12a. DISTRIBUTION/AVAILABILITY STATEMENT

Unclassified - Unlimited
Subject Category 02
Distribution: Nonstandard
Availability: NASA CASI (301) 621-0390

12b. DISTRIBUTION CODE

13. ABSTRACT (Maximum 200 words)

The surface modeling and grid generation requirements, motivations, and methods used to develop Computational Fluid Dynamic volume grids for the X34-Phase I are presented. The requirements set forth by the Aerothermodynamics Branch at the NASA Langley Research Center serve as the basis for the final techniques used in the construction of all volume grids, including grids for parametric studies of the X34. The Integrated Computer Engineering and Manufacturing code for Computational Fluid Dynamics (ICEM/CFD), the Grid Generation code (GRIDGEN), the Three-Dimensional Multi-block Advanced Grid Generation System (3DMAGGS) code, and Volume Grid Manipulator (VGM) code are used to enable the necessary surface modeling, surface grid generation, volume grid generation, and grid alterations, respectively. All volume grids generated for the X34, as outlined in this paper, were used for CFD simulations within the Aerothermodynamics Branch.

14. SUBJECT TERMS

Grid Generation, X34, Numerical Methods, Surface Modeling, Vehicle Design

15. NUMBER OF PAGES
117

16. PRICE CODE
A06

17. SECURITY CLASSIFICATION OF REPORT Unclassified	18. SECURITY CLASSIFICATION OF THIS PAGE Unclassified	19. SECURITY CLASSIFICATION OF ABSTRACT Unclassified	20. LIMITATION OF ABSTRACT